



University of  
Stavanger

Faculty of Science and Technology

## MASTER'S THESIS

Study program/ Specialization: Petroleum Engineering / Drilling Technology	Spring semester, 2015  Open
Writer: Annbjørg Fiveland	..... (Writer's signature)
Faculty supervisor: Mesfin Belayneh	
Thesis title: <b>Effect of Nano silica and Salts on Xanthan gum polymer-Bentonite fluid system</b>	
Credits (ECTS): 30	
Key words: Salts (KCl, NaCl) Xanthan gum, XC Nano Silica Bentonite Rheology Filtrate Hydraulics Viscoelasticity	Pages: .....109.....  + enclosure: .....22.....  Stavanger, ..... Date/year

## Abstract

The application of nanotechnology shows positive results in the oil and gas industry, with respect to cement, drilling fluid and enhanced oil recovery. In this thesis, an optimized nano-fluid in Xanthan gum (XC) polymer treated bentonite mud system was investigated. The composition of the best-formulated nano-system is: *500g H<sub>2</sub>O+ 25g Bentonite+ 0.5g XC+ 2.5g KCl+ 0.1g Nano silica.*

The best-formulated mud system was further analysed for its viscoelastic behaviour. Simulation of its hydraulic and hole cleaning performance were also conducted.

The overall result shows that the addition of 0.02 wt.% nano-silica:

- Reduces filtrate by 16.67 %.
- Improves cutting transport efficiency.
- Increases the yield stress and apparent viscosity.

Details of the main findings can be found in the conclusion part.

# Acknowledgment

First of all, I want to express my outmost thankfulness to my supervisor Mesfin Belayneh, who has motivated me and provided excellence guidance throughout this process. I want to thank you for always having the door open at your office. You really care for the students. I wish you all the best in the future to come.

I am also very thankful to Bernt S. Aadnøy for providing me this thesis, and giving me the exciting opportunity to study nano technology.

Furthermore, I would also like to thank Thomas Sharman for practical guidance in the use of Anton Paar rheometer.

At last, my sincerest gratitude goes to my family and friends for always encouraging and supporting me.

# Contents

<b>Abstract</b> .....	<b>2</b>
<b>Acknowledgment</b> .....	<b>3</b>
<b>1 Introduction</b> .....	<b>7</b>
<b>1.1 Background</b> .....	<b>8</b>
<b>1.2 Problem formulation</b> .....	<b>11</b>
<b>1.3 Objective</b> .....	<b>12</b>
<b>1.4 Method of investigation</b> .....	<b>12</b>
<b>2 Literature review</b> .....	<b>14</b>
<b>2.1 Rock mechanics</b> .....	<b>14</b>
2.1.1 Fracture models.....	15
2.1.2 Collapse model.....	18
<b>2.2 Lost circulation</b> .....	<b>18</b>
2.2.1 Lost circulation formations.....	18
2.2.2 Effect of particle additives on mechanical strength and loss circulation control.....	20
<b>2.3 Drilling fluids and function and additives</b> .....	<b>22</b>
2.3.1 Function of drilling fluids.....	22
2.3.2 Additives.....	24
2.3.2.1 Bentonite.....	24
2.3.2.2 Salts.....	30
2.3.2.4 Polymers.....	31
<b>2.4 Nano technology and applications</b> .....	<b>34</b>
2.4.1 Emulsion based nano solution on filtrate reducing.....	35
2.4.2 Emulsion based nano solution on wellbore strengthening.....	37
2.4.3 Water based nano effect on permeability reduction.....	37
<b>3 Theory</b> .....	<b>38</b>
<b>3.1 Rheology</b> .....	<b>38</b>
3.1.1 Reynolds number.....	38
3.1.2 Flow regimes.....	39
3.1.3 Viscosities and gel strengths.....	39
<b>3.2 Rheological models</b> .....	<b>40</b>
3.2.1 Newtonian fluids.....	41
3.2.2 Non Newtonian fluids.....	42
3.2.2.1 Bingham plastic.....	42
3.2.2.2 Power Law.....	43
3.2.2.3 Herschel-Buckley.....	43
3.2.2.4 Robertson-Stiff.....	44
3.2.2.5 Unified.....	44
<b>3.3 Viscoelasticity</b> .....	<b>45</b>
3.3.1 Fundamentals.....	45
3.3.2 Amplitude Sweep Test.....	48
3.3.3 Frequency Sweep Test.....	49
<b>3.4 Hydraulics</b> .....	<b>49</b>

3.4.1 Friction pressure drop.....	50
<b>3.5 Cutting transport .....</b>	<b>51</b>
<b>4 Experimental work.....</b>	<b>54</b>
<b>4.1 Drilling fluid formulation and testing.....</b>	<b>54</b>
4.1.1 Equipment used for experiment.....	54
4.1.1.1 Cup and Bob viscometer (Fann VG 35).....	54
4.1.1.2 API filter .....	55
4.1.1.3 Density .....	56
4.1.2 Description of Nano silica (SiO <sub>2</sub> ).....	57
4.1.3 Effect of XC concentration-Screening test.....	58
4.1.3.1 Description of fluid systems .....	58
4.1.3.2 Test result and analysis.....	59
4.1.4 Temperature effects on 0.5g XC fluid system .....	65
4.1.4.1 Drilling fluid description .....	65
4.1.4.2 Test result and analysis .....	65
4.1.5 Effect of KCl and NaCl on polymer system .....	67
4.1.5.1 Drilling fluid description.....	67
4.1.5.2 Test result and analysis .....	67
4.1.6 Effect of nanoparticles on polymer system .....	69
4.1.6.1 Drilling fluid system description.....	70
4.1.6.2 Test result and analysis .....	70
4.1.7 Effect of salt types on Nano based system (NaCl and KCl) .....	74
4.1.7.1 Drilling fluid description .....	74
4.1.7.2 Test results and analysis.....	74
<b>4.2 Visco-elasticity Test .....</b>	<b>76</b>
4.2.1 Anton Parr equipment.....	76
4.2.2 Oscillatory amplitude sweep test results.....	77
4.2.3 Oscillatory frequency sweep test results .....	79
<b>4.3 Rheology Modeling and Analysis of nanoparticles fluid system.....</b>	<b>80</b>
<b>5 Drilling fluid performance simulation studies .....</b>	<b>83</b>
<b>5.1 Hydraulics performance simulation .....</b>	<b>83</b>
5.1.1 Simulation arrangement .....	83
5.1.2 Description of drilling fluids.....	84
5.1.3 Simulation results.....	85
<b>5.2 Cutting transport .....</b>	<b>86</b>
5.2.1 Simulation arrangement .....	87
5.2.2 Description of drilling fluids.....	87
5.2.3 Simulation result.....	88
5.2.3.1 Minimum flow rate .....	88
5.2.3.2 Bed height deposition.....	90
<b>6 Summary and discussion.....</b>	<b>92</b>
<b>6.1 Effect of Xanthan concentration .....</b>	<b>92</b>
<b>6.2 Temperature effects on 0.5g XC fluid system .....</b>	<b>92</b>
<b>6.3 Effect of KCl and NaCl on polymer system .....</b>	<b>93</b>
<b>6.4 Effect of nanoparticles on polymer system .....</b>	<b>93</b>
<b>6.5 Effect of salt types on Nano based system (NaCl and KCl).....</b>	<b>93</b>
<b>6.6 Rheology Modeling and Analysis of nanoparticles fluid system.....</b>	<b>94</b>
<b>6.7 Viscoelasticity .....</b>	<b>94</b>

<b>6.8 Hydraulics .....</b>	<b>95</b>
<b>6.9 Cutting transport .....</b>	<b>95</b>
<b>7 Conclusion .....</b>	<b>96</b>
<b>References .....</b>	<b>98</b>
<b>Abbreviations .....</b>	<b>103</b>
<b>Nomenclature .....</b>	<b>105</b>
<b>List of Figures .....</b>	<b>107</b>
<b>List of Tables .....</b>	<b>109</b>
<b>Appendix .....</b>	<b>110</b>
<b>Appendix A: Effect of temperature on polymer system.....</b>	<b>110</b>
<b>Appendix B: Effect of nano on salt system (NaCl) .....</b>	<b>114</b>
<b>Appendix C: Effect of nano on polymer system.....</b>	<b>117</b>
<b>Appendix D: Effect of nano on polymer system (with NaCl).....</b>	<b>119</b>
<b>Appendix E: Unified model.....</b>	<b>122</b>
<b>Appendix F: Hole and drill string, and well inclination data hole cleaning simulation</b>	<b>125</b>
<b>Appendix G: Well plan cutting transport models.....</b>	<b>127</b>

# 1 Introduction

Drilling fluids play key roles in drilling operations. The main types of drilling fluids used in the oil industry are water based (WBM) and oil based (OBM) fluid systems. Except with regards to cost and environmental issues, the application of oil based mud system has several advantages compared to the water based mud system. For instance, oil based mud has a low friction coefficient, and avoids shale swelling. Due to environmental policy such as in Norway, when the drilling environment is susceptible, one should use inhibitive water based mud system. The common approach is to use KCL, Glycol, and other filtrate reducing polymers in the water based mud system. However, the “inhibitive” WBM doesn’t completely solve swelling problem.

Presently, the application of nanotechnology has shown proven results in several industries such as biomedicine. Preliminary test results in petroleum industry also show positive effect on cement, drilling fluid and enhanced oil recovery.

This thesis presents an investigation of the effect of nano on polymer Xanthan gum (XC) based bentonite mud system. Several conventional (without nano) and nano based water based mud systems were formulated and tested. The systems were evaluated in various concentration of polymer, KCL and NaCl.

The main objective was to come up with nano system with the idea of improving conventional system by the use of nano technology. After several tests, an optimized nano based polymer was obtained. The viscoelasticity of the system was further investigated based on Anton Paar rheometer measurements. Additionally, hydraulic and hole cleaning efficiency of the system was simulated.

## 1.1 Background

Drilling is a process that connects the reservoir to surface, recovering potential hydrocarbons. In conventional drilling operations, high-pressure mud pumps pump drilling fluid through the circulation system. From mud pits, drilling fluid is injected to the well through standpipe, rotary house and swivel. Further on, it flows through kelly, drill string and collar and across the bit. Then, it enters into the annulus and flows up in the annular clearance to the surface, carrying cuttings and dust. Figure 1 shows schematics of the drilling fluid circulation system. The ability to transport cuttings and cavings from the bottom of the borehole to the surface is partly dependent on the physical properties of the drilling fluid, such as rheology and density, and partly dependent on the velocity of the fluid.

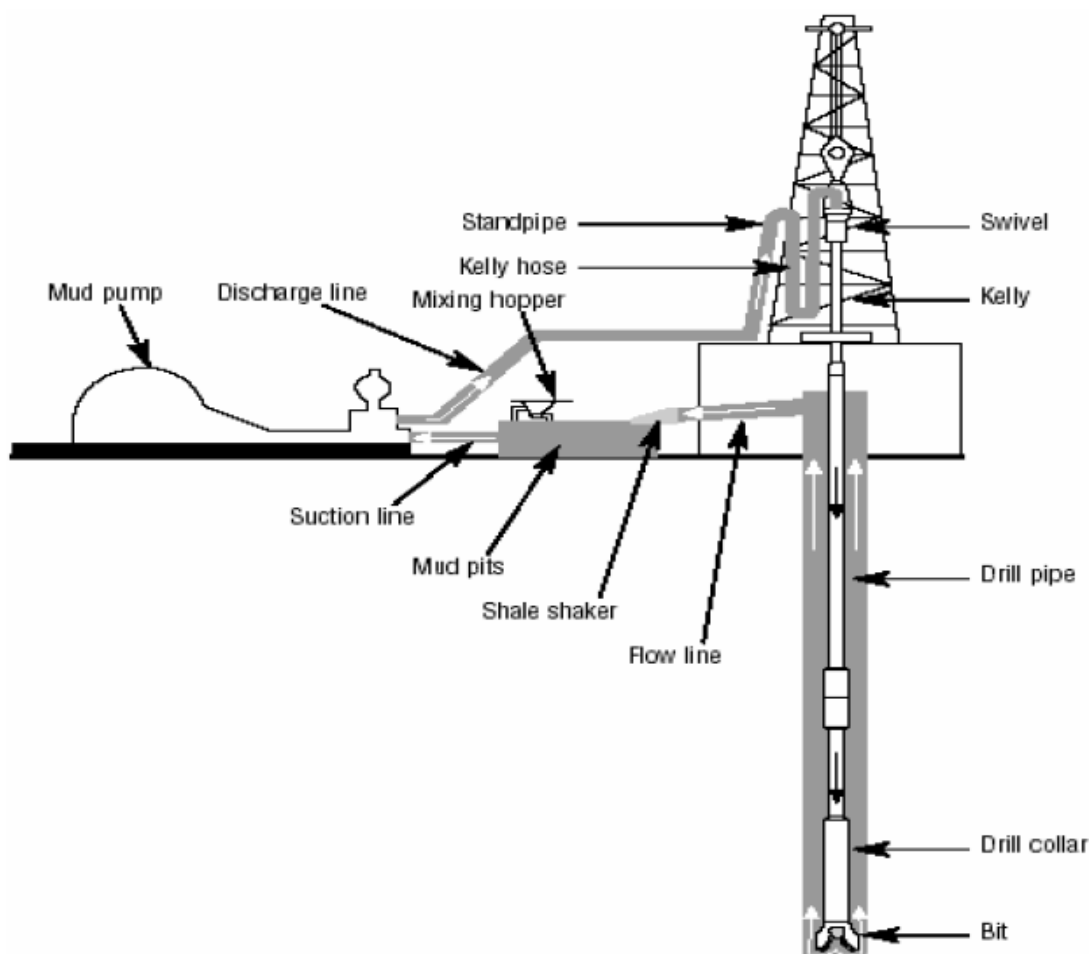
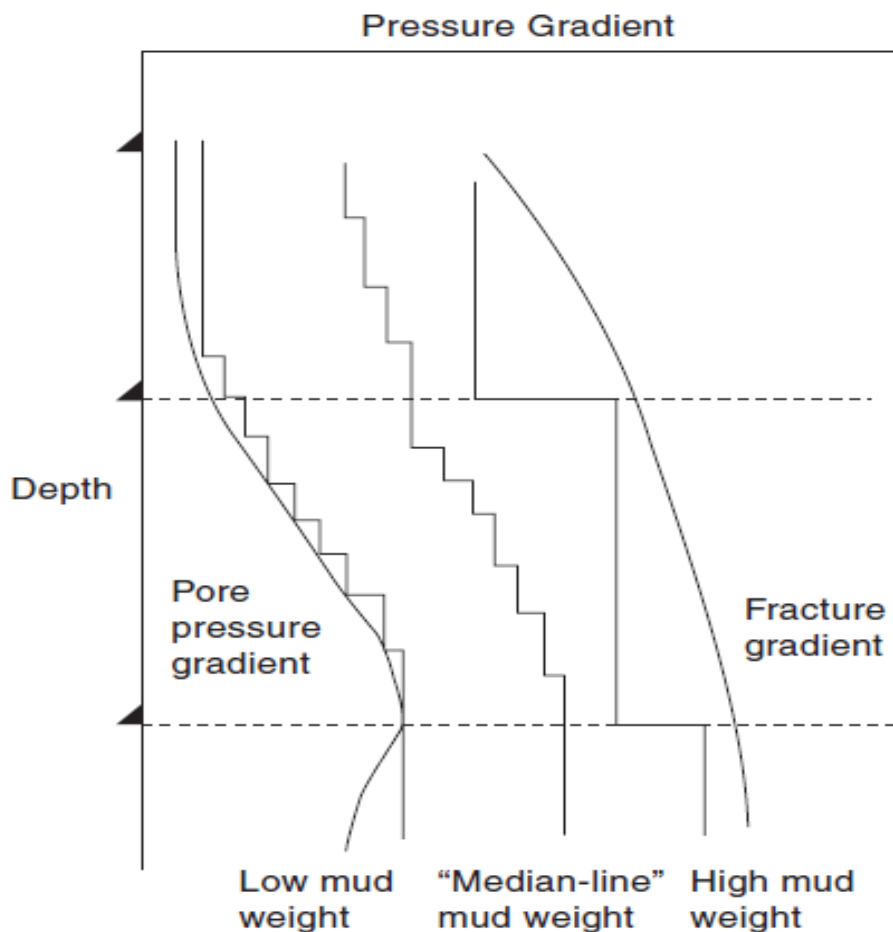


Figure 1: Drilling fluid circulation system [30]



Besides removing cuttings from the well, the drilling fluids have several important tasks. Among others, it should lubricate and cool the bit and prevent formation damage. However, one of the most important tasks is to maintain the pressure in the borehole within a safe operational window. If the pressure is outside this window, as when the well pressure is lower than the formation pressure or close to it, the formation fluids will influx the well because of the differential pressure. If this pressure is not controlled it may lead to a kick, and in worst-case, a blow out. On the other hand, if the well pressure is higher than the fracturing pressure of the well, unwanted situations such as differential sticking and formation fracturing may occur. Therefore, in conventional drilling, it is crucial to maintain the well pressure within the allowable drilling window to avoid severe drilling issues. Figure 2 displays the safe operational window for certain a well in terms of ECD (Equivalent circulation density).



**Figure 2: Median line principle weight selection [31]**

The well pressure is the calculated from static mud density and pressure loss in the annulus, given as:

$$ECD = \rho_{st} + \frac{\Delta P_{annulus}}{0.052.TVD} \quad 1.1$$

Where:

- $\rho_{st}$  = Static mud density (ppg).
- $\Delta P_{annulus}$  = Pressure loss in the annulus (psi).
- TVD = True vertical depth (ft).

The pressure loss is determined from the drilling fluid properties (rheology & density), and flow rate (Q).

Because of the overpressure needed when drilling conventionally, mud will be pushed through wards the formation. If the formation is permeable, drilling fluid will be lost to it. Simultaneously, the solid content in the mud will settle along the hole wall, creating a filter cake. Figure 3 illustrates the described phenomenon. A thin, firm and impermeable filter cake will limit further losses of drilling fluid into the formation. [6]

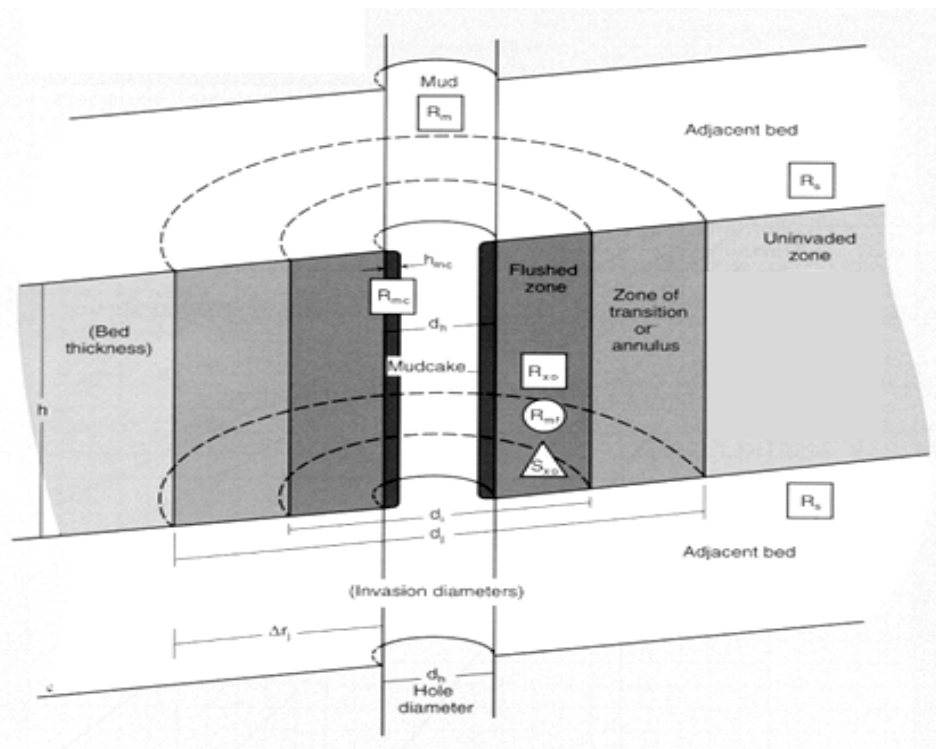


**Figure 3: Mud invasion [17]**

Drilling fluids are therefore a vital element in the success of drilling process. It is important to predict hydraulic behavior and rheology of the drilling fluids at all times while drilling a well.

Poorly designed drilling fluid causes several drilling related problems such as formation damage, inefficient cutting lifting capacity that as a result causes an increase in torque and drag. To overcome these problems, one needs to formulate an efficient drilling fluid. This is the motivation of this thesis.

## **1.2 Problem formulation**

As mentioned in the introduction part, nanotechnology improves the performances of conventional technology. Nanotechnology research in petroleum industry is in its early stage and not yet fully exploited. Since an “inhibitive” water based mud system doesn’t solve shale swelling and lubricity related problems, the possible application of nano particles in improving water based mud systems creates a potential for research activities.

This thesis is primarily a laboratory work, with the objective of formulating bentonite fluid system with nano additives. In order to make the fluid system more realistic, salts (KCL & NaCl) and polymer (Xanthan Gum, XC) were added to the bentonite solution.

This thesis is going to address issues such as:

- Effect of XC polymer on bentonite fluid system.
- Temperature effects on XC polymer treated bentonite fluid system.
- Effect of salt on XC polymer treated bentonite fluid system.
- Effect of nano particles on polymer treated bentonite fluid system.
- Hydraulic and hole cleaning performance of an optimized nano fluid system compared to a nano free system.

### 1.3 Objective

The main object of this thesis is to formulate a nano silica based fluid system. The activities are:

- Literature review of rheological and hydraulic models.
- Review of drilling fluid additive properties.
- Formulation of various combination additives and characterization of the formulated fluid systems through experimental measurement.
- Formulate an optimized nano treated fluid system.
- Further study the viscoelastic behaviour of the optimized nano treated system.
- Hole cleaning and hydraulics performance of the optimized nano treated system.

### 1.4 Method of investigation

To meet the objectives of this thesis, as shown on Figure 4, the research investigation methodology comprises of two parts:

- **Part I:** *Experimental*
- **Part II:** *Performance simulation*

The idea of the experimental part was to formulate a mud system containing nano particles that exhibited favorable rheology and filtrate properties. Secondly, the viscoelastic properties of the obtained mud system were further investigated. In Part II, the performance of the nano treated mud was tested with respect to cutting transport and hydraulics.

In the experimental part, the effect of nano particles, polymer Xanthan and salt on bentonite was investigated based on the following four systems seen in Figure 5: dispersion, aggregation, flocculation and de-flocculation. The terms will be described later on, in section §2.3. The idea is to get low filtrate losses and enhanced rheological properties. The rheological

properties can be characterized in terms of apparent viscosity (AV), plastic viscosity (PV), yield point (YP) and gel strength (gel) of the fluid systems. [23]

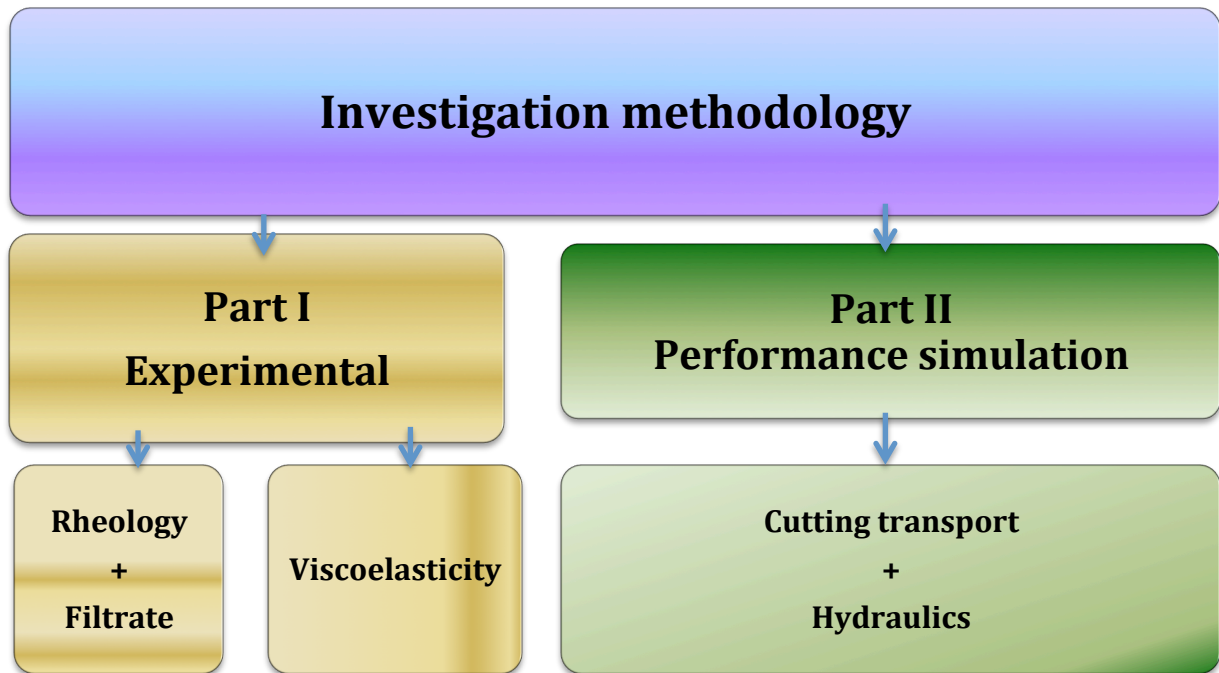


Figure 4: Investigation methodology

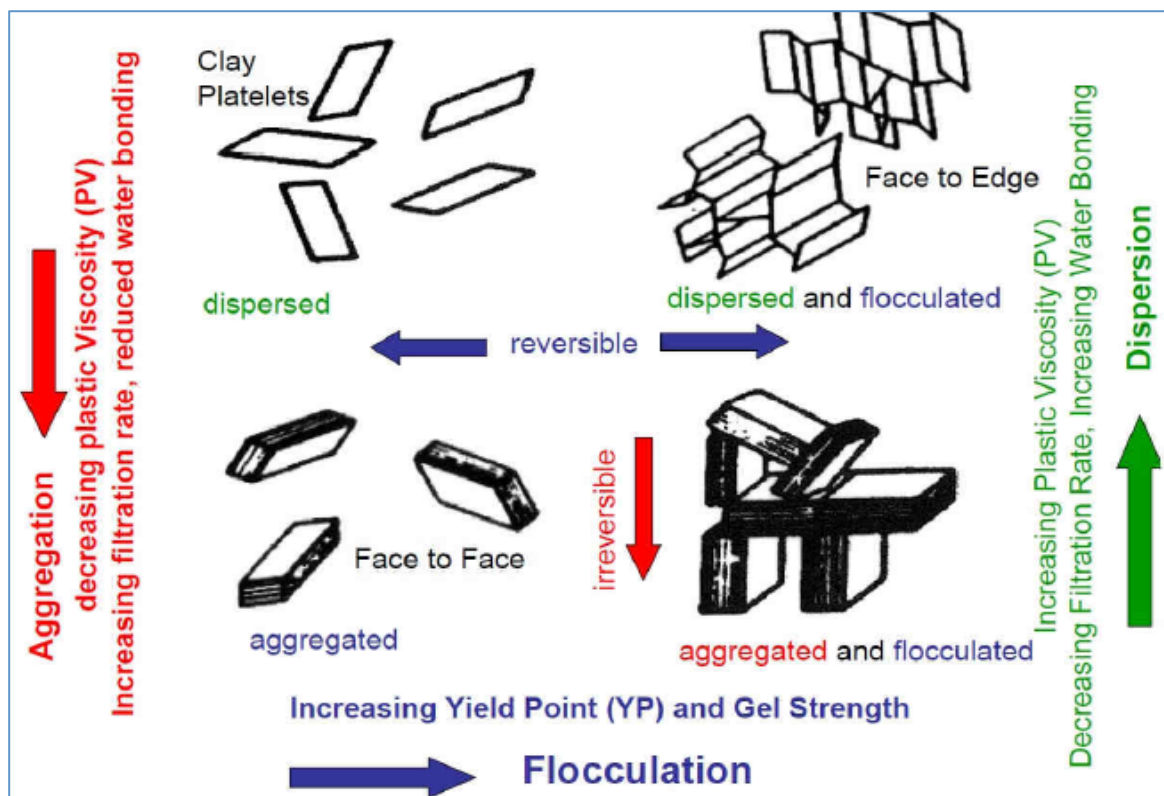


Figure 5: Different behaviors of clay pellets with respect to rheology and filtrate of fluid systems [32]

## 2 Literature review

This chapter presents topics associated with drilling fluids. In addition, it presents the description of chemical additives used in chapter 4.

### 2.1 Rock mechanics

Petroleum rock mechanics deals with the prediction of deformation, compaction, fracture, collapse and faulting of oil and gas reservoir rock formations that are caused by drilling and production. Since drilling fluid is related to well instability issues, this section presents types of well failures mechanisms. The instability problems can be managed by appropriately designed drilling fluid in terms of density, rheology and chemistry. Wellbore instability problems are challenging and cost factors for the oil industry. There are several factors that contribute to well bore instability. These are related to stress, thermal and chemical means. Tensile and shear are the two primary well failure mechanisms, which cause well fracturing and well collapse. [1] Figure 6 illustrates the consequences of typical drilling challenges when drilling through:

- Highly fractured formations results in loss circulation.
- Unconsolidated formations results in mechanical pack-off.
- Moveable formations results in drill string sticking.
- Reactive shale results is shale swelling.

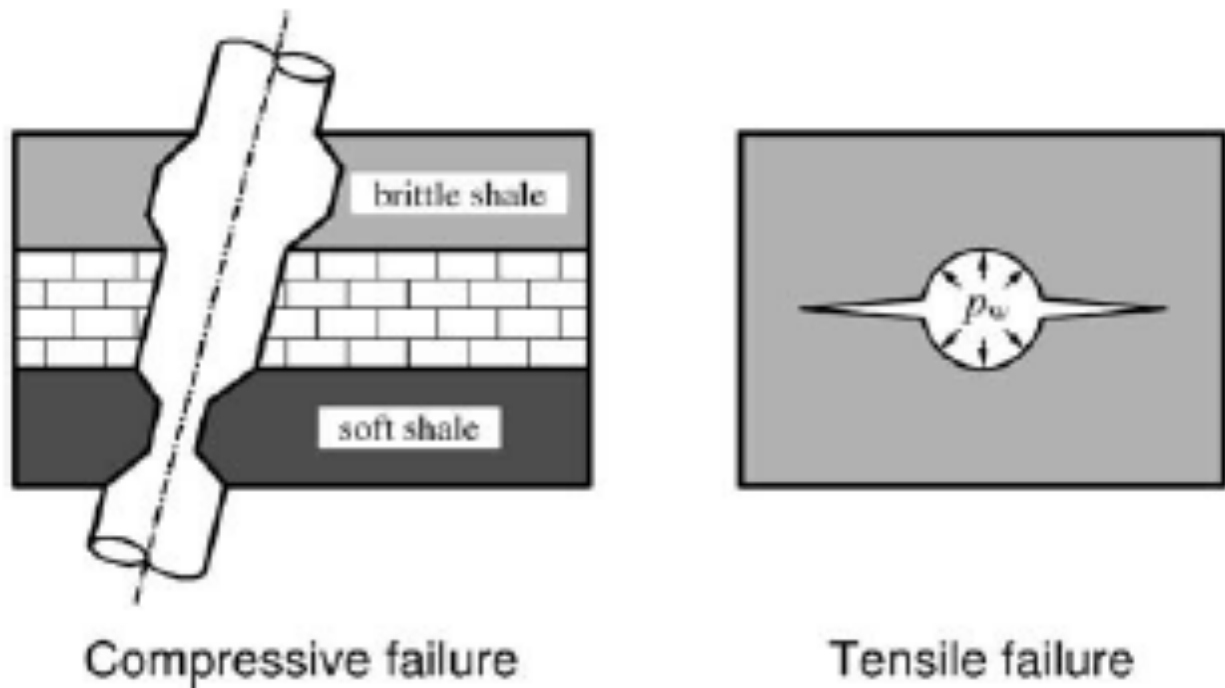


**Figure 6: Compressive and tensile failure in shale formation [3]**

### **2.1.1 Fracture models**

Fracturing models often used in the oil industry are derived from the Kirsch equation. The Kirsch equation defines the hoop stress around the borehole circumference. The fracturing models are linear models that are used for predicting fracture initiation pressure.

The following sections will review two models, the penetrating model and the non-penetrating model. [1]

#### **2.1.1.1 The penetrating model**

The penetrating model states that pressurising borehole will cause fracture using clean fluids like water against the bore wall, exceeding the minimum in-situ stress in the rock [2]. As we can see from Figure 7, the pore pressure builds up inside the wall, resulting in an equalized pore and well pressure at the wellbore.

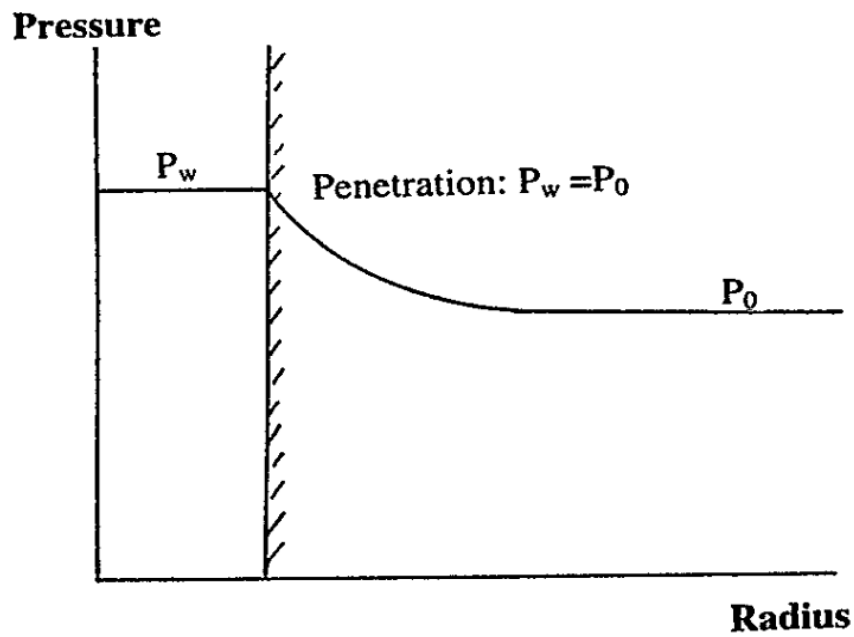


Figure 7: The penetrating model [2]

A poro-elastic solution has been derived and is given as: [2]

$$P_w = \sigma + (1 - 2\nu)(\sigma - P_0) + (1 - \nu)\sigma_t \quad 2.1$$

Where:

- $P_w$  = Well pressure
- $P_0$  = Pore pressure
- $\sigma$  = In situ stress, external load
- $\sigma_t$  = Tensile rock strength
- $\nu$  = Poisson's ratio
- $P_0$  = Pore pressure



### 2.1.1.2 The non - penetrating model

When drilling in a non-permeable formation or using a drilling fluid that builds a filter cake on the bore wall, fracturing can be calculated and analysed by the use of the non-penetrating model. As shown on Figure 8, the well pressure and the formation pressure are not communicating.

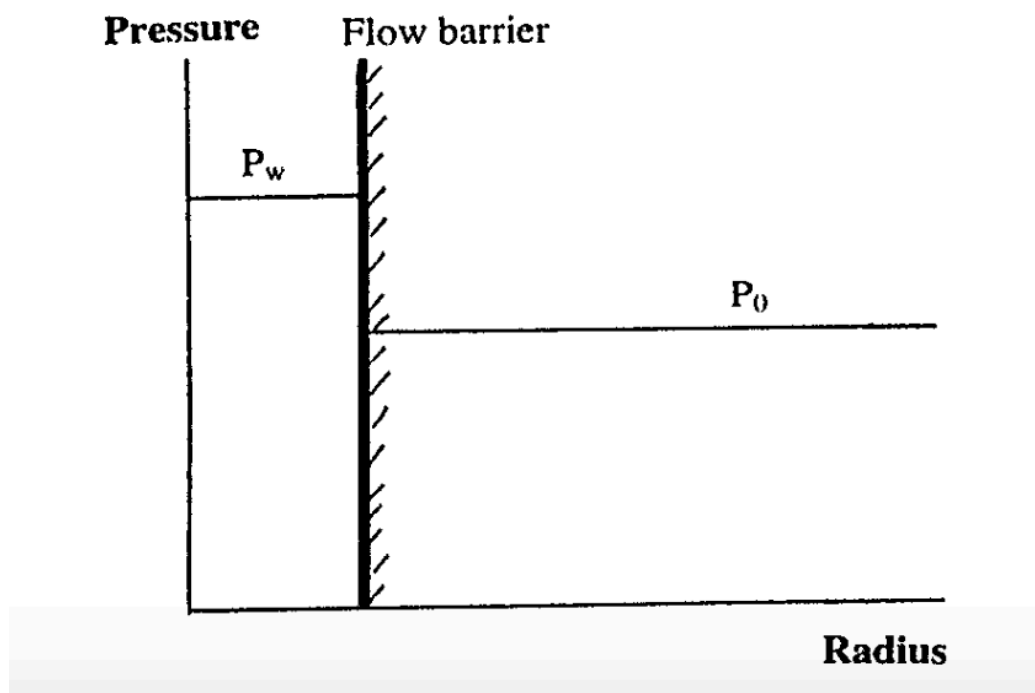


Figure 8: The non-penetrating model [2]

For non-penetrating type boundary condition and elasto-plastic material deformation behaviour, the fracturing equation is given as: [1]

$$P_{wf} = 3\sigma_h - \sigma_H - P_0 + P_y \quad 2.2$$

Where:

- $P_{wf}$  = Fracturing pressure
- $\sigma_H$  = Minimum horizontal stress
- $\sigma_h$  = Maximum horizontal stress
- $P_0$  = Pore pressure
- $P_y$  = Plasticity term

In contrast to a linear elastic model, this model is elastic-plastic; meaning that there is considered a plastic barrier at the bore wall. The plastic barrier, formed by the filter cake and the borehole wall, will deform instead of crack. This will again allow higher fracture pressures, even with low in situ stress. [1][5]

### **2.1.2 Collapse model**

Hole-collapse is caused by shear failure mechanism. The fragments of the near well formation fall into and fill the hole. This problem results in drill string sticking. The problem mainly occurs at lower well pressures. There are several well collapse models available in literature. One of the most common failure criteria used for petroleum rock mechanics analysis is the Mohr-Coulomb (M-C) criterion. The M-C models are a function of in-situ stresses, pore pressure, uniaxial compressive strength and internal friction angle. [3][1]

## **2.2 Lost circulation**

Lost circulation is defined as the flow of fluid into a formation. There are several reasons for lost circulation to occur. Lost circulation problem is a cost factor for the industry.

### **2.2.1 Lost circulation formations**

Circulation losses occur due to drilling induced fractures and drilling in naturally fractured formations. Because of overpressure, naturally, mud will have a tendency to penetrate into the formation. These formations include unconsolidated, permeable and naturally fractured zones [6][8]. Drilling induced losses occur when the well pressure exceeds the fracture strength of the formation.

Figure 9 illustrates the formations that can cause lost circulation: [17]

- Formations that are unconsolidated or that have high permeability (gravel) (A).
- Formation with open channels (chalk layers hollowed by water) (B).
- Formations with natural fractures (chalk, shale) (C).
- Formations with fractures caused by drilling operations (axial load from drill string) (D).

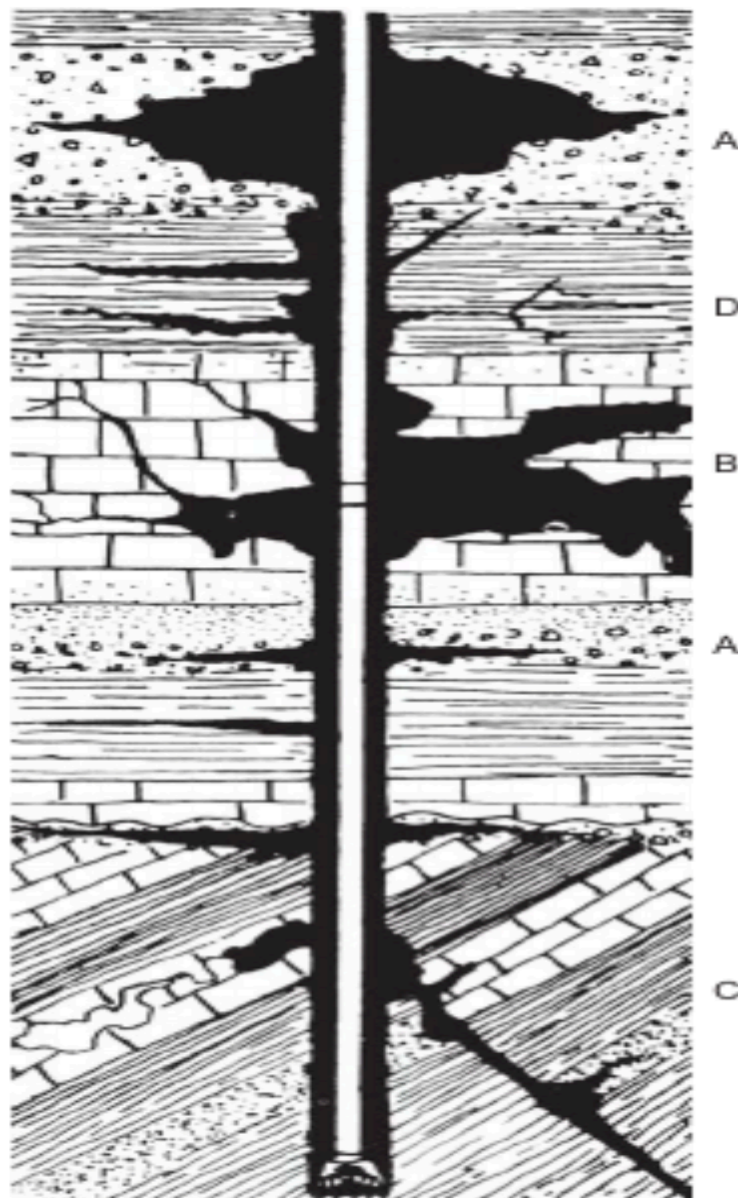


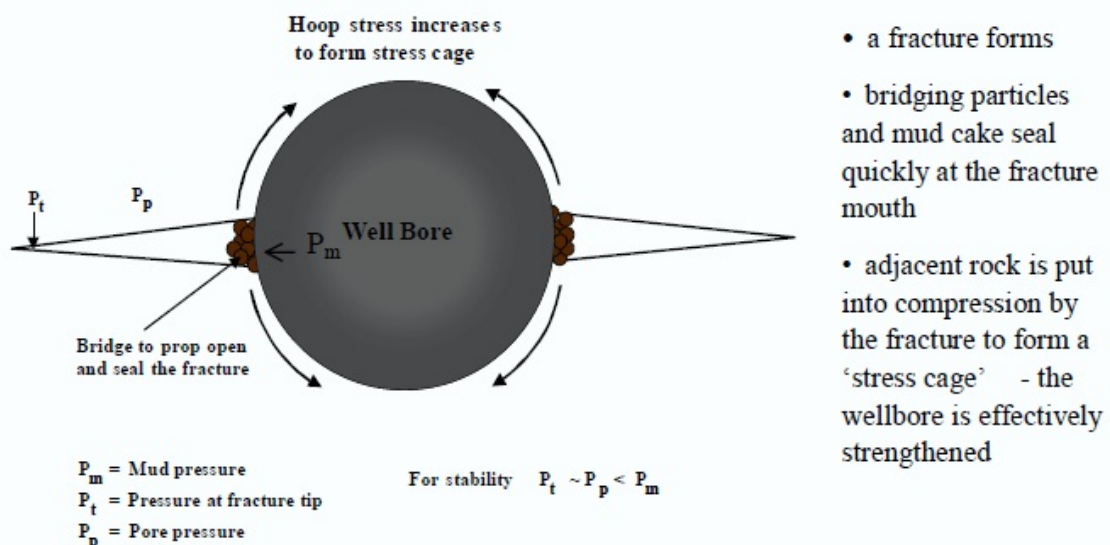
**Figure 9: Lost circulation formations [18]**

### 2.2.2 Effect of particle additives on mechanical strength and loss circulation control

As shown on Figure 9, drilling formations experiences lost circulation. In addition to operational costs, it is reported that the downtime associated with lost circulation accounts for a higher percentage as compared with other downtime causing problems.

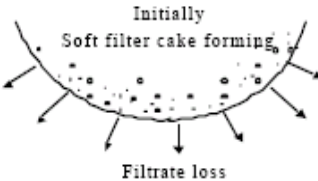
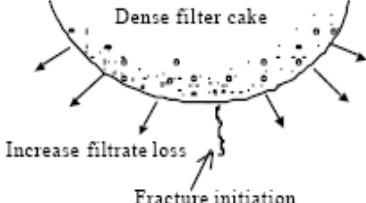
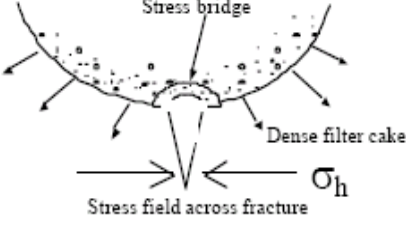
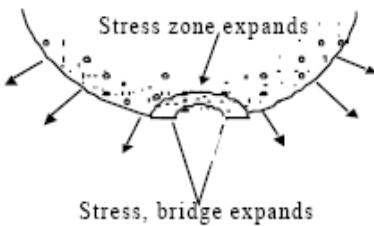

However, fluid loss control can be achieved by viscosity and the creation of an ultralow permeability filter cake. The filter cake must be tough, thin, and easily removable. In that way the cake will clog the pores and create a barrier to prevent further loss of mud. The viscosity of the filtrate plays an important role in order of minimizing the filter invasion depth. [6][8]

To reduce lost circulation, adding lost circulation materials (LCM) in drilling fluid is a common practice. As the fluid is treated with LCM, the particles screen out at the gate of the fracture and hinder mud loss. Solid deposits also increases the strength of the wellbore, and this is called the principle of stress cage theory. This is illustrated in Figure 10. The quality of bridging at the fracture depends on the quality of drilling fluid and the strength of LCM. [33]



**Figure 10: Stress cage concept to enhance wellbore strength [33]**

Figure 11 illustrates the process of filter cake formation and the main controlling parameters. [34] The particle deposited in mud cake creates a bridge during well fracture. As the well pressure increases and reaches to the collapse pressure, particles and drilling fluid flows into the fracture.

Event	Fig	Main controlling parameters
Filter cake formation		Filtrate loss
Fracture initiation		Filtrate loss, Stress
Fracture growth		Bridge stress Rock stress
Further fracture growth		Bridge/rock stress Particle strength
Filter cake collapse		Particle strength

**Figure 11: Description of the filtrate cake formation, fracture process and bridging mechanisms. [34]**

## 2.3 Drilling fluids and function and additives

The term drilling fluid, also known as drilling mud, comprises of several additives such as viscosifiers, salts, weight materials and fluid loss control materials.

### 2.3.1 Function of drilling fluids

Drilling fluids have many important functions, such as: [6][23][14]

- Balance formation pressure.
- Transport cuttings from bottom to surface.
- Filter loss control.
- Keep cuttings floating when circulation stops.
- Cooling and lubrication of drill bit.
- Stabilize well and protect the formation.
- Provide buoyancy to drill string and casings.
- Control corrosion.
- Secure maximal well information.

**Balance formation pressure:** To prevent gas or liquid from entering the well, the hydrostatic pressure of the mud must be larger than the pore pressure. The pore pressure depends on the pressure of the porous formation, the density of the formation fluid and geological conditions.

**Transport cutting from bottom to surface:** Removal of cuttings from the bottom of the well is important in order to keep up the drilling speed. During drilling, mud is pushed through nozzles in the drill bit. The mud cleans the hole by removing all the cuttings from the bottom of the hole, through the annulus and up to surface. Generally, higher viscosity fluids improve cutting transport.

**Keep cuttings floating when circulation stops:** During the time it takes drilling a well, the circulation has to stop for each new connection. Even

though it is not preferable having too much cuttings in the mud before the circulation stops, there will always be some cuttings left. Mud has properties that keep the cuttings floating when circulation stops. These properties are called thixotropic, meaning that the mud becomes gel when it's static, and becomes fluid again under pressure and movement.

**Filter loss control:** As mentioned in the introduction section, the hydrostatic pressure of the mud must be larger than the pore pressure to prevent inflow of gas and liquid from the formation. The purpose of the creation of a filter cake in the borehole is to get a thin, low permeable film that prevents the liquid phase in the mud to escape into the formation. Low filter losses alone are not necessarily indications of good filtrate control, as minimum filter losses are not equivalent with minimum filter cake thickness. Therefore, it is necessary to control the filter cake periodically when drilling.

**Cooling and lubrication of drill bit:** When the drill bit is pushed and scraped against the bottom of the hole, and when drill string and collars rotates against the hole wall, a severe amount of heat will occur. All this heat cannot be absorbed by the formation. Fortunately, mud has thermic capacity and conductivity, so it can absorb this heat and transport it to the surface. Mud has also a lubricating effect on the drill bit and decreases the friction between collars and casings.

**Stabilize well and protect the formation:** The mud has to be designed in such a way that it does not react with the formation, making it unstable. For instance water in the mud can react with clay in the formation, making it swell.

**Provide buoyancy to drill string and casings:** The weight of a drill string or a section of casings can be, measured in air, up to 200 tons. This kind of weight would give an enormous tension in the surface equipment. The natural buoyancy of the mud will give a relief in this tension.

**Control corrosion:** Mud must not have a corroding effect on drill string, casing nor drilling equipment. To avoid this, an alkaline mud can be used with pH below 9.5.

**Secure adequate well information:** Accurate formation evaluation is essential to ensure the success of the drilling operation. Besides its primary tasks, the drilling fluids also gather all the necessary geological and formation related evaluation data. This kind of information is obtained through analyses of cuttings, electrical logs, core samples and dissolved oil and gas.

### **2.3.2 Additives**

In this section, additives used to prepare experimental drilling fluids (chapter 4) will be presented.

#### **2.3.2.1 Bentonite**

Bentonite is a type of fine-grained clay with strong swelling properties that are added to water based mud for one or all of following purposes: [7]

- to increase hole-cleaning capability.
- to reduce water seepage or filtration into permeable formations.
- to form a thin, low-permeability filter cake.
- to promote hole stability in poorly cemented formations.
- to avoid or overcome loss of circulation.

#### **Particle association**

The behaviour of the clay particles in aqueous solution is important because it affects important mud properties such as viscosity, yield strength and filter loss. [17]

The following associations describe the colloidal dispersion of bentonite in water: **Deflocculated system, flocculated system, aggregated system and dispersed system.** Figure 12 illustrates this.



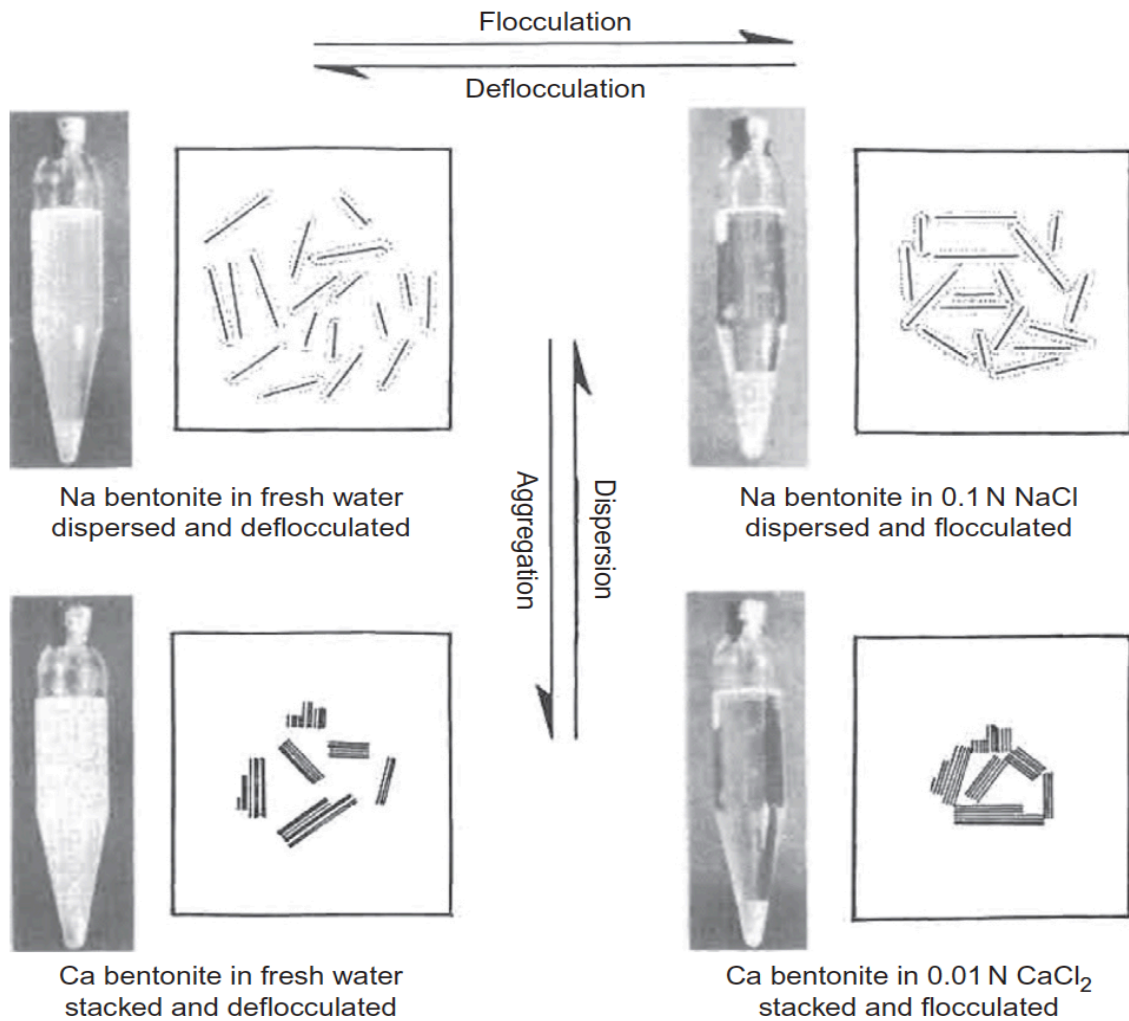


**Figure 12: Schematic representation of flocculation and deflocculating, dispersed and aggregation mechanisms [8]**

Primarily, the condition of the mud depends on the chemical/electrical interaction between the individual montmorillonite crystals. In turn, this interaction depends on the chemical condition of the solution, at which the crystals are added, such as pH and salt content (concentration and types of cations present) and the type of clay minerals in the solution. [6]

**Deflocculated system:** A solution with suspended particles can be described as “deflocculated” when only repulsive forces act between the individual particles. This can normally be achieved under conditions at which the particles have the same charge. [7] A complete de-flocculation is only achieved by adding chemicals such as lignosulfonate, which neutralizes

the negative charges on the surfaces resulting in net negative charges. This negative charge makes the crystals repel on each other. [6] Due to no electrical attraction between the clay particles in deflocculated mud, filter losses and yield limit will be low. [23]

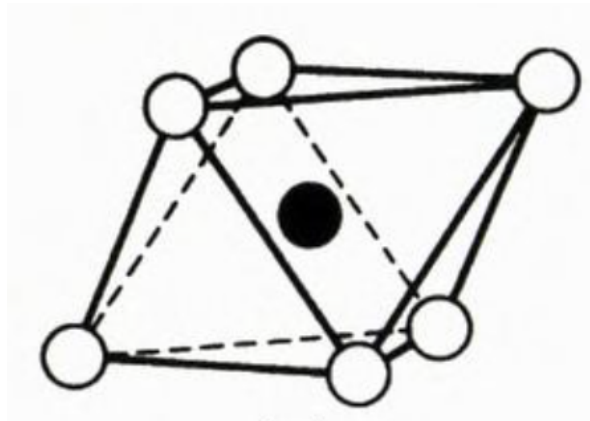
**Flocculated system:** A solution with suspended particles can be described as “flocculated” when there exist attracting forces between the particles. The particles bonds together either edge to edge or edge to surface. This occurs when the clay crystals have free positive charges on the fracture surface. The particles then form a loose three-dimensional network, that “locks” the water molecules inside, and thereby increases the viscosity [6][7][23] When mud containing bentonite flocculates, filter losses increases as well as a major increase in yield limit.

**Aggregated system:** A solution with suspended particles can be described as aggregated when individual particles bound together creating an aggregate. Generally, for clay systems the basic structure consists of sheets, while the crystal structure consists of sheets bonded together as in a deck of cards. For bentonite (montmorillonite) the sheets can be separated by mechanical impact or hydration. The flakes and stack of flakes can be deflocculated or flocculated. Generally, bentonite mud that is strongly flocculated will over time go into an aggregated state. By that, one will get fewer particles in the mud and the surface of each mud particle will be smaller. Typical characteristics of such a mud are that both the apparent viscosity and plastic viscosity will be low, and the filter loss will be high. [6][7][23]

**Dispersed system:** A solution with suspended particles can be described as dispersed when all the aggregates are completely broken down into individual sheets or small groups of crystals. When bentonite hydrates in freshwater, the clay particles will be in an almost dispersed state. A dispersed system can either be flocculated or deflocculated. A deflocculated and dispersed system indicates a favourable bentonite mud. [6][7]

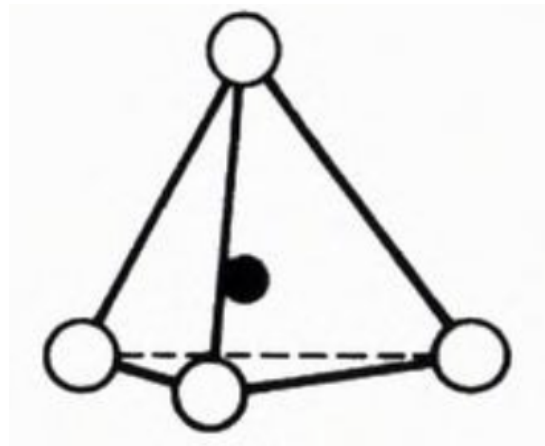
### **Montmorillonite**

Montmorillonite is the dominating mineral in bentonite. As illustrated in Figure 13, most minerals are built by two fundamental building blocks called the “octahedron sheet” and the “tetrahedral sheet”. The “octahedron sheet” consists of two layers with packed oxygen (O) or hydroxide (OH) with aluminium atoms. The aluminium atom is bonded to all the oxygen and hydroxide in an octahedron structure. It can be replaced by Iron (Fe) and magnesium (Mg).



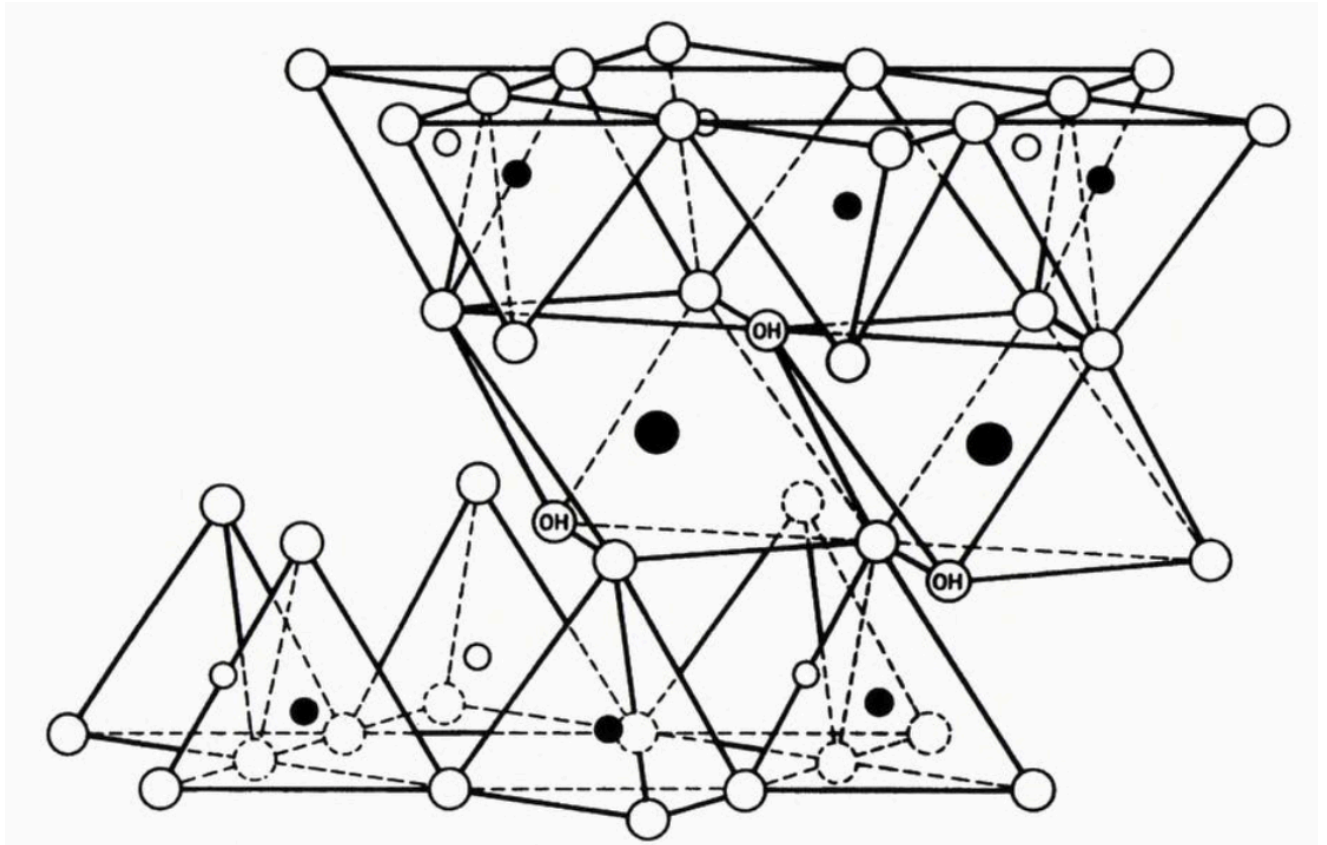
**Figure 13: Simple Octahedron structure. Oxygen and aluminum atoms [6]**

Figure 14 shows a simple tetrahedral structure. The “tetrahedral sheet” contains oxygen (O) or hydroxyl (-OH) and silicon (Si) formed as a tetrahedral structure, with oxygen or hydroxyl placed in the corners and the silicon atom in the middle.



**Figure 14: Simple tetrahedral structure. Oxygen and Silicon atoms. [6]**

As shown in Figure 15, the “octahedron sheet” and the “tetrahedral sheet” can bond chemically by sharing oxygen or hydroxyl, creating crystals. The montmorillonite mineral consists of two layers of “tetrahedral sheet” with one “octahedron sheet” in the middle.



**Figure 15: Tetrahedral sheet with octahedron sheet in the middle [6]**

#### 2.3.2.1.1 Swelling of montmorillonite

Figure 16 shows distribution of charges in a montmorillonite crystal. Montmorillonite has the special swelling and thixotropic properties that are associated with bentonite. When added to water, it can swell up to several times its original volume. This is due to chemical interactions in the montmorillonite crystal. An ideal montmorillonite crystal would be electrical neutral. In reality, this is not the case due to crystal faults, making them electrical and chemical active. Substitution of atoms will mainly take place in the “octahedron sheet”, where divalent Magnesium 2+ often replaces trivalent Aluminium 3+. The result is a source of negative charge on the “octahedron sheet” attracting positive charges cationes to the surface of the

crystal. The cations will have trouble getting in close contact to the negative charges due to their placement. The result is a net, weak and positive field that will attract polar molecules like water. The special swelling properties for montmorillonite are due to the water molecules splitting the weak bonding between the crystals, increasing inter layer space, which in turn generate a huge potential area for adsorption. [6][17][10]

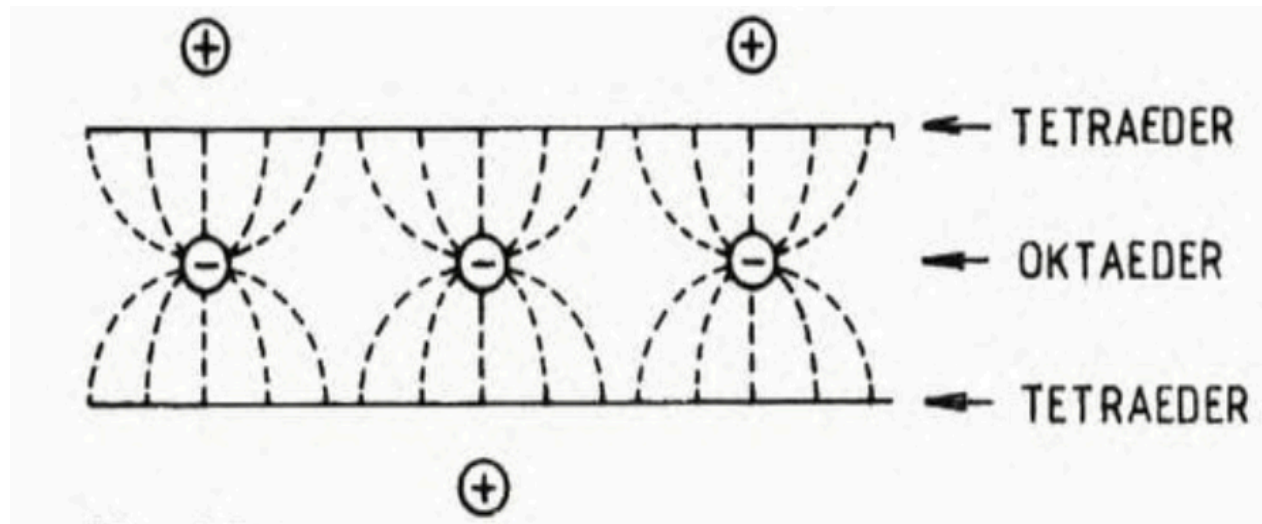


**Figure 16: Distribution of charges in a montmorillonite crystal [6]**

### 2.3.2.1.2 CEC- Cation Exchange capacity

Montmorillonite has a much higher cation exchange capacity than other minerals, meaning cations attracted to the surface of the montmorillonite have a high ability to substitute. The relative attraction potential is as follows: [7]



For example, at the same concentration, Ca<sup>++</sup> will have a greater attraction than Na<sup>+</sup>. It should be mentioned that the concentration of cations would affect the cation exchange capacity. A high concentration of Li<sup>+</sup> will for instance replace Ca<sup>2+</sup>.

A methylene blue test will give an estimate of how much montmorillonite or other clay that are present in the mud. The test will measure how much organic cation (methylene blue: colour) that is absorbed by the clay. [17]

### 2.3.2.2 Salts

During drilling, contact between water sensitive formation clay (e.g montmorillonite clay) and water based mud may induce clay hydration. The hydration of water may arise problems such as well instability problems and collapse. An adequate degree of shale stabilization can usually be achieved by cation exchange reactions, usually the replacement of Na<sup>+</sup> by K<sup>+</sup>. [8] The potassium ion (K<sup>+</sup>) size and low hydration energy makes it more effective compared to other inhibitive ions. It is small enough to enter the hole in the hexagonal structure in the “tetrahedral sheet” and bind the clay crystal surfaces closer together, and thereby prevent hydration. [17] As we can see from Figure 17, potassium chloride (KCl) is more effective in reducing swelling than other salts such as sodium chloride (NaCl) at the same concentration. [8]

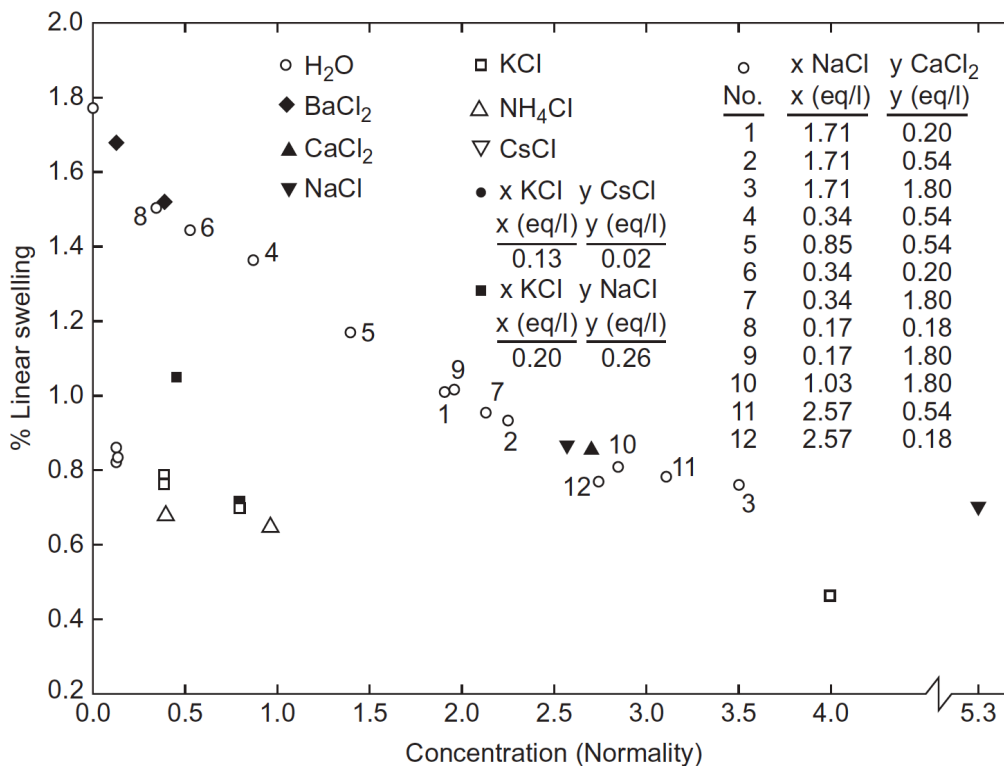


**Figure 17: Effect of cation concentration and species on linear swelling. Clay mineral analysis of shale: 9.2% montmorillonite, 11.2% mixed layer, 35% illinite, 5.5% chlorite, 4.4% kaolonite.**

### **2.3.2.4 Polymers**

Ever since 1937, polymers have been used in drilling technology as an additive in drilling mud. At that time, corn-starch was used as an additive to control fluid losses. Later, polymers have been developed more sophisticated to control fluid properties. Today they are practically a part of all water based mud system as they can be specially designed to fit a particular drilling situation. [9][7] Their application largely depends on parameters such as molecular weight (length) of the polymers and charges. Some are added primarily to provide higher viscosity and reduce filter losses. Others are added to inhibit clay and encapsulate cuttings. There are also combined effects, raising transitional forms. [7]

#### *2.3.2.4.1 Structure of polymers*

Basically, a polymer consists of small units called *monomers* that are chemically bonded together (polymerized) forming a chain. The chains can have few repeating units, or be long with many repeating units. The properties of the polymer are determined by the properties of the monomer, and how they are connected. As shown on Figure 18, the polymer structure can be divided into three main groups: [6]

- a) **Linear structure:** Can give polymers high or low viscosity depending on whether the chain is long or short. A linear structure gives low gel strength.
- b) **Branched structure:** An example of a branched structure is the Xanthan gum (XC) polymer. The XC polymer has good gel strength and high viscosity.
- c) **Cross-linked structure:** This structure is not that common for polymers related to mud. They are more common for polymers that can create hard, not fusible substances.

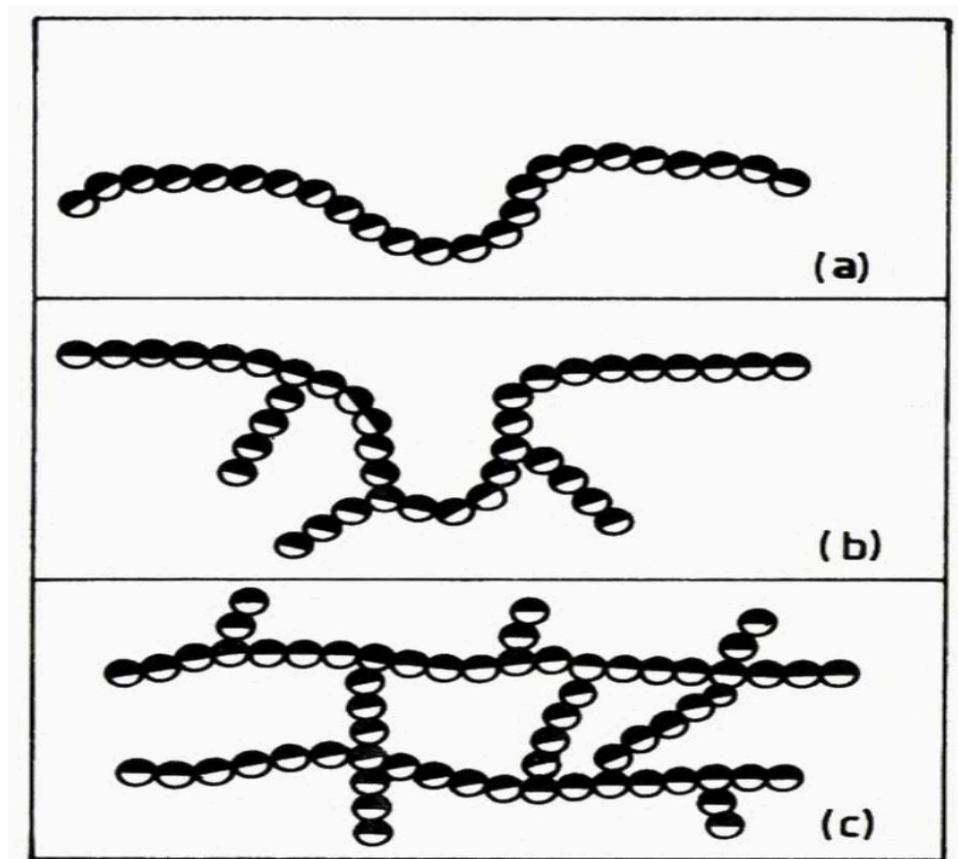


**Figure 18: Structure of polymers: a) linear b) branched c) cross linked [6]**

#### 2.3.2.4.2 Xanthan gum polymer

Xanthan gum (XC) is classified as a naturally occurring polymer and is often used in the oil industry for a number of reasons. It is water soluble and used to thicken water based drilling mud due to its viscous properties on e.g. brines (seawater).

As can be seen from Figure 19, Xanthan gum composes of a five-ring structure: A three-ring side chain with a two-ring backbone. Coupled to the side chain are different functional groups such as carbonyl and hydroxyl. This unique branching structure gives Xanthan gum thixotropic properties, that in simple terms means that the fluid will flow under normal conditions and thicken under dynamic conditions. When a certain amount of polymer is reached, the polymer branches will connect by hydrogen bondings. This is the original viscous state of the system. Since the hydrogen bondings are weak, they will break when shear is applied to the system. For practical purposes, high shear conditions would be when the fluid is pushed through



the nozzles in the drill bit. Under these conditions the fluid will act almost like water. Under low shear rate conditions, such as in the annulus, the hydrogen bondings will again connect, and viscosity goes back to initial state. [9]

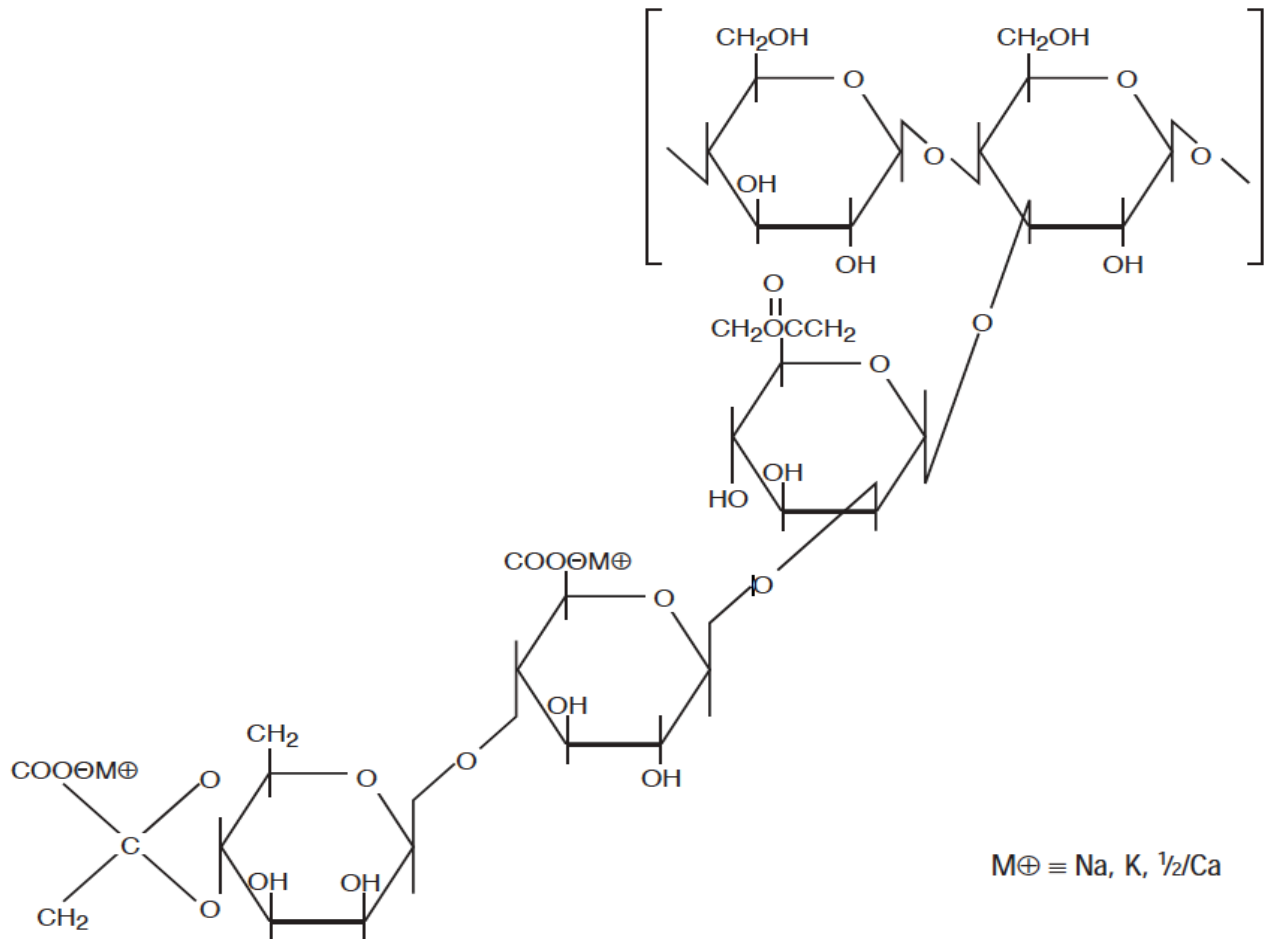


**Figure 19: Structure of Xanthan gum [8]**

## 2.4 Nano technology and applications

Nanoparticles are small solid particles with a size within a range of 1- 100 nm. As shown on Figure 20, nanoparticles are smaller and have a higher surface/volume ratio than micro particles. At low concentrations and additives, they also have the capability of performing superior fluid properties. [11]

The application of nanotechnology has shown proven results in several industries such as medical treatments and electronics. Research projects have shown that nanotechnology has the potential to solve or manage several problems in the petroleum industry, such as enhancing productivity and well integrity along with improving recovery.

Nanotechnology could create a lot of opportunities for research and development programs. Therefore, this thesis will look at the effect of nano-silica on water based mud system (chapter 4)

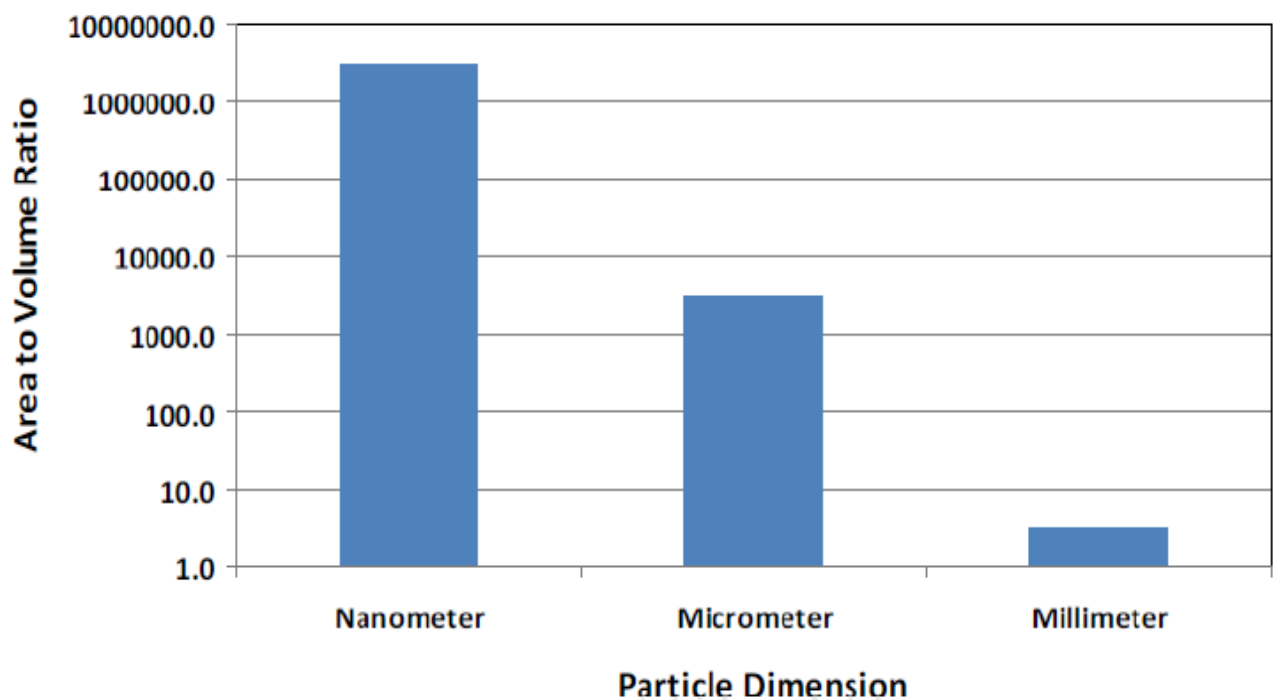
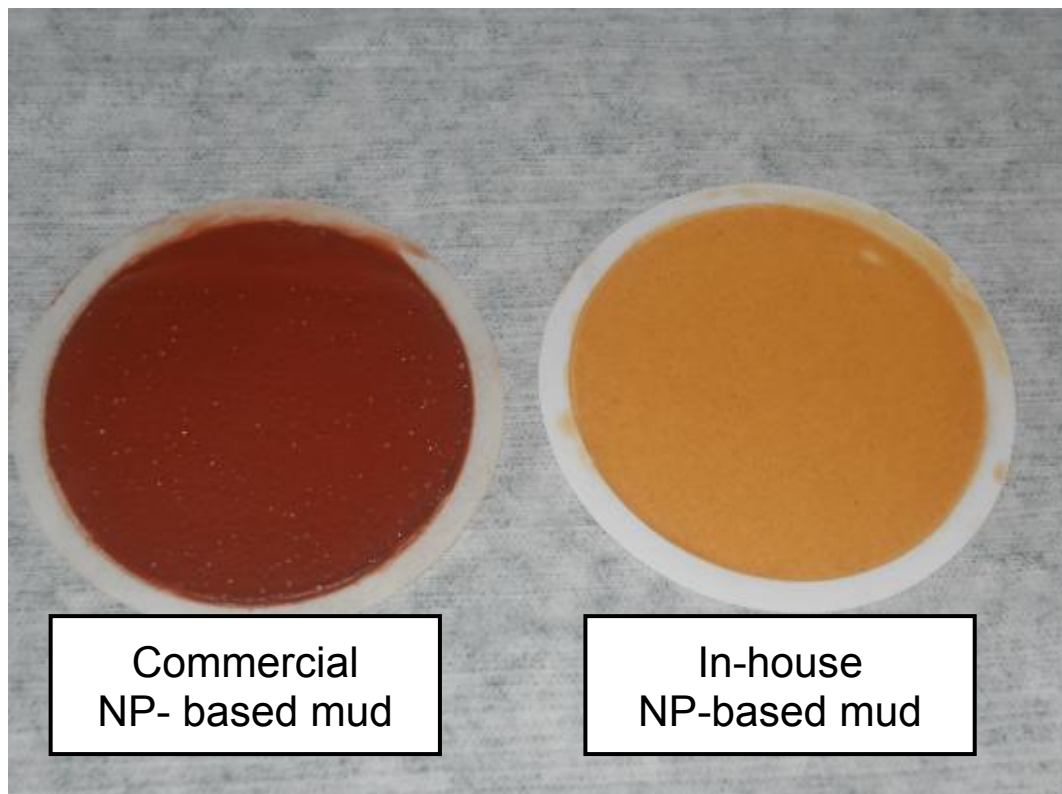


Figure 20: Surface area to volume ratio versus particle diameters [38]

### 2.4.1 Emulsion based nano solution on filtrate reducing

At the University of Calgary, Zakaria et al. (2012) [11] have formulated nano particles. The method of preparation is by micro-emulsion where the fluid system consists of 90% oil and 10% water.



**Figure 21: Mud cakes of commercial and in house nano particles [11]**

Both commercial and proprietary nano particles were used, for comparison. The filter loss was tested in the standard API 30 minutes filter loss test. Visual observations were used to determine the stability of the fluids with the nano particles. Figure 21 shows the picture of mud cakes obtained from commercial and in house nanoparticles. [11]

First, the commercial nano particles were mixed with the mud. This would work as bench marking. The effect on the filter loss was poor, as can be seen from **Table 1**. Small "fish eyes" occurred in the filter cake, and it was not possible to get it away, even with more mixing. The same test was conducted

with the proprietary nano particles. These showed significantly improved protection against filter loss. **Table 2.** There were also noticed that the filter cake that was created by stable and dispersed nano particles was relatively dense and had a greater flow resistance than the filter cake formed by commercial nano particles. The proprietary nano particles accumulated on the surface of the filter cake and acted as a “shut-off” valve.

The in-situ mixture of where the propriety nano particles were used, gave an improvement in filter loss of 80%. This shows potential with the right choice of nano particles, as it is clear that the nano particles can contribute to a significant reduction in filter losses and formation damage. [11]

Samples Types	NPs	Time (min)	LPLT Fluid Loss (mL)		Fluid Loss Reduction %
			DF	DF with commercial NPs	
90:10 (v/v) Oil: Water	Commercial NPs (20-40 nm)	7.5	1.7±0.6	1.7±0.6	0
		30	4.5±0.6	4.2±0.6	6.67

**Table 1: API LPLT Fluid loss of drilling samples using commercial nanoparticles [11]**

Samples Types	Time (min)	LPLT Fluid Loss (mL)			
		DF	DF with LCM	DF with In-house ex-situ NPs	DF with In-house in-situ NPs
90:10 (v/v) Oil: Water	7.5	2.0±0.2	1.4±0.2	0.15±0.1	-
	30	3.96±0.2	3.6±0.1	1.25±0.2	0.9±0.2

**Table 2: Comparative study of API LPLT fluid loss property of in-house prepared nanoparticle and drilling fluids [11]**

The use of improved NP-based invert emulsion drilling fluid showed an excellent fluid loss control, rheological properties together with a good lubricity profile.

### **2.4.2 Emulsion based nano solution on wellbore strengthening**

At the University of Calgary, Charles et al. (2013) [35] have formulated an emulsion-based nanoparticle, which is based on Iron III hydroxide and CaCO<sub>3</sub> nano particles. In order to test the sealing performance of the nano-fluid system, fracturing and re-fracturing experimental tests have been carried out.

The authors have treated (Iron III hydroxide NPs) with graphite in water based mud system. The fracturing test results show that the nano treated system increase the well strength by 70% compared to nano untreated fluid system. They have also tested another nano system, which is CaCO<sub>3</sub> based. The Calcium carbonate NPs and graphite system test result increased the fracture pressure by 36% over the unblended invert emulsion mud. [35]

### **2.4.3 Water based nano effect on permeability reduction**

At the University of Texas, Sharma et al. (2012) [36] have developed a new environmentally friendly nano particle. The authors have tested this nano particle in water-based drilling fluids. The main objective of the test was to evaluate the interaction of the nano system with shale. The test result shows that the fluid system reduces the filtrate by 10 to 100 times. This is an indication that the fluid system have a capacity of minimizing formation damage, shell swelling and hence wellbore instability. [36]

## 3 Theory

This chapter presents the theory used to analyse the experimental data measured in chapter 4.

### 3.1 Rheology

*Rheology* is the study of deformation and flow of all types of matter. [11] Prior to starting drilling, one should know the rheological properties of a drilling fluid, because of their ability to characterize the properties of the mud, such as: well cleansing, cuttings removal, erosion preservation, pump system and hydraulic calculation. [13] Hydraulic calculations such as the friction pressure drop are for instance important in order to drill within the “safe operational window”, as reviewed in the introduction section. Various flow models have been proposed to describe the behaviour of fluids, using the concepts of shear stress and shear rate. Most drilling fluids do not conform exactly to either of the models. [8] However, the models have accuracy sufficient for practical purposes.

#### 3.1.1 Reynolds number

This is dimensionless number, which is defined by the ratio of fluid’s inertia forces and its viscous forces. Reynolds numbers are used to characterize different flow regimes, such as laminar or turbulent flow. For laminar flow, Reynolds number is given as: [12]

$$R_e = \frac{\rho \cdot \bar{V} \cdot D}{\mu} \quad 3.1$$

Where:

- D = Hydraulic diameter of the pipe (m)
- $\bar{V}$  = Mean fluid velocity (m/s)
- $\mu$  = Dynamic viscosity of the fluid (Pa·s or N·s/m<sup>2</sup> or kg/m·s)
- $\rho$  = Density of the fluid (kg/m<sup>3</sup>)

### **3.1.2 Flow regimes**

As mentioned earlier, the flow patterns are distinguished based on the Reynolds number. The flow regimes are laminar, transitional or turbulent.

Laminar flow is generally associated with Reynolds number typically lower than 2000. This occurs at low fluid velocities and is typical for the annular regions of a wellbore. A uniform layer characterizes the fluid pattern, which is parallel to the flow direction.

The laminar flow described as telescopic flow, where the lower velocity is closer to the wall of the flow channel and higher velocity at the center. The flow profile is a parabolic.

Turbulent flow is characterized by higher Reynolds number, typically greater than 4000. This mainly occurs at high velocities and random/chaotic flow patterns of drilling fluid.

There exists also a flow pattern that is a transition period as the flow pattern changes from uniform to chaotic. This flow regime occurs when the Reynolds number is between 2000 and 4000.

### **3.1.3 Viscosities and gel strengths**

The parameters to be presented here will be used to characterize the drilling fluids to be formulated in chapter 4. [17]

#### **Plastic viscosity (PV):**

Plastic viscosity is a term used to describe mechanical friction between the particles in the mud, between the particles and the mud and between the liquid elements mutually. Plastic viscosity depends on the concentration of the particles, the size and shape of the fluid and viscosity of the fluid.

### **Yield point (YP)**

The yield point describes the part of flow resistance that arises due to attractive forces between the particles. These attractive forces are caused by electrical charges (forces). The yield limit will depend on shear rate. As the shear rate increases the yield limit will decrease. This property is called shear thinning.

### **Gel-strength (gel)**

Gel strength is related to the attractive forces between the particles in the mud, when the mud is at rest, and is measured as function of time. It expresses the thixotropic properties of the fluid, meaning that the shear stress is not fixed for a certain rate, but changes with shear time.

### **Apparent viscosity (AV) and Funnel viscosity (“marsh funnel”):**

Apparent viscosity is a measure of the fluids total viscosity. It is affected by gel strength, plastic viscosity and yield limit. Because of that, this is often used as a control parameter for the mud. To describe the causes of the changes, the other rheological parameters need to be determined.

## **3.2 Rheological models**

There exist several rheological models in the literature, which are relating shear stress with shear rate in laminar flow conditions. Using the measured rheological data and the models, one can determine the viscosity and gel strength of the fluid systems. These parameters are used to determine several important issues related to the performance of the drilling fluid, such as:

- Pressure loss through pipe, annulus and bit hydraulics, hence ECD.
- Swab and Surge pressures.
- Cutting transport efficiency.
- Bottom hole pressure.
- Well control.



Determination of the right rheological model to describe the behavior of the fluid system is vital. In this thesis, both Newtonian and non-Newtonian rheology models will be reviewed to analyze the formulated fluid systems. The non-Newtonian models are: Bingham Plastic, Power Law, Unified, Robertson & Stiff and Herschel-Bulkley. Figure 22 illustrates the different rheological models describing typical behaviour of each model.

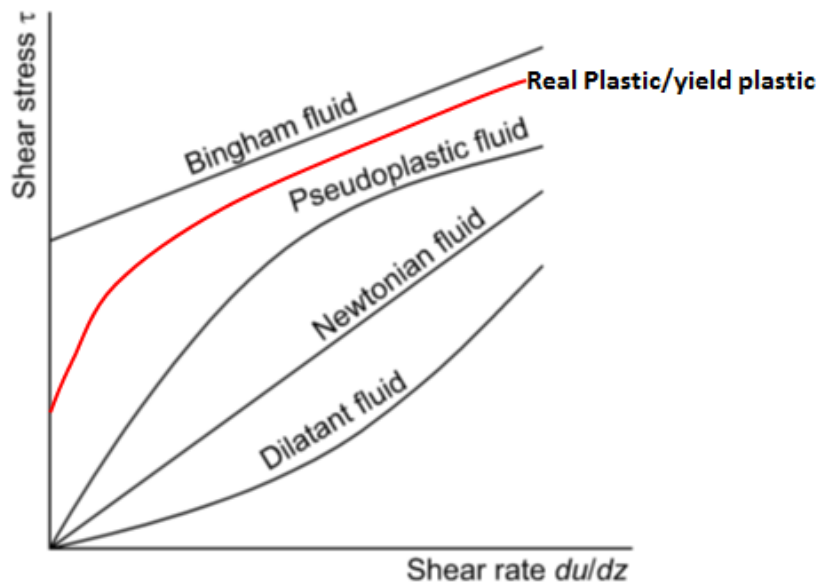


**Figure 22: Rheological models [12]**

### 3.2.1 Newtonian fluids

A fluid is characterized as Newtonian if it exhibits a constant viscosity for any shear rate at constant temperature and pressure. Examples of Newtonian fluids are gases, water and high-gravity oils. The Newtonian model states that the shear stress is directly proportional to the shear rate, where the constant of proportionality is the viscosity. [14]

$$\tau = \mu \gamma \quad 3.2$$

Where:

- $\mu$  = Viscosity
- $\gamma$  = Shear rate
- $\tau$  = Shear stress

The relationship between the shear rate and shear strain is shown as a linear line through origin, as shown on Figure 22.

### **3.2.2 Non Newtonian fluids**

Most drilling fluids are non – Newtonian, i.e. they don't obey the laws and equations that apply for Newtonian fluids. Their viscosity is too complex to be characterized by one single value.

#### **3.2.2.1 Bingham plastic**

Bingham plastic is a two-parameter model. As in a Newtonian fluid, the relationship between the shear strain and shear rate is illustrated by a straight line. The intercept of the Bingham yield point, is the shear stress that has to be overcome so that the fluid can start to flow.

Once the yield point has been exceeded, the changes in shear rate will be proportional to changes in shear stress forming the constant of proportionality, called the plastic viscosity. [14]

$$\tau = \mu_p \gamma + \tau_y \tag{3.3}$$

Where:

- $\tau_y$  = Yield point
- $\mu_p$  = Plastic viscosity

Yield point and plastic viscosity can either be read from a graph or measured using Fann viscometer and then calculated using the following equations.

$$\mu_p = PV = R_{600} - R_{300} \tag{3.4}$$

$$\tau_y = YS = R_{300} - PV \tag{3.5}$$

### 3.2.2.2 Power Law

Like Bingham, the Power law model requires two parameters to characterize the fluid. The model is given by the following equation: [14]

$$\tau = k\gamma^n \quad 3.6$$

Where:

- $k$  = Consistency index
- $n$  = Flow behaviour index.

The Power-law parameters can be estimated from following equations:

$$n = 3.32 \log\left(\frac{R_{600}}{R_{300}}\right) \quad 3.7$$

$$k = \frac{R_{300}}{511^n} = \frac{R_{600}}{1022^n} \quad 3.8$$

The Power-law model can represent more than one fluid, i.e when:

- $n < 1$  a pseudo plastic fluid
- $n = 1$  a Newtonian fluid
- $n > 1$  a dilatant fluid

### 3.2.2.3 Herschel-Buckley

Most drilling fluids are more likely to correspond to the Herschel Buckley model than the other reviewed models, since it is the most complete model currently in use. [7] It is also known as the yield pseudo plastic model and can be expressed as followed: [4]

$$\tau = \tau_0 + k\gamma^n \quad 3.9$$

Where:

- $\tau_0$  = Yield point
- $k$  = Consistency index
- $n$  = Flow behaviour index

The  $n$  and  $k$  values can be determined graphically.

$\tau_o$  can be determined as:

$$\tau_o = \frac{\tau^{*2} - \tau_{min}\tau_{max}}{2\tau^* - \tau_{min} - \tau_{max}} \quad 3.10$$

Where:

$\tau^*$  is the shear stress value corresponding to the geometric mean of the shear rate,  $\gamma^*$ , and can be determined as:

$$\gamma^* = \sqrt{\gamma_{min}\gamma_{max}} \quad 3.11$$

#### **3.2.2.4 Robertson-Stiff**

Robertson-Stiff is a model that can describe rheological behaviour for both drilling fluid and cement slurries. The basic mathematical equation is: [15]

$$\tau = A(\gamma + C)^B \quad 3.12$$

Where:

A, B and C represent model parameters and A and B corresponds to  $k$  and  $n$  in Power law model. C is considered a correction factor to the shear rate.

$$C = \frac{(\gamma_{min}\gamma_{max} - \gamma^{*2})}{2\gamma^* - \gamma_{min}\gamma_{max}} \quad 3.13$$

Where:

$\gamma^*$  is determined by interpolation of  $\tau = \sqrt{\tau_{min} * \tau_{max}}$

#### **3.2.2.5 Unified**

The Unified model is another simplified version of Herschel-Bulkley. The model uses lower shear yield point, instead of  $\tau_o$ , as presented in equation 3.9. The model reads: [15]

$$\tau = \tau_{yL} + k\gamma^n \quad 3.14$$

Where:

$$\tau_{yL} = (2R_3 - R_6) 1.066 \quad 3.15$$

### 3.3 Viscoelasticity

Viscoelastic fluids, such as drilling fluids, exhibit both elastic and viscous behaviour when they undergo deformation. Viscosity is a property that liquid exhibits, and elasticity is a property that a solid exhibits. When stress or strain is applied to the system, viscoelastic fluids display time dependent behaviour. When the viscous portion is deformed, it will dissipate energy as heat. The elastic portion of the drilling fluid will store energy when deformed and not dissipate energy. The elastic portion has a strong effect on the pressure drop and flow behaviour. The viscoelastic properties of drilling fluid are important in order to determine gel strength and structure, barite sag, solid suspension and hydraulic modelling. [25]

Two parameters that describe the viscoelastic behaviour of a fluid are the Storage Modulus ( $G'$ ) and the Loss Modulus ( $G''$ ). The Storage Modulus stores the energy when undergoing deformation, and describes the elastic behavior of the fluid. It is therefore also known as the elastic modulus. The Loss Modulus  $G''$ , also known as the viscous modulus, dissipates energy when undergoing deformation, and describes the viscous behavior of the fluid. Both parameters are measured in shear, and are described in the relationship of strain and stress.

#### 3.3.1 Fundamentals

Many phenomena related to fluid behaviour cannot be described by viscos properties alone. Although the viscous part is dominating in common operations, the gel structure shows viscoelastic response under infinitesimal deformation. [25]

To determine the viscoelastic response of the fluids one can use dynamic tests, called oscillatory tests. The basic principle is the fluid being exposed to periodic oscillations. Figure 23 describes it. The fluid is placed between to plates. One plate is stationary and the other is oscillatory. The oscillating plate causes shear to the fluid, by dynamic movement. [26]

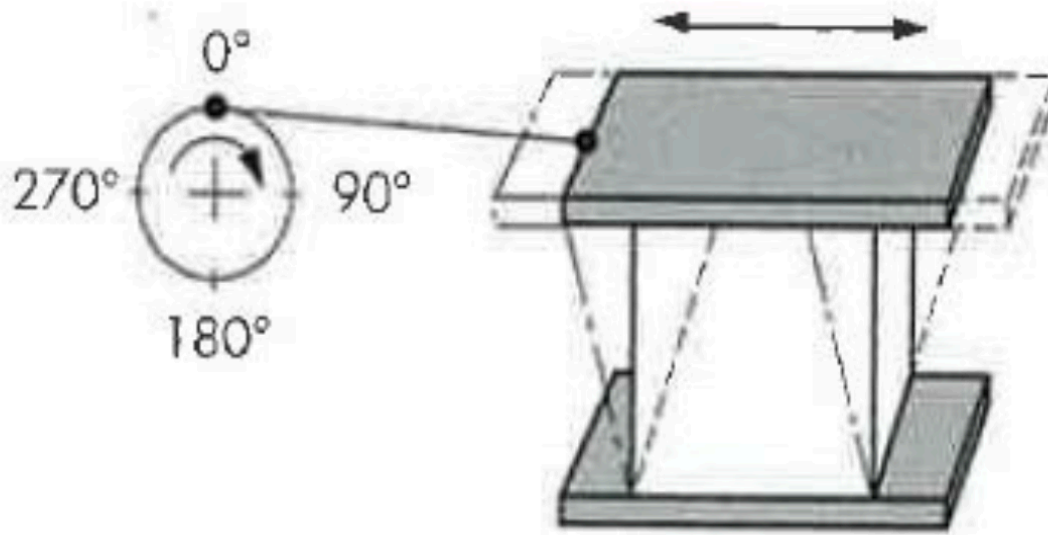


**Figure 23: Periodic oscillations illustrated by two plate model [26]**

The sample (fluid) is object to a sinusoidal force causing deformation and the resulting fluid response to stress is measured. The two following equations show the stress written in terms of strain. [25]

$$\tau(t) = \gamma_o \left[ \left( \frac{\tau_o}{\gamma_o} \cos \delta \right) \sin(\omega t) + \left( \frac{\tau_o}{\gamma_o} \sin \delta \right) \cos(\omega t) \right] \quad 3.16$$

$$\tau(t) = \gamma_o [G' \sin(\omega t) + G'' \cos(\omega t)] \quad 3.17$$

The Storage Modulus can be described as an in-phase component and measures the energy stored per cycle. The Loss Modulus can be described as an out of phase component, and measures the energy lost per cycle of sinusoidal deformation.

$$G' = \left( \frac{\tau_o}{\gamma_o} \cos \delta \right) \quad 3.18$$

$$G'' = \left( \frac{\tau_o}{\gamma_o} \sin \delta \right) \quad 3.19$$

The damping factor,  $\tan(\delta)$ , describes the ratio between the viscous and the elastic deformation.

$$\tan \delta = \frac{G''}{G'} \quad 3.20$$

The phase shift angle,  $(\delta)$ , is an expression for energy dissipated of the material. For a purely viscous fluid, the phase angle  $(\delta)$  is equal to  $90^\circ$ . For a purely elastic material, the phase angle is equal to  $0^\circ$ . For a viscoelastic material, the phase angle ranges between  $0^\circ$  and  $90^\circ$ . The phase angle is illustrated between response and deformation in Figure 24. [25]

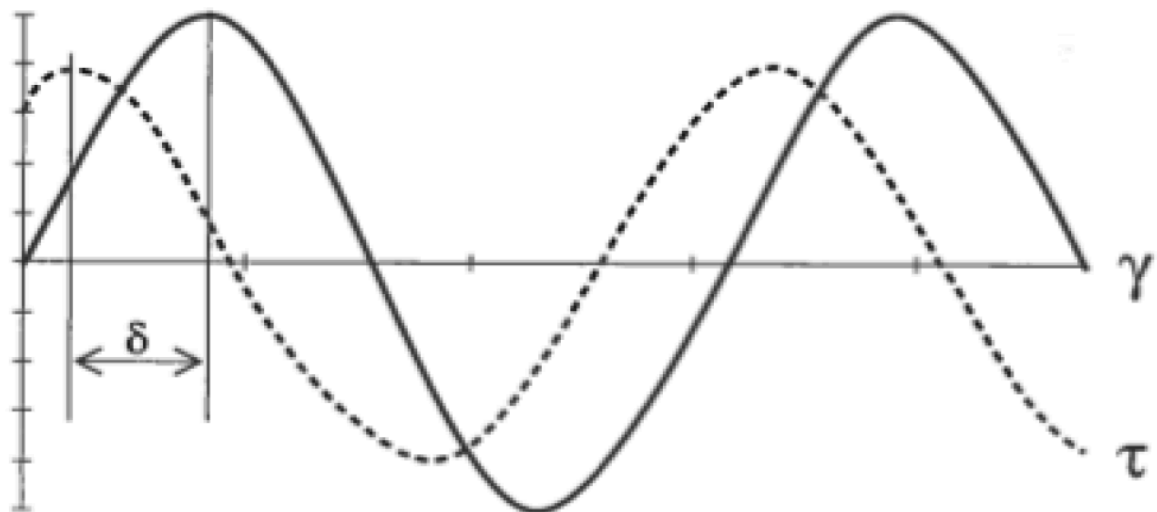


**Figure 24: Oscillatory test showing viscoelastic behaviour [26]**

### 3.3.2 Amplitude Sweep Test

Amplitude Sweep tests are tests done in oscillation, where the amplitude of oscillation is ramped while the frequency is held constant. This test is done to determine the Linear viscoelastic (LVE) range. At this range the Storage Modulus ( $G'$ ) and the Loss Modulus ( $G''$ ) are constant. By finding the LVE range one detect for which strains the sample remains intact and the structure remains unchanged. If  $G' > G''$  the fluid has characteristic as a solid or a gel. If  $G'' > G'$ , viscous behavior dominates the elastic part. In other words, the difference in value between the two parameters will tell whether the viscous or the elastic behavior dominates the other. The different behaviors can be seen in Figure 25.

From the curves one can determine the flow point of the fluid, where the fluid starts to flow. This point is found where the Storage Modulus is equal to the Loss Modulus. The yield point is found at the limit of the LVE range, where LVE plateau begins to deviate.

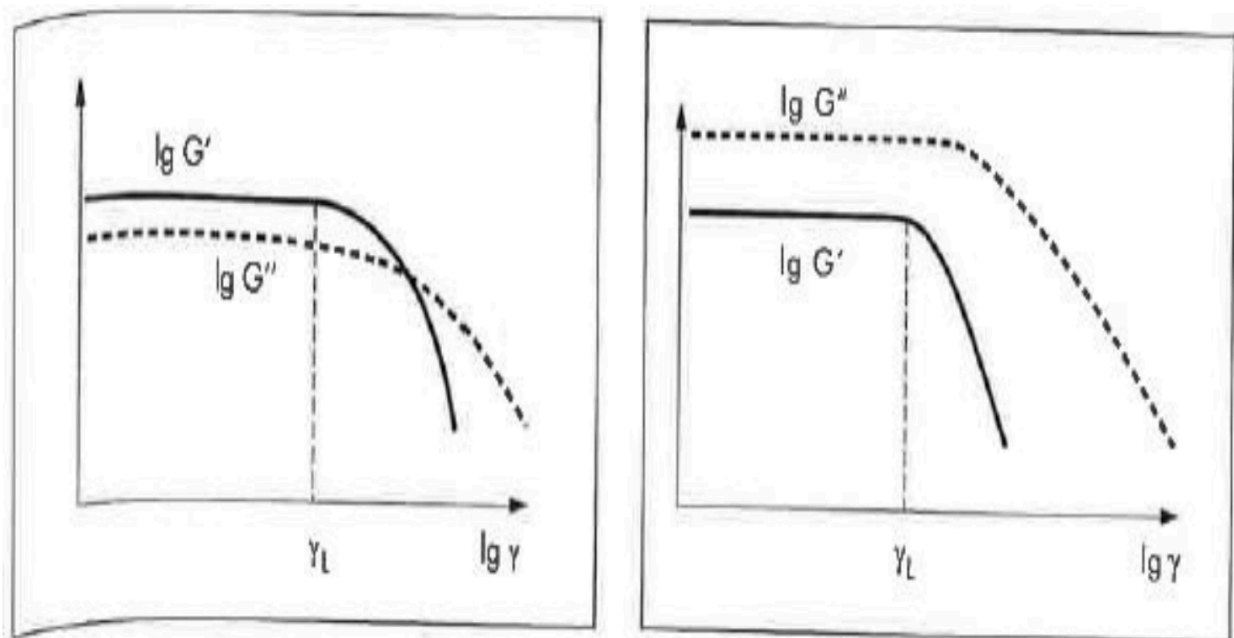


**Figure 25: Left figure: Illustrates a strain amplitude showing a gel-like character in the LVE range. Right figure: Illustrates a strain amplitude sweep of a sample showing the character of a viscoelastic liquid in the LVE range. [26]**



### 3.3.3 Frequency Sweep Test

Oscillatory tests performed with constant amplitude, while varying the frequency, are called Frequency sweep tests. This test is used to detect time-dependent deformation, as the frequency is the inverse value of time. Before conducting the frequency tests, one have to find the LVE range, as the tests are only valid within this area.

High frequency corresponds to fast deformation and low frequency corresponds to slow deformation. To evaluate if the response of the sample to deformation is a viscous or elastic response, the frequency sweep data can be used. If the Storage Modulus ( $G'$ ) is higher than Loss Modulus ( $G''$ ), the samples response to deformation is dominated by elastic behavior. Conversely, if the Storage Modulus is smaller than the Loss Modulus, the sample behaves more viscously. [25]

### 3.4 Hydraulics

Dynamic pressure loss occurs during circulation of the drilling fluid caused by nozzle pressure drop and friction pressure drop in pipe, annulus and at surface equipment. Figure 26 illustrates how the flow behaviour shows higher fluid resistance at wall.

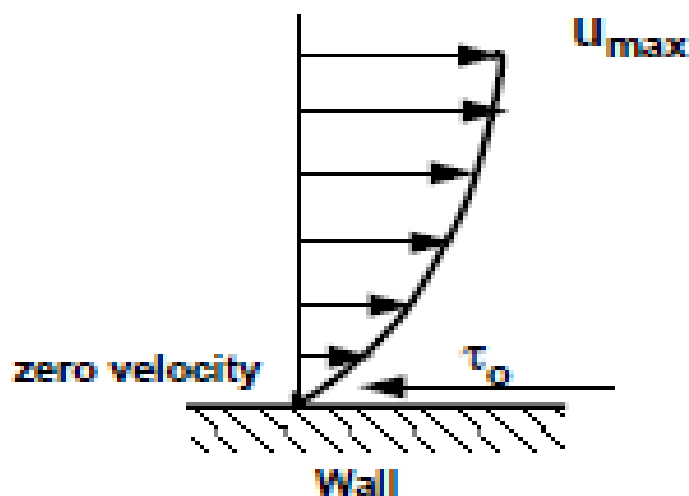


Figure 26: Pressure drop [12]

### 3.4.1 Friction pressure drop

During circulation of drilling fluid energy will be lost due to friction between the drilling fluid and the wall of the drill pipe and the annulus. The loss is dependent of several factors such as: rheology of the fluid, wellbore geometry, volume of the flow, properties of the fluid (viscosity and density), flow rate and geometry of the drill string. [15] The energy lost due to friction (and nozzle pressure drop) has to be compensated by the mud pump. [16] These are important parameters to calculate and add in the planning of a drill program. As illustrated on Figure 27, the friction pressure drop that the mud pump has to deliver is the sum of the following friction pressure losses: [15]

- Inside the drill string,  $\Delta P_{ds}$ .
- In the annulus around the drill string,  $\Delta P_a$ .
- In the surface equipment such as kelly, swivel, standpipe.  $\Delta P_s$ .
- Across the bit,  $\Delta P_b$ .

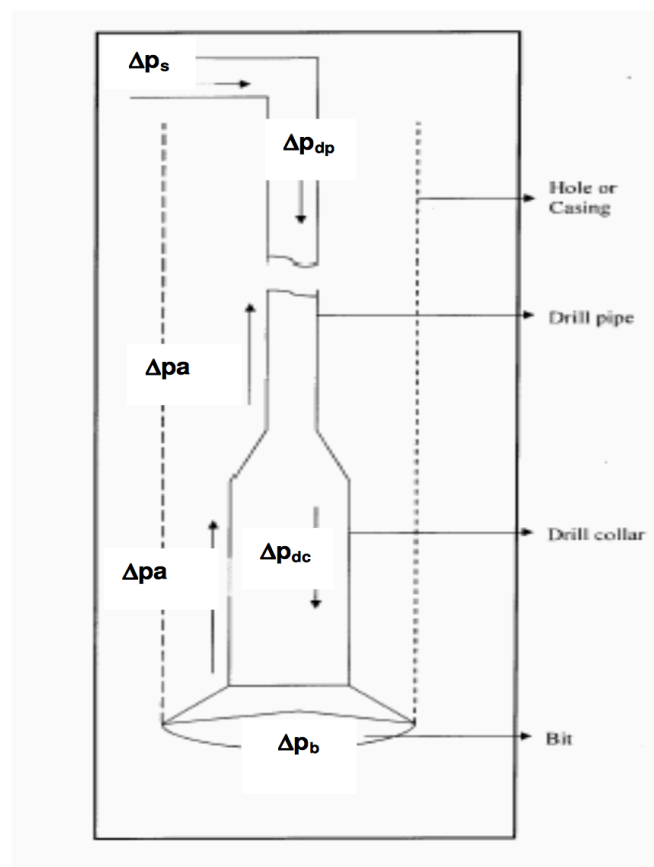


Figure 27: Drilling Fluid Circulation System [15]

The sum of the friction pressure losses can be expressed as given:

$$\Delta P_{\text{pump}} = \Delta P_s + \Delta P_{\text{ds}} + \Delta P_b + \Delta P_a \quad 3.21$$

The frictional pressure losses in the annulus,  $\Delta P_a$ , are used to calculate the ECD, as reviewed in the introduction section. In this thesis, in order to evaluate how the selected drilling fluid affects the ECD, the Unified model was selected. The model is summarized in Appendix E, which shows pressure losses in pipe, annulus and at bit.

### **3.5 Cutting transport**

It is essential to determine the carrying capacity of drilling fluids. Cutting transport is a critical issue for the drilling engineers. In literature, several correlations have also been proposed for determining particle slip velocity.

Insufficient hole cleaning can cause drilling problems such as mechanical pipe sticking, channelling problems and high torque and drag, if not handled [21][22]. Deviated wells may be particularly challenging because of reduction in lifting capacity of the mud. The reduction in lifting capacity happens due to the mud having a tendency to accumulate at the wall of the low side of the annulus instead of being circulated out. This accumulation of mud may induce the formation of cutting beds. [22]

Other factors that are known to affect hole cleaning, besides inclination, are: Drill pipe rotation, rate of penetration (ROP), mud rheology and density, cutting size and flow rate.

By increasing the flow rate, for instance, one may have a positive effect on hole cleaning. Increasing the flow rate will cause an increase in frictional pressure loss, which includes an increase in ECD. [21] [12] As reviewed in section § 1.1, the ECD should be kept within the safe operation window. Too high flow rate may cause fracturing. To avoid this issue, a compromise between cutting transport and well stability should always exist, so that an appropriate flow rate can be found. [12]

Cutting transport is a function of annular/pipe and cutting settling velocity.

- The annular / pipe velocity are a function of:
  - Pump rate (Q)
  - Annular geometry (D<sub>1</sub>, D<sub>2</sub>)
- Cutting settling velocity depends on:
  - Mud properties (rheology – viscosity and density)
  - Cutting parameters (diameter and shape)

Figure 28 illustrates forces acting on a single particle in an inclined well. The forces are hydrodynamic forces caused by fluid flow, lifting, drag, gravitational and sticking forces, which are caused by drilling fluid. These are the main cutting transport governing forces. Details are beyond the scope of this thesis.

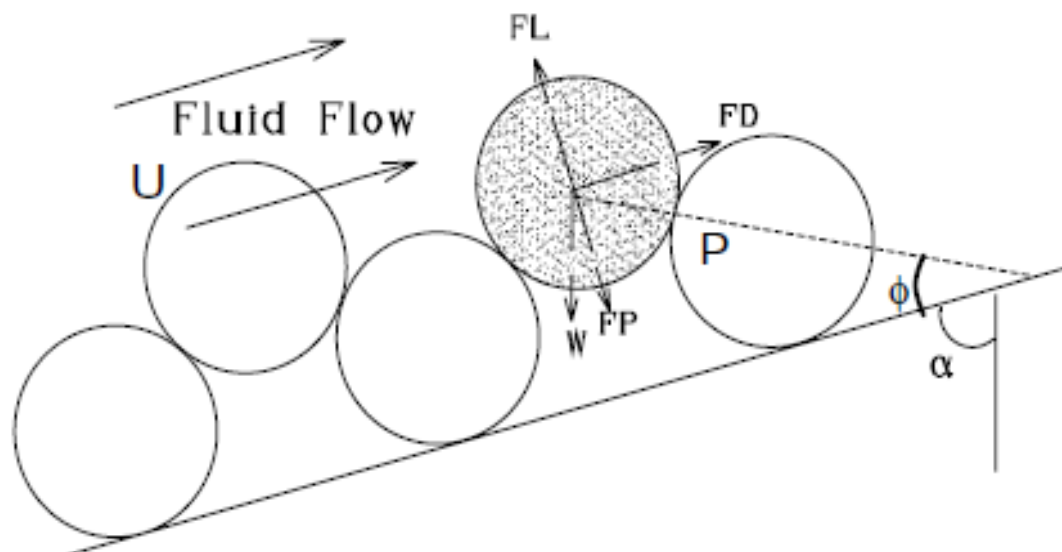


**Figure 28: Forces acting on a single particle at an active erosion site of a cutting bed [37]**

Using force balance, one can derive the settling velocity as:

$$v_s = \left( \frac{4 \cdot g d_p (\rho_p - \rho_f)}{\rho_f \cdot C_D} \right)^{0.5} \quad 3.22$$

$C_D$  is particle drag coefficient, which is a function of a particle Reynolds number. This is also a function of cutting and fluid parameters.

In this thesis, Wellplan<sup>TM</sup>/Landmark module was used to simulate the cutting transport carrying capacity of the best nano-treated fluid system. The model is given in Appendix G. As shown, the model is a function of fluid behavior.

## 4 Experimental work

This chapter presents drilling fluid formulations and measurements (rheology, density & pH). The drilling fluid additives have been reviewed in chapter 3. Basically the drilling fluid is formulated from 500g H<sub>2</sub>O mixed with 25g bentonite. The additives are Xanthan gum (XC) polymer, salts (KCl & NaCl) and nano silica.

### 4.1 Drilling fluid formulation and testing

#### 4.1.1 Equipment used for experiment

##### 4.1.1.1 Cup and Bob viscometer (Fann VG 35)

Fann VG 35 viscometer is used to measure the rheology of the fluid systems. The viscometer consists of an outer cylinder that rotates around a stationary inner bob. Figure 29 illustrates a schematic of the viscometer and heating (thermo) cup in which fluid is filled during testing. The heating cup is regulated to desired temperature. The rheometer works as follows: A part of the rheometer is lowered into a container with mud, such that the space between outer and inner cylinder is filled with mud. The inner cylinder is suspended from a torsion spring. When the outer cylinder rotates, the fluid layer closest to it will rotate with equal speed. The fluid layers further away, closer to the inner cylinder will rotate slower and slower. The fluid layer closest to the inner cylinder will transmit torque to it. The torsion spring will work as a counterforce, but when it is overcome, the inner cylinder will turn. The impact is an expression of the fluid shear stress and is measured in degrees  $\theta$  impact. [17][6]. Eight Fann viscometer dial readings were measured for varying rates of shear at 600, 300, 200, 100, 60, 30, 6 and 3 rev/min. Prior to the rheometer measurements, the fluids were mixed with Hamilton Beach mixer for two minutes to achieve homogeneity. Some of the sample fluids were also heated up using Tufel heating cup before placed in the rheometer. This was done to study thermal effects on the fluid.

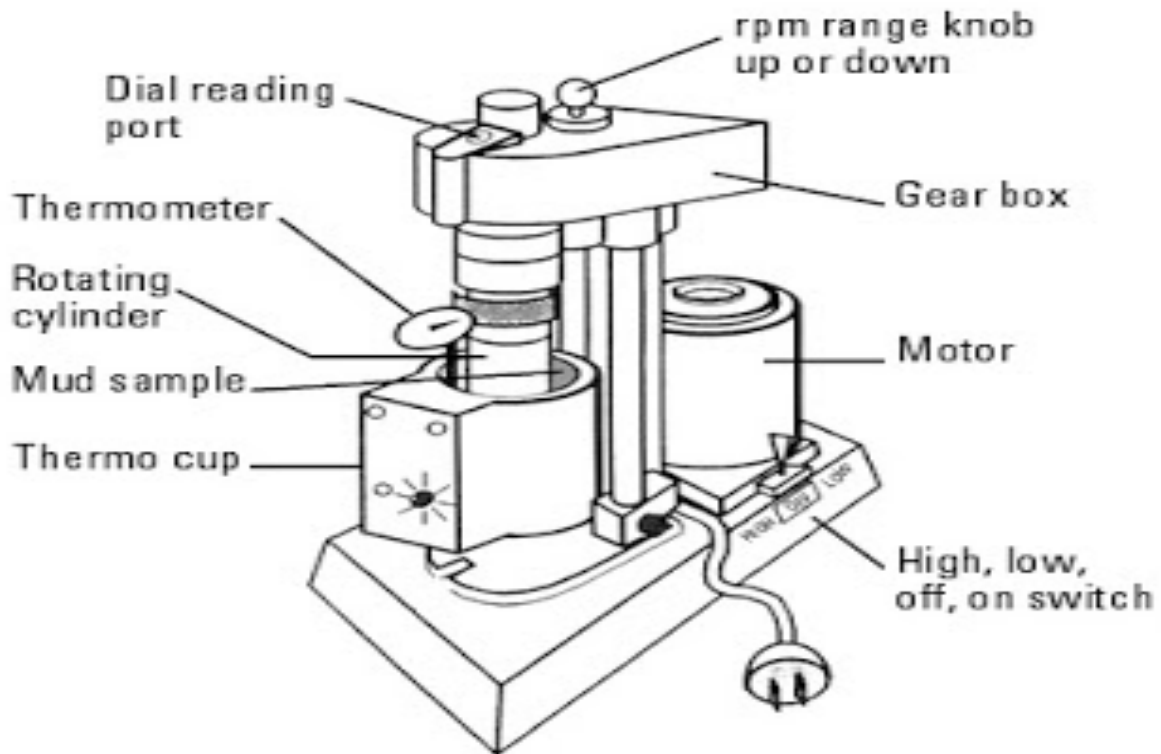


**Figure 29: Parts of Fann VG 35 viscometer [27]**

#### **4.1.1.2 API filter**

Figure 30 is a picture of API filter test. API filter measurements provide important information from the filter cake properties such as strength, smoothness and thickness, as well as filter losses. These parameters form the basis in how to optimize the filter properties of the mud. [17] The API instrument simulates how the drilling fluid is being pushed through the formation under pressure, by using filter paper. The tests were performed at room temperature and operation pressure of 100 psi. The filter loss volumes were reported after 7.5 minutes.

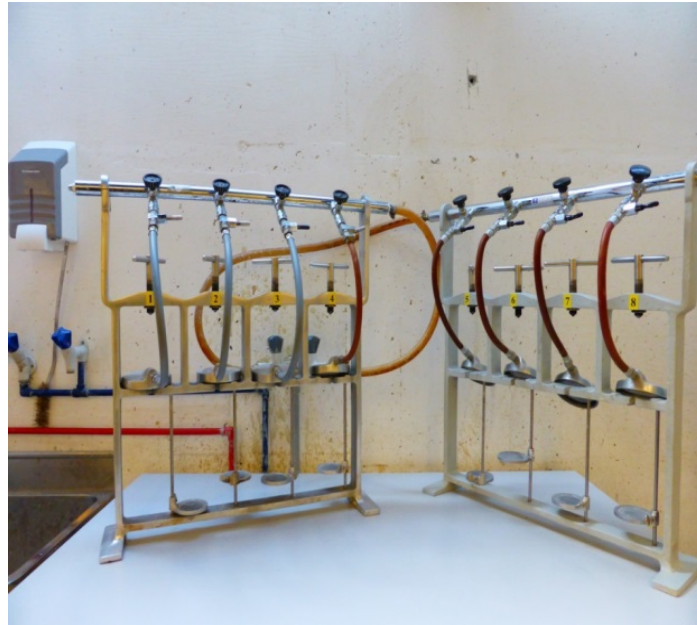


**Figure 30: Photograph picture of API filter test**

#### **4.1.1.3 Density**

The density measurements were conducted by using Baroid mud weight as can be seen in Figure 31. During the test, the measuring cup is first filled with mud and adjusted so that the mud is balanced at a certain weight. As the volume of the measuring cup is known, it is possible to read the density directly of the mud weight. To control the mud weight, one can calibrate it to water that should have a specific gravity (s.g) of 1.0. This is a straightforward test, but one of the deficiencies is the occurrence of gas and air bubbles in the mud, that will give inaccuracies in the measurements. [17]



**Figure 31: Photograph picture of density measuring equipment**



#### 4.1.2 Description of Nano silica (SiO<sub>2</sub>)

The nano-silica particles (15nm) that are used in this thesis were supplied from EPRUI Nanoparticles and Microspheres Co. Ltd, China. [19] There were done analyses of the particles in-house at the University of Stavanger, due to lack of specifications from the distributor. The analysis composed of Scanning Electron Microscopy (SEM) for imaging and Elemental Dispersive Spectroscopy (EDS) to characterize the particle for elemental identification. The results are given in Figure 32. The figure shows the content of the nano-silica particle: Silicon (Si), Oxygen (O) and some Carbon (C). The Palladium (Pd) is not a part of the particle, it is only a coating before the analysis was done. Figure 33 shows the SEM image.

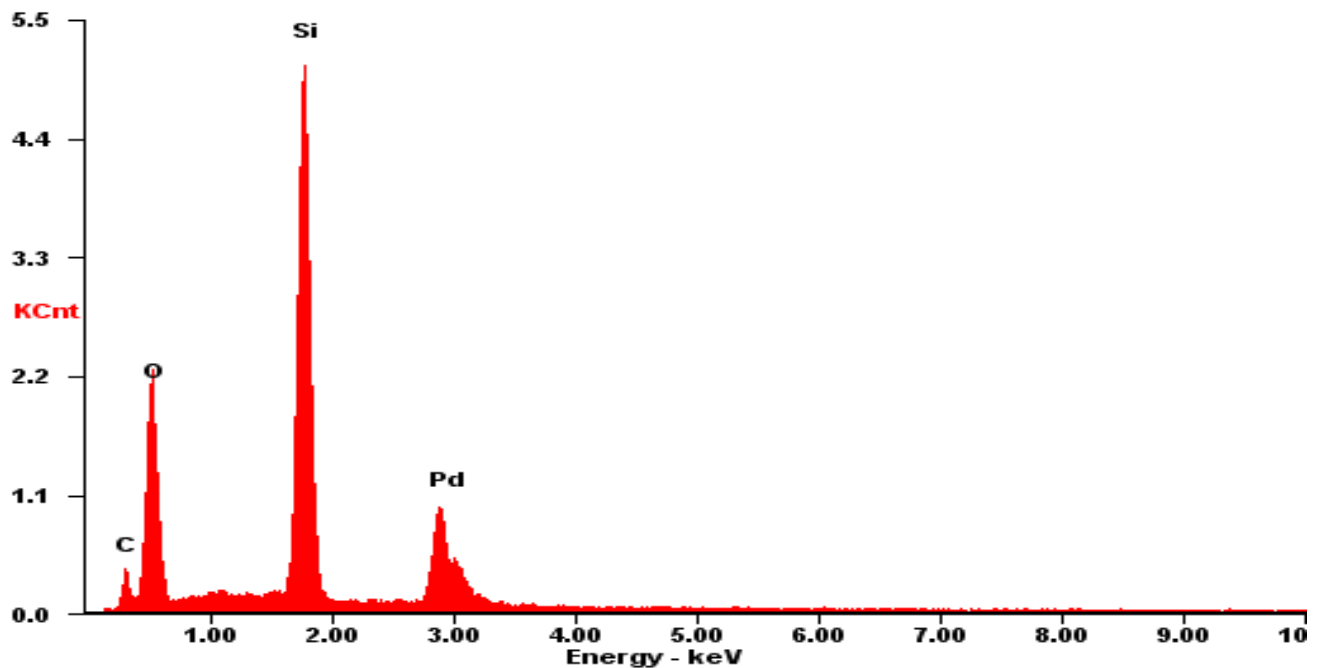
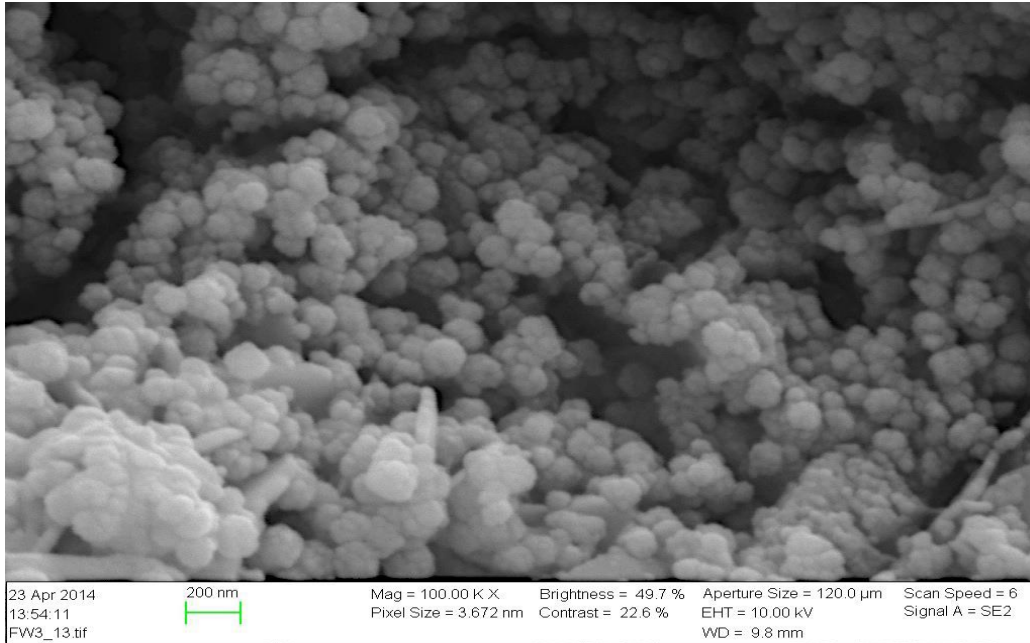


Figure 32: Element analysis of Nano- Silica



**Figure 33: SEM picture of Nano- Silica**

#### **4.1.3 Effect of XC concentration-Screening test**

The objective of this test was to screen out the right concentration of XC, which provides reasonable rheology properties and better filtrate loss. Based on the selected XC concentration, the rest of the experimental studies will be carried out.

##### **4.1.3.1 Description of fluid systems**

A screening test was conducted to look at the effect of the various concentrations of the polymer Xanthan in 500g H<sub>2</sub>O and 25g bentonite. From this study, a Xanthan concentration, which provides reasonable viscosities, will be selected and will be used for the rest of experimental analysis. The selection is based on visual inspection. As shown in Table 3, a total of five fluid systems were considered for screening test. Xanthan polymer free fluid system, which is mixture of 500g H<sub>2</sub>O and 25g bentonite, is used as control system. This will be referred to as “REF mud“. The formulated fluid systems were characterized in terms of their rheology, pH, density and filter loss properties. In addition, the temperature effects on the rheological properties of these fluid systems were studied at three different

temperatures (72 °F, 120 °F, 150 °F). The measured rheology data is shown in Appendix A.

As we can see from the table, the fluid samples were prepared by keeping the amount of water and bentonite constant, and vary the amount of polymer Xanthan. For samples #2 to #5, the amounts of Xanthan gum added were 0.5, 0.75, 1.0 and 1.5g, respectively. First, the specified polymer was added step-by-step to 500 gram of water, and mixed using Hamilton Beach mixer in 5 minutes. Xanthan gum was, deliberately, carefully added to the water to avoid lumping of the polymer. At last, bentonite was added, step-by-step, into the mixture of water and polymer and mixed properly using the Hamilton Beach mixer. Prior to rheology measurements, the mixture was set for 3 days, allowing the bentonite to swell.

Sample	Water (ml)	Bentonite (gram)	Polymer Xanthan (gram)
<b>1 (REF)</b>	<b>500</b>	<b>25</b>	<b>0,00</b>
<b>2</b>	500	25	0,50
<b>3</b>	500	25	0,75
<b>4</b>	500	25	1,00
<b>5</b>	500	25	1,50

**Table 3: Fluid sample composition of screening test**

#### **4.1.3.2 Test result and analysis**

As reviewed in section §3.2, rheological behavior is essential to determine the properties of drilling fluid. These properties are directly proportional to the chemical composition of the fluid systems. When the dynamics of the mud is analyzed it can be easier to select a proper mud for a certain well. Figure 34 shows the rheological measurements of the screening test at 72°F.

As we can see from the figure, for the same shear rate, the shear stress is increasing with the increasing amount of Xanthan. Comparing the reference system sample #1 (REF) with sample #5 at 600 RPM, 1.5g XC additive increases the shear stress by 188.89%. Similarly, comparing sample #1

(REF) with sample #2, the addition of 0.5g XC increases the shear stress by 77.78%.

Table 4 lists the computed viscosity and yield strength parameters from the screening tests at 72°F as well as physical parameters such as filter loss, pH and density.

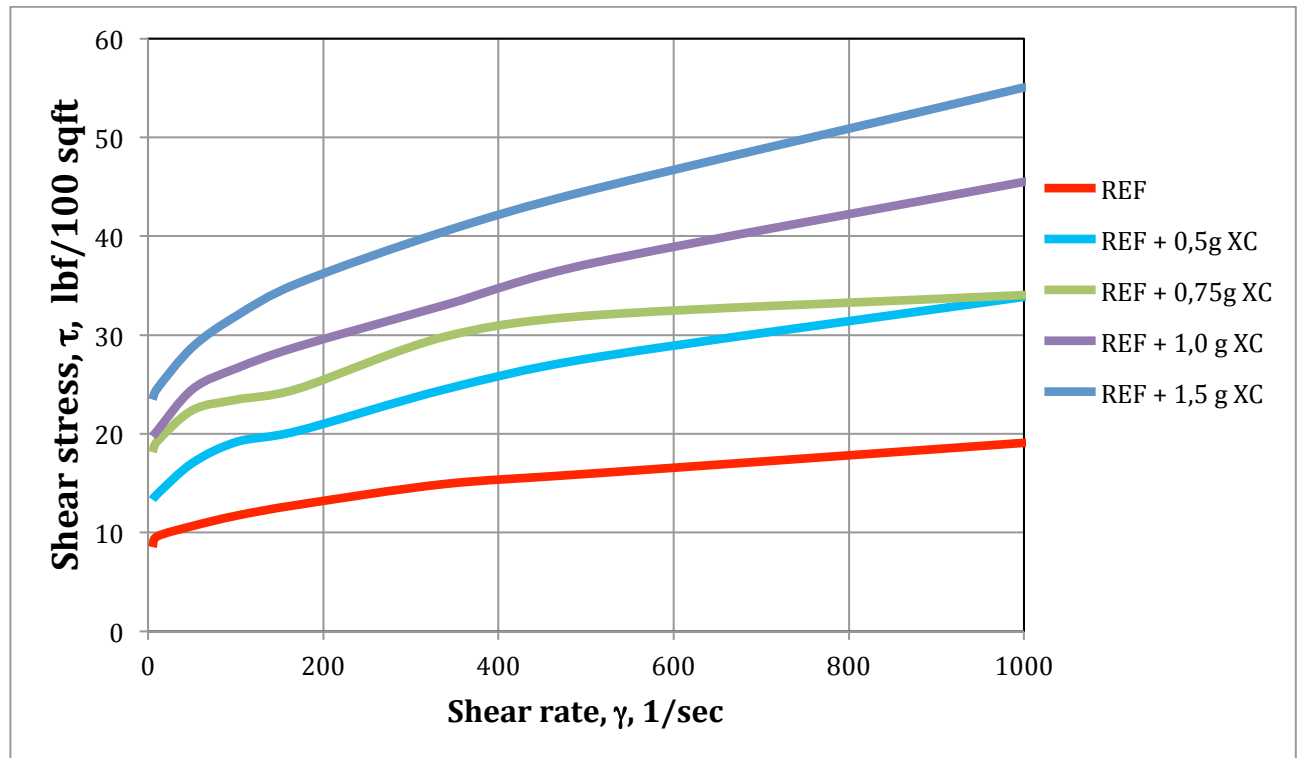


**Figure 34: Rheology measurements for screening test at 72°F**

The Fann data was put into the Bingham model to directly determine AV (apparent viscosity), YS (yield strength) and PV (plastic viscosity). Using the Power law model, “n” values (flow behaviour index) and “k” (consistency index) was calculated. The physical parameters were directly measured in the laboratory.

Parameters	Mudsystems				
	REF	REF + 0,5g XC	REF+ 0,75g XC	REF+ 1,0g XC	REF+ 1,5g XC
<b>Bingham</b>					
AV [cP]	9,00	16,00	2,00	8,00	10,00
PV [cP]	3,00	6,00	16,00	21,50	26,00
YS [lbf/100sqft]	12,00	20,00	28,00	27,00	32,00
<b>Power Law</b>					
n	0,26	0,30	0,09	0,30	0,31
k [lbf <sup>n</sup> /100sqft]	2,91	4,02	16,79	5,50	6,15
<b>Physical parameters</b>					
Filter Loss 7.5min [ml]	7,50	5,75	5,25	5,00	4,50
PH	10,10	9,95	9,95	10,00	9,80
Density [SG]	1,03	1,02	1,02	1,02	1,02

**Table 4: Extracted parameters from screening test performed at 72 °F**

As expected, we see from Table 4 that the filter losses decrease with increasing amount of Xanthan. There are no significant deviations in density measurement, since no weighing agents were added to the fluid systems. The pH is stable around the value of 10.

#### 4.1.3.2.1 Effect of temperature

The variation of consistency index (k), flow behavior index (n), YS, PV and AV as a function of concentration of Xanthan is visualized by the use of the Figures 35-39. As some of the calculations shows major deviations from an either declining or increasing trend at temperature of 72°F, the graphs also shows measurements taken at 120°F and 150°F to compare. It seems that measurements taken at higher temperature shows less deviation than the ones taken at 72°F. This could be indication of errors in the 72°F measurements.

An all over observation is that all graphs, except flow behavior index have an increasing trend with an increasing amount of Xanthan. According to Figure 5, an increase in gel strength, yield point, and plastic viscosity as well as decrease in filter loss, indicates that the fluid system becomes more dispersed and flocculated by increasing the amount of Xanthan.

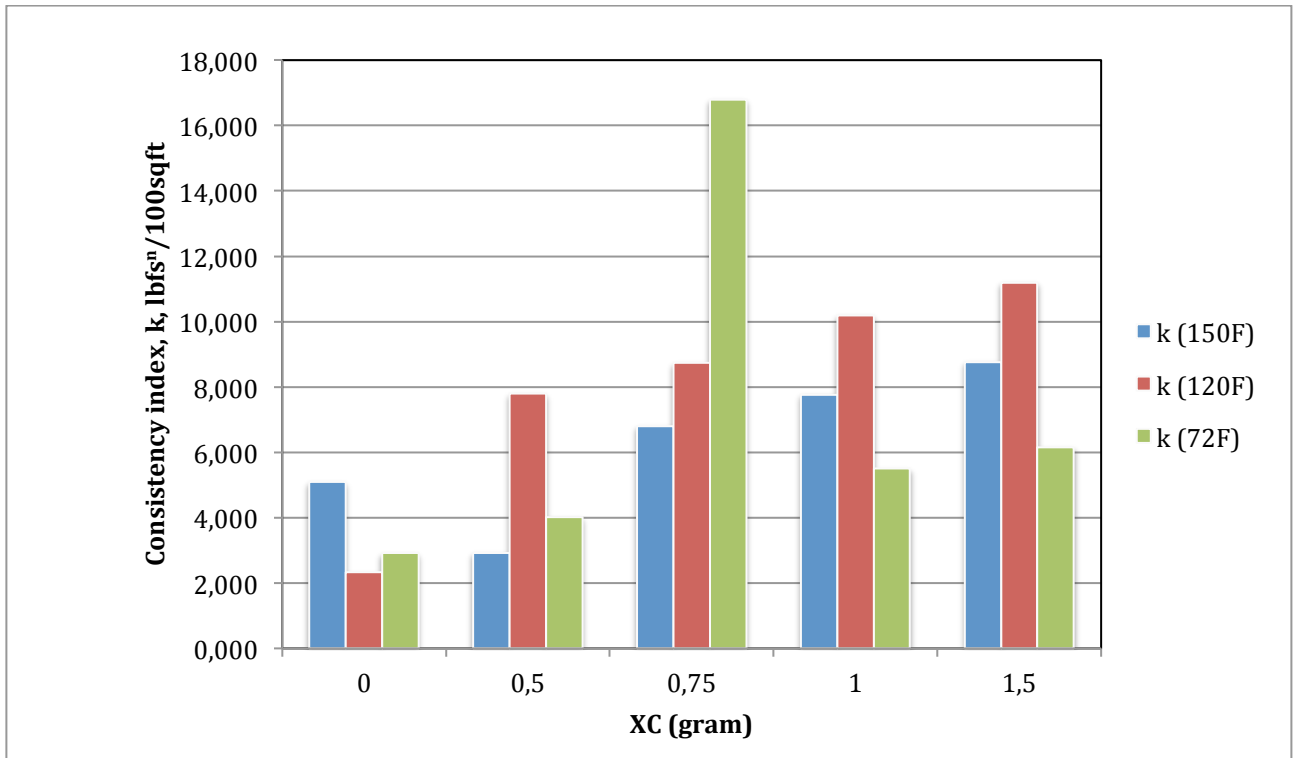


**Figure 35: Consistency index (k) for screening system at 72, 120 and 150 °F**

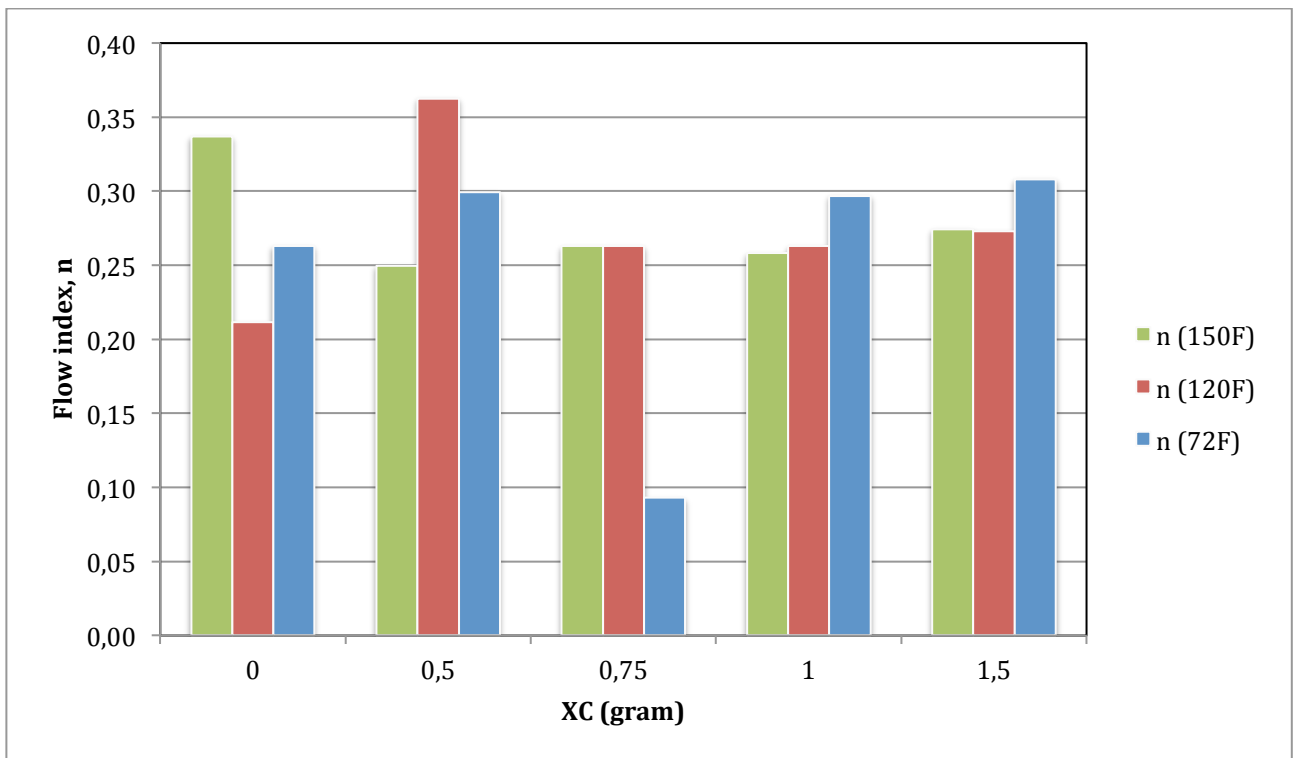


**Figure 36: Flow behaviors flow index (n) for screening system at 72, 120 and 150 °F**

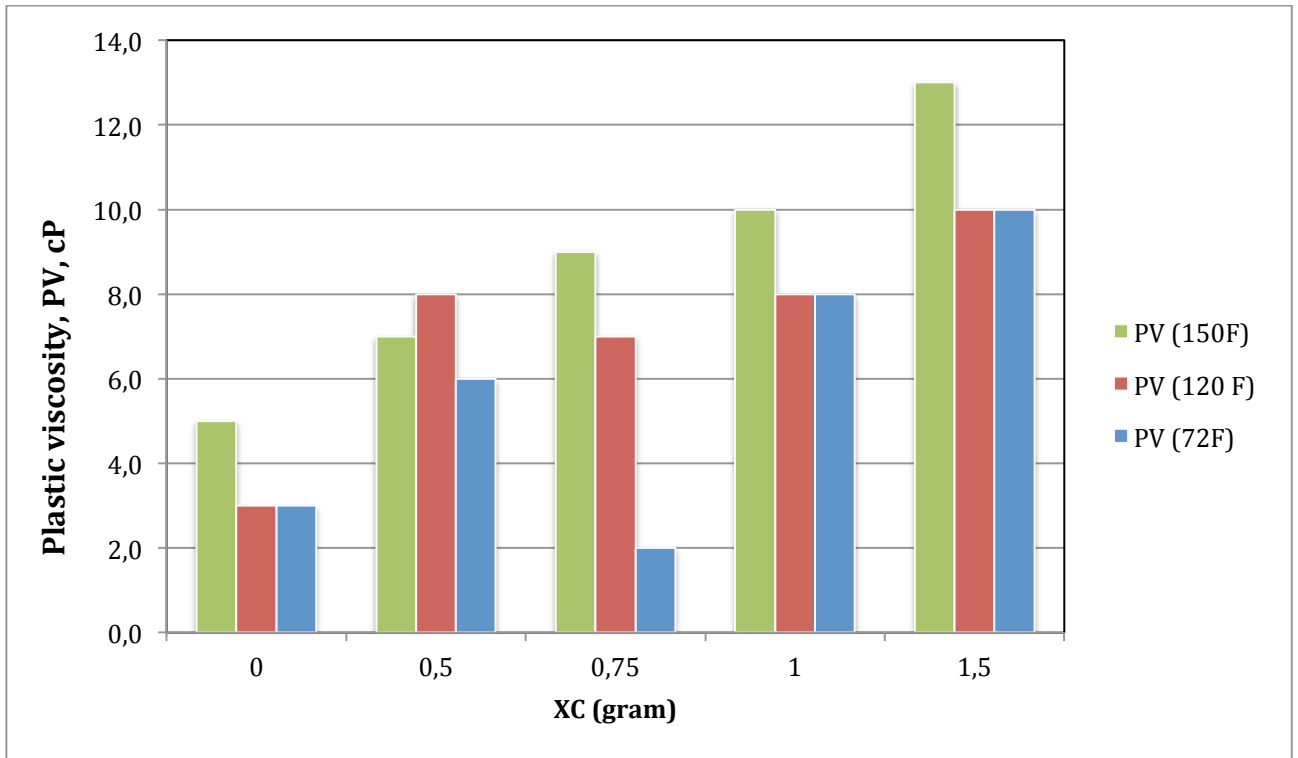


**Figure 37: Plastic viscosity for screening system at 72, 120 and 150 °F**

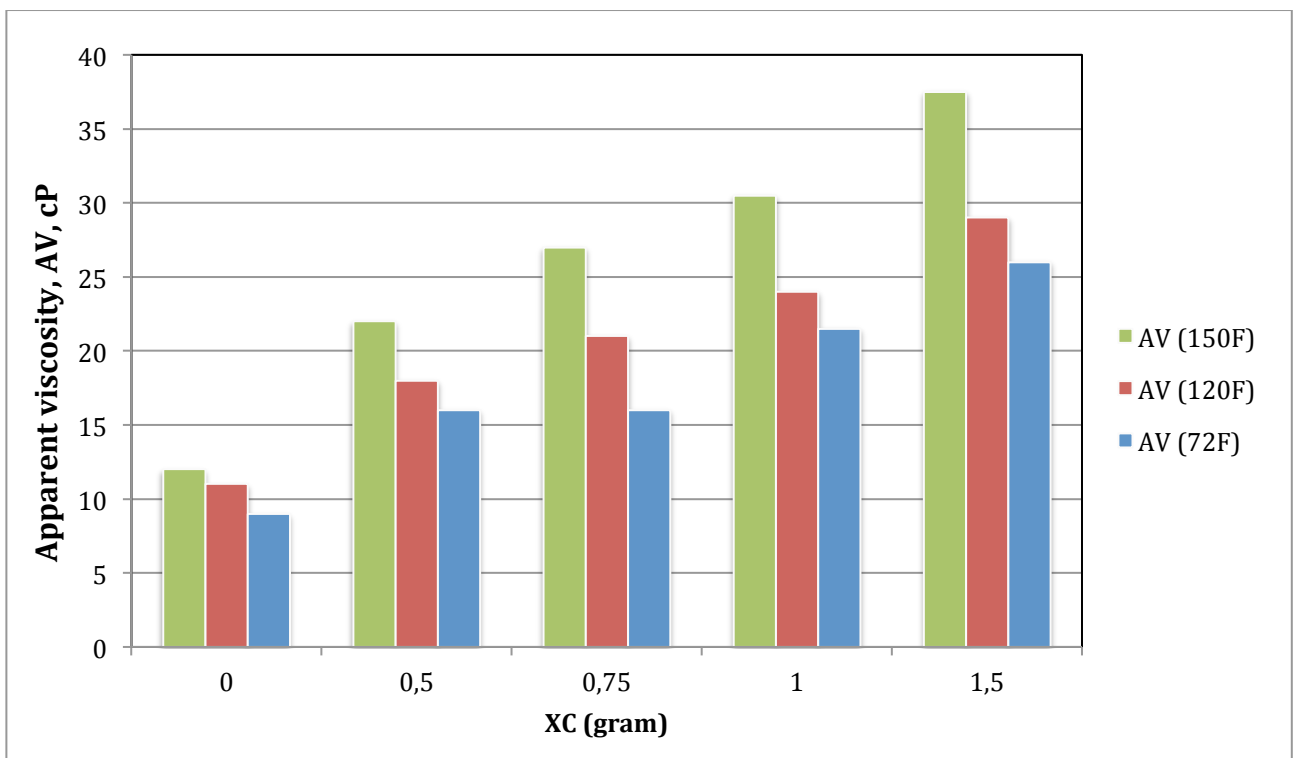


**Figure 38: Apparent viscosity for screening system at 72,120 and 150 °F**

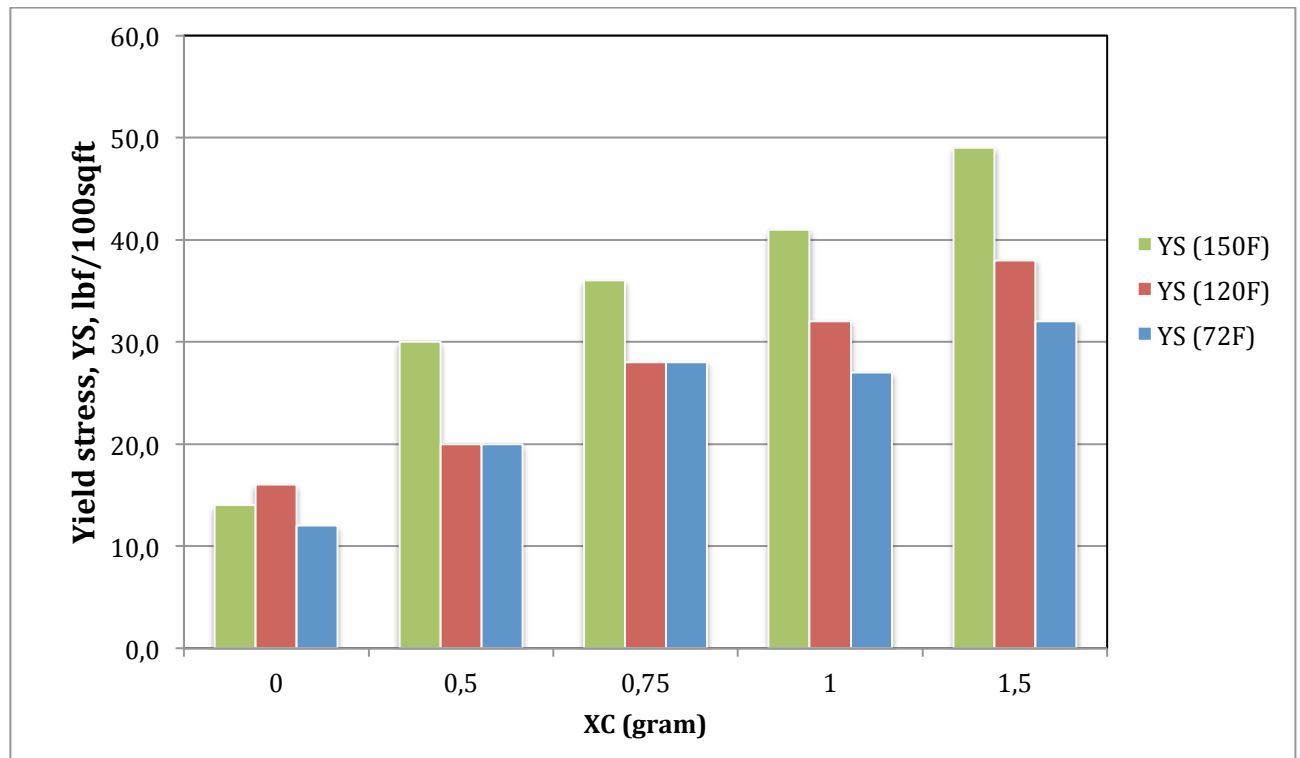


**Figure 39: Yield strength for screening system at 72, 120 and 150 °F**

#### 4.1.3.2.2 Screening

By visual inspection of the fluid samples (#2-#5), the systems with polymer concentrations larger than 0.5g shows too high viscosity for practical operations, even though the filter losses were low. It is well known that higher viscous fluid systems require higher energy to pump. Good alternatives for further enhancement of viscosity would be low molecular weight molecules such as polyanionic celluloses (PACs) or carboxyl methyl celluloses (CMCs). [24]

From an economical point of view, by using a mixture with minimum amounts of Xanthan as a base for further additives, one will be spared considerable costs. Xanthan gum costs approximately 40NOK/kg. For comparison, bentonite costs approximately 2.8NOK/kg. Therefore, based on the overall analysis, we selected the 0.5g XC system for further investigation.



#### 4.1.4 Temperature effects on 0.5g XC fluid system

This section presents temperature effects on the rheological properties of the 0.5g XC treated fluid system. The fluids were heated up to 72, 120 and 150°F using Tuefel heating cup. The reason for performing this test was to simulate how the fluid system will act in a well. When drilling, temperature conditions will raise as going deeper into the formation.

##### 4.1.4.1 Drilling fluid description

Table 5 shows the considered fluid system that was heated to study the temperature effect.

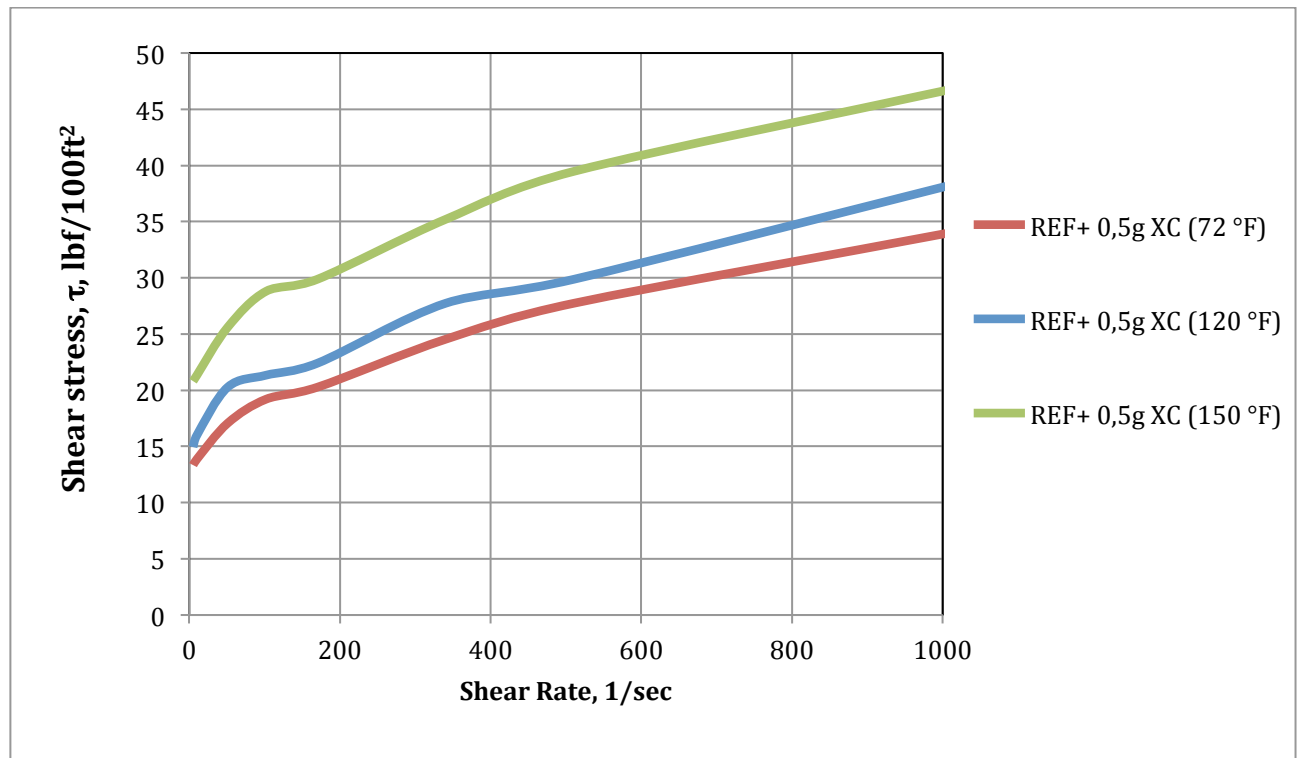
Sample	Water (ml)	Bentonite (gram)	Polymer Xanthan (gram)
1	500	25	0,50

Table 5: Fluid sample composition of screening test

##### 4.1.4.2 Test result and analysis

Figure 40 shows the effect of temperature on chosen system, REF + 0.5g XC, on the rheological properties. As temperature increase from 72°F to 150°F, at the higher shear rate, the shear stress increases by 37.5%.

The trend of increasing stress as temperature rises can be found observing viscosity curves for the remaining screening systems with various amounts of Xanthan in Appendix A.



**Figure 40: Rheology measurements for REF+ 0,5gXC at 72, 120 and 150 °F**

Bingham and Power law parameters from the REF system with 0.5g XC are listed in Table 6. We observe a slight increase in apparent viscosity as the temperature increases. This was found in all the polymer systems. Similar trend can be found when observing the plastic viscosity. The yield strength would either increase or be the same at 120°F as at 72°F and then increase at 150°F for the polymer systems. The consistency index ( $k$ ) and flow behavior index ( $n$ ) did not show the same consistency as the apparent and plastic viscosity. This is an indication of the bentonite system becoming more aggregated and flocculated.

Parameters	Mud systems		
	REF + 0,5g XC (72°F)	REF + 0,5g XC (120°F)	REF + 0,5g XC (150°F)
<b>Bingham</b>			
AV [cP]	16,00	18,00	22,00
PV [cP]	6,00	8,00	7,00
YS [lbf/100sqft]	20,00	20,00	30,00
<b>Power Law</b>			
n	0,30	0,36	0,25
k [lbf <sup>n</sup> /100sqft]	4,02	2,92	7,79
<b>Physical parameters</b>			
Filter Loss 7.5min [ml]	5,75		
PH	9,95		
Density [SG]	1,022		

**Table 6: Extrated parameters for REF + 0,5gXC system at 72,120 and 150 °F**

#### 4.1.5 Effect of KCl and NaCl on polymer system

This experiment was designed to investigate how different amounts of NaCl and KCl influence the rheological properties.

##### 4.1.5.1 Drilling fluid description

Table 7 shows the fluid systems considered for the investigation. A salt free 0.5g XC-bentonite mud system was used as a reference system. On the reference fluid system, 2.5g and 5.0g NaCl and KCl was treated.

Sample	Water (gram)	Bentonite (gram)	Polymer Xanthan (gram)	KCl (gram)	Nacl (gram)
Ref: 1	500	25	0,50	0,0	0,0
2	500	25	0,50	2,5	0,0
3	500	25	0,50	5,0	0,0
4	500	25	0,50	0,0	2,5
5	500	25	0,50	0,0	5,0

**Table 7: Fluid composition for reference system + 0,5gXC with various amounts of NaCl and KCl**

##### 4.1.5.2 Test result and analysis

Figure 41 shows the test results. The samples with NaCl exhibit a higher shear stress than samples with KCl. It is observed that the addition of 2.5g NaCl on the REF system increase the shear stress and the addition of 5.0g

NaCl reduces the shear stress. Whereas, the addition of 2.5g and 5.0g KCl reduces the shear stress as compared with the reference salt free system. Increasing the amount of KCl salt in general shift the shear stress curve downwards as compared with salt free system.

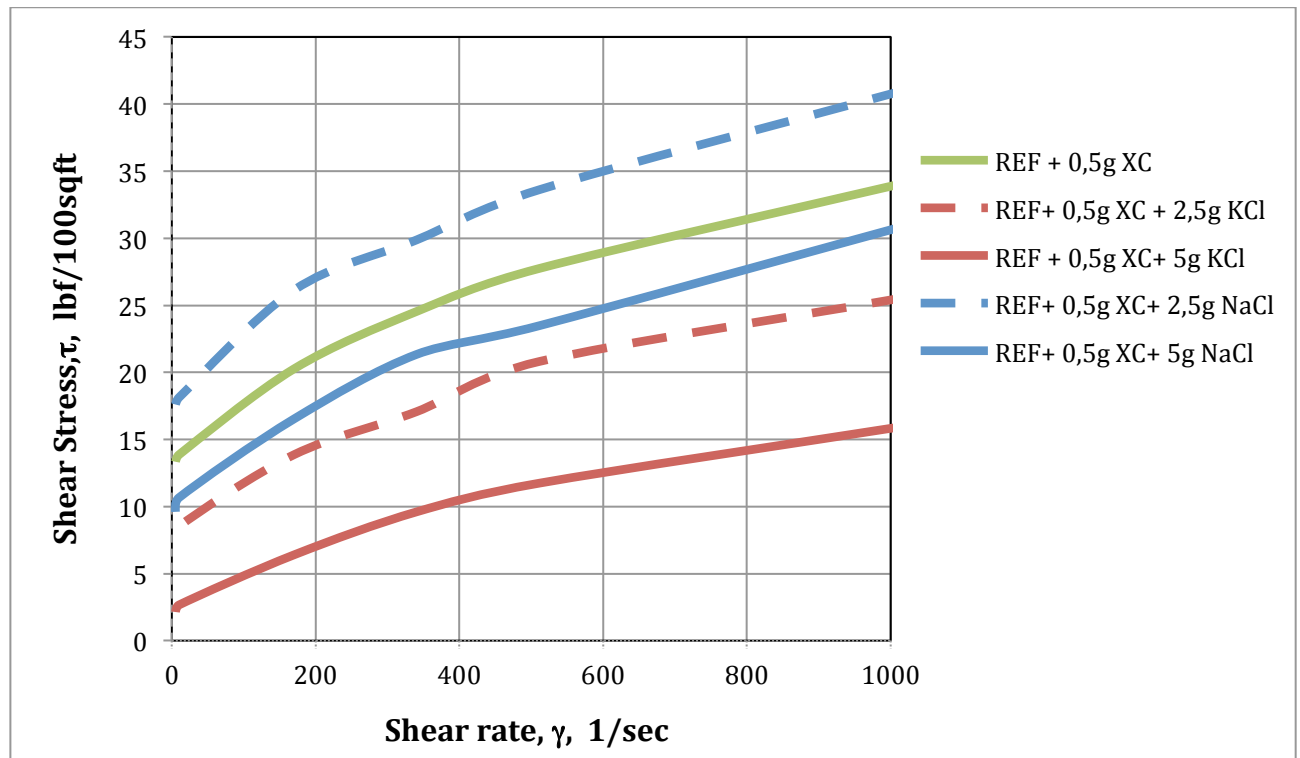


**Figure 41: Rheology measurements for REF+0,5gXC system with various amounts of salt. (72 °F)**

The calculated viscosity and yield stress, “n” and “k” parameters for the salt systems can be found in Table 8. By comparing the reference system (without salt) to the systems with KCl, a decrease in apparent viscosity is observed. A similar reduction can be found observing the plastic viscosity and yield strength. According to Figure 5, decrease in plastic viscosity, along with enhanced filter losses, indicates that system goes from a dispersed state towards an aggregated state.

In contrast to the KCl systems, the system with 2.5g NaCl shows an increase in apparent viscosity to the reference system with no salt. However, by increasing the concentration of NaCl to 5g, we see that the apparent

viscosity decreases. A similar reduction can be found comparing the yield strength for the two KCl systems, while the plastic viscosity stays constant. Comparing the flow behaviour index (n) for the two salt systems with 2.5g salt, to the initial flow behavior index (n), where there is no salt in the system, we see no significant deviations. However, by increasing the amounts of salt to 5.0g, a slight increase in flow behavior index occur is seen for both the NaCl and KCl fluid system. The consistency index (k) decreases for all the systems to the reference system, except from the one with 2.5g NaCl. The system with 2.5g NaCl, is also the only salt system that exhibits lower filter losses than the reference system without salt.

Parameters	Mud systems				
	REF+ 0,5g XC	REF+0,5g XC +2,5g KCl	REF+0,5g XC +5g KCl	REF+0,5g XC +2,5g NaCl	REF+0,5g XC +5g NaCl
<b>Bingham</b>					
AV [cP]	16,00	12,00	7,50	19,25	14,50
PV [cP]	6,00	4,50	4,00	7,00	7,00
YS [lbf/100scft]	20,00	15,00	7,00	24,50	15,00
<b>Power Law</b>					
n	0,30	0,30	0,45	0,29	0,40
k [lbf <sup>n</sup> /100sqft]	4,02	3,01	0,68	5,18	1,83
<b>Physical parameters</b>					
Filter Loss 7.5min [ml]	5,75	7,5	11	5,5	6,5

**Table 8: Extracted paramters for REF + 0,5gXC with various amounts of salt**

#### 4.1.6 Effect of nanoparticles on polymer system

According to studies done by Ammanullah M.D et al. [28], there have been a proven reduction in filter loss by the use of nanoparticles. They state that the huge surface area of the nanoparticles, together with van der Waals, molecular and atomic forces can change the properties of the fluid significantly with only a small amount of nano particles (<1%). In this study we will look into how different concentrations of nano silica from our supplier EPRUI Nanoparticles and microspheres [19] have any effect on the

filtrate and rheological properties of water based system without nano particles.

#### 4.1.6.1 Drilling fluid system description

Table 9 shows the fluid systems considered for the investigation. A nanoparticle free bentonite mud system was used as a reference system. Various amounts of nano particles were added to investigate the effects on rheological and filtrate properties.

Sample	Water (gram)	Bentonite (gram)	Polymer Xanthan (gram)	KCl (gram)	Nanoparticles (gram)
Ref: 1	500	25	0,50	2,5	0,0
2	500	25	0,50	2,5	0,1
3	500	25	0,50	2,5	0,2
4	500	25	0,50	2,5	0,3
5	500	25	0,50	2,5	0,4
6	500	25	0,50	2,5	0,5

**Table 9: Fluid composition for polymer system (with KCL) with various amounts of nano particles**

#### 4.1.6.2 Test result and analysis

Figure 42 shows the obtained viscosity curves from the tests. For all the fluid samples with various amounts of nano particles, there is a shift upwards compared to the curve without nano. The system with 0.1g nano shows the greatest change, with 91.67% increase in shear stress for the highest measured shear rate of 600 RPM (1021.8 sec<sup>-1</sup>). To comparison, the system that exhibited the least change in shear stress was the system with the highest amount of nano (0.5g), with an increase of 29.17%. The fluid systems with 0.2, 0.3 and 0.4g nano shows an increase in shear stress of 75, 58.33 and 70.83%, respectively.

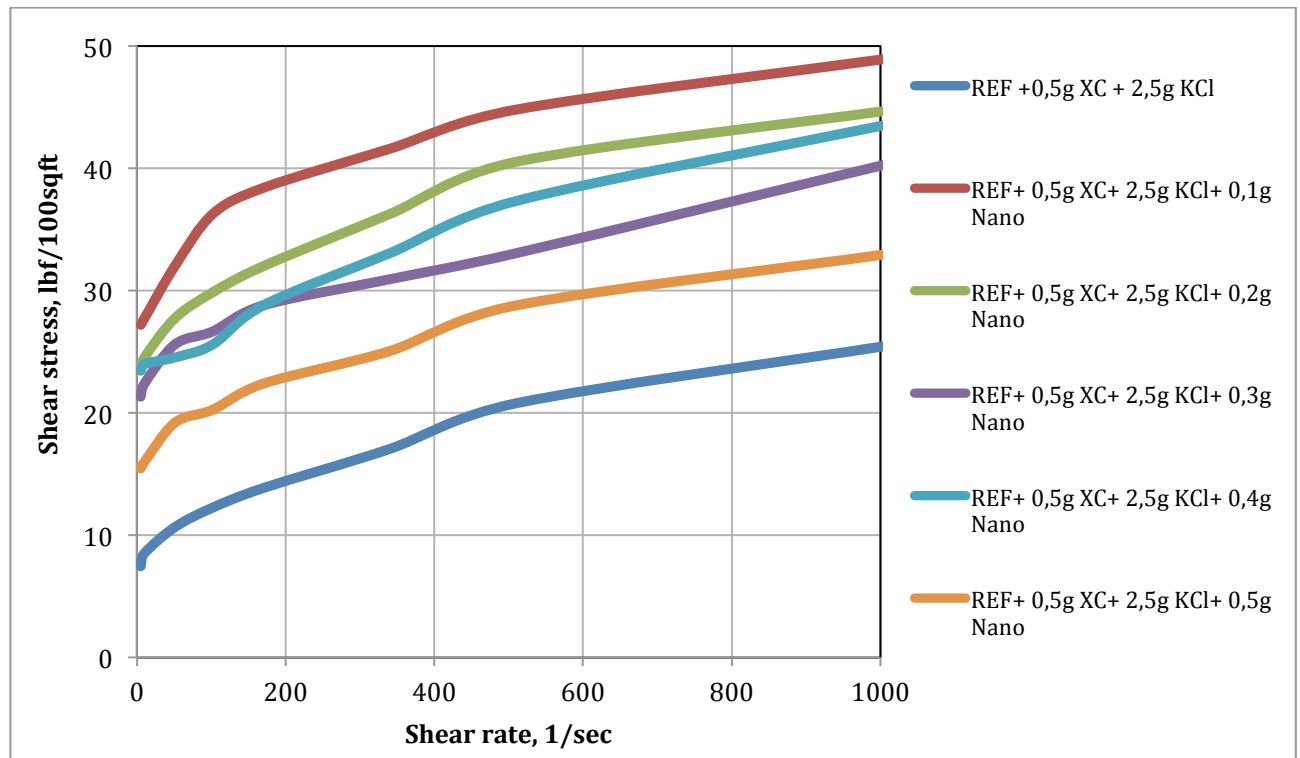


**Figure 42: Rheology measurements for REF+ 0,5gXC +2,5gKCl and various amounts of nano**

The computed drilling fluid parameters for the fluids systems can be found in Table 10. Comparing the fluid system with nano particles to the fluid systems without nano an obvious increase in AV and YS is observed for all systems. The fluid system that affected the AV and YS the least was the system with the largest amount of nanoparticles (0.5g), with an increase of 29.17% and 53.33%, respectively.

The fluid system with 0.1g nano particles increase the apparent viscosity (AV) and yield strength (YS) of 91.67% and 153.33%, respectively. According to Figure 5 an increase in YS and gel strength indicates that the fluid system becomes more flocculated. YS is used to evaluate the ability of a mud to lift cuttings out of the well. Higher YS done by the nanoparticles implies a mud that can transport cuttings better than the mud without nano, which has a lower YS and a similar density. Improved hole cleaning by the use of nanoparticles can lead to fewer hole related issues. Seen from an economical point of view, this may lead to a significant reduction in total drilling costs. Also, by the use of nano based muds, one can eliminate additional polymer

and chemical costs, mud treating costs, recovery costs etc. Although the nano particles can be more expensive than conventional drilling muds, in challenging drilling conditions, they may have the potential to reduce the total drilling costs. [28]

Observing the consistency index (k) for the fluid systems, a substantial increase of 515.6% is seen at the system with 0.1g nano. To comparison, the fluid system with the 0.3g nano has an increase of 65.12%. The consistency index is directly proportional to the annular viscosity. By increasing the consistency index one will normally improve the suspension effectiveness and hole cleaning of a fluid, but not without a corresponding decrease in flow behavior index, “n”. Without a reduction in “n”, the viscosity of the entire circulation system is increased, resulting in a higher circulating pressure drop. [9][29] Studying Table 10, we see that the preferable reduction in “n” is seen for all the systems for nanoparticles compared to the system without nanoparticles. A reduction in “n” means that the fluid becomes more shear thinning of over that corresponding shear rate. [9] The greatest reduction of 56.67% is seen for the nano system with 0.1g nanoparticles.

Four out of five nano- containing fluids exhibit lower filter loss than the one fluid without nano. A noticeable increase in filter losses is observed as the amount of nanoparticles is increased. The fluid containing the least amount of nano (0.1g) shows a reduction in filter loss of 16.67%. For comparison, the fluid containing 0,5g nano exhibits an increase in filter loss of 16.67%.





**Figure 43: Mud cake from fluid system with 0.1g nanoparticles**

The main finding from this study is the fluid system with 0.1g nano, which exhibits the best rheological properties and lowest filter losses. It will be further investigated for cutting transport, viscoelasticity and hydraulic performance later on.

Parameters	Mud systems					
	REF+ 0,5g XC +2,5g KCl	REF+ 0,5g XC+ 2,5g KCl+ 0,1g Nano	REF+ 0,5g XC+ 2,5g KCl+ 0,2g Nano	REF+ 0,5g XC+ 2,5g KCl+ 0,3g Nano	REF+ 0,5g XC+ 2,5g KCl+ 0,4g Nano	REF+ 0,5g XC + 2,5g KCl+ 0,5g Nano
<b>Bingham</b>						
AV [cP]	12,00	23,00	21,00	19,00	20,50	15,50
PV [cP]	4,50	4,00	4,00	7,00	6,00	4,00
YS [lbf/100scft]	15,00	38,00	34,00	24,00	29,00	23,00
<b>Power law</b>						
n	0,30	0,13	0,14	0,29	0,23	0,20
k [lbf <sup>n</sup> /100s <sup>n</sup> qft]	3,01	18,53	15,45	4,97	8,44	7,80
<b>Physical parameters</b>						
Filter Loss 7.5min [ml]	7,5	6,25	7	6,75	7,25	8,75

**Table 10: Extracted parameters for REF + 0,5g XC + 2,5g KCl with various amounts of nanoparticles**

#### 4.1.7 Effect of salt types on Nano based system (NaCl and KCl)

The objective of this test was to determine if a mixture of concentration NaCl and KCl on nano system shows an improved effect on rheology parameters and filter losses on the nano fluid system.

##### 4.1.7.1 Drilling fluid description

The nano system that was used as a reference along with the other systems is listed in Table 11. The amount of KCl was held constant, while increasing the amount of NaCl.

Sample	Water (gram)	Bentonite (gram)	Polymer Xanthan (gram)	KCl (gram)	NaCl (gram)	Nanoparticles (gram)
Ref:1	500	25	0,50	2,5	0,0	0,2
2	500	25	0,50	2,5	0,2	0,2
3	500	25	0,50	2,5	0,4	0,2
4	500	25	0,50	2,5	0,6	0,2

Table 11: Fluid composition for 0.2g nano fluid system with various amounts of NaCl

##### 4.1.7.2 Test results and analysis

The results from Fann viscometer can be found in Figure 44. Adding 0.2g NaCl to the reference system provides no major impact on the viscosity curve. By further increasing the concentration of NaCl, the sample with 0.4g NaCl exhibits a higher shear stress at given shear rates than the corresponding shear stresses of the sample with 0.6g NaCl.

Observing the Bingham parameters in Table 12, the yield strength decreases when increasing salts to the system. The fluid system with 0.6g NaCl has shown a reduction in yield strength by 44.12% as compared with the reference system. A slightly increase in AV is observed for the fluids containing 0.2g and 0.4g NaCl, respectively. As for the system with 0.6g NaCl there is a reduction in AV of 9.52%. Regarding the PV, the system that stands out, is the fluid system with 0.2g NaCl with an increase of 75%.

The results shows increasing filter loss for all the samples, except the fluid sample with 0.2g NaCl, where filter loss reduction is found.

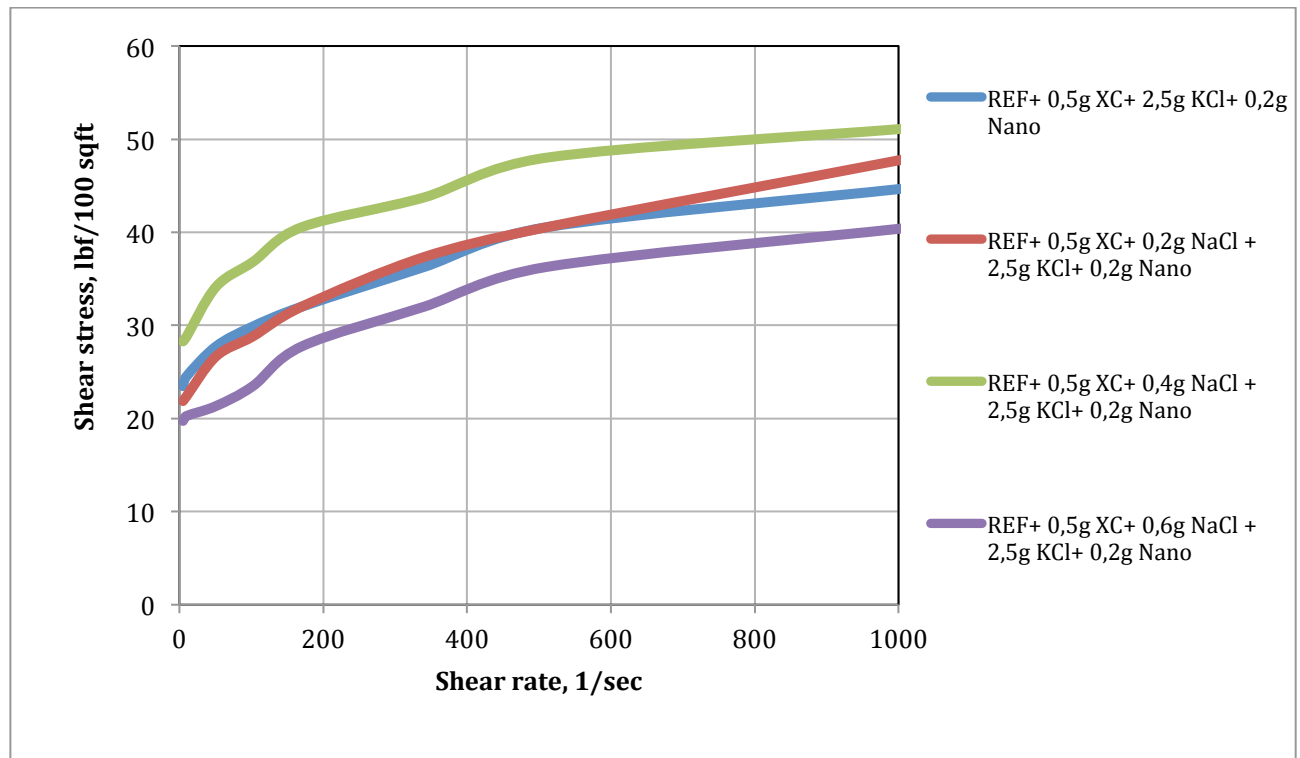


Figure 44: Rheology measurements for 0.2g nano system with various amounts of NaCl

However, the Power law parameters exhibit decreasing consistency index ( $k$ ) and increasing flow behavior index ( $n$ ). Based on this evaluation, none of these fluids samples will be taken further for viscoelastic and hydraulic performance examination.

Parameters	Mud systems			
	REF+ 0,5g XC+ 2,5g KCl+ 0,2g Nano	REF+ 0,5g XC+ 0,2g NaCl + 2,5g KCl+ 0,2g Nano	REF+ 0,5g XC+ 0,4g NaCl + 2,5g KCl+ 0,2g Nano	REF+ 0,5g XC+ 0,6g NaCl + 2,5g KCl+ 0,2g Nano
<b>Bingham</b>				
AV [cP]	21,00	22,50	24,00	19,00
PV [cP]	4,00	7,00	3,00	4,00
YS [lbf/100sqft]	34,00	31,00	24,00	19,00
<b>Power Law</b>				
$n$	0,14	0,24	0,09	0,16
$k$ [lbf <sup><math>n</math></sup> /100sqft]	15,45	8,31	25,19	12,51
<b>Physical parameters</b>				
Filter Loss 7.5min [ml]	7	6,8	7,5	7,75

Table 12: Extracted parameters for 0,2g nano particles with various amounts NaCl

## 4.2 Visco-elasticity Test

The oscillatory amplitude- and frequency sweep tests were performed using Anton Paar rheometer illustrated in Figure 45.

### 4.2.1 Anton Parr equipment

The gap between the two parallel plates was set to be 1 mm. Prior to testing, the fluid samples were mixed with Hamilton Beach mixer for 10 minutes in order to create homogeneity in the fluids. The rheometer was adjusted to not start testing before the fluids were measuring 20°C, thereby creating the most equal temperature conditions for the samples.



**Figure 45: Anton Paar rheometer**

The tests were performed on the two fluids system, one with and one without nanoparticle additives. The compositions of the fluids are given in Table 13.

Sample	Water (gram)	Bentonite (gram)	Polymer Xanthan (gram)	KCl (gram)	Nanoparticles (gram)
(REF)	500	25	0,5	2,5	0,0
(REF+ 0,1g nano)	500	25	0,5	2,5	0,1

**Table 13: Fluid composition for viscoelasticity test**

#### 4.2.2 Oscillatory amplitude sweep test results

The amplitude sweep tests were conducted to determine the yield point, flow point and the linear viscoelastic range, i.e. the range where the Storage Modulus ( $G'$ ) and the Loss Modulus ( $G''$ ) are constant. The tests were done on both fluids samples, at a strain ramp from 0.0001% to 1000% and an angular frequency of 10 rad/s.

The results from the amplitude sweep test for the two fluids are presented in Figure 46. One can observe a nearly identical behaviour for the fluids within the LVE range that has a limit close to 1%. Both Storage Modulus and Loss Modulus overlap within this area. Also, we can see that the Storage Modulus ( $G'$ ) is greater than the Loss Modulus ( $G''$ ) in the LVE area. This indicates that the fluids exhibit gel like behaviour, because the elastic portion dominates the viscous one. At low shear stress, the fluid will show certain stability. When the LVE range is exceeded, the viscous behaviour will become more dominating, as the gel structure breaks.

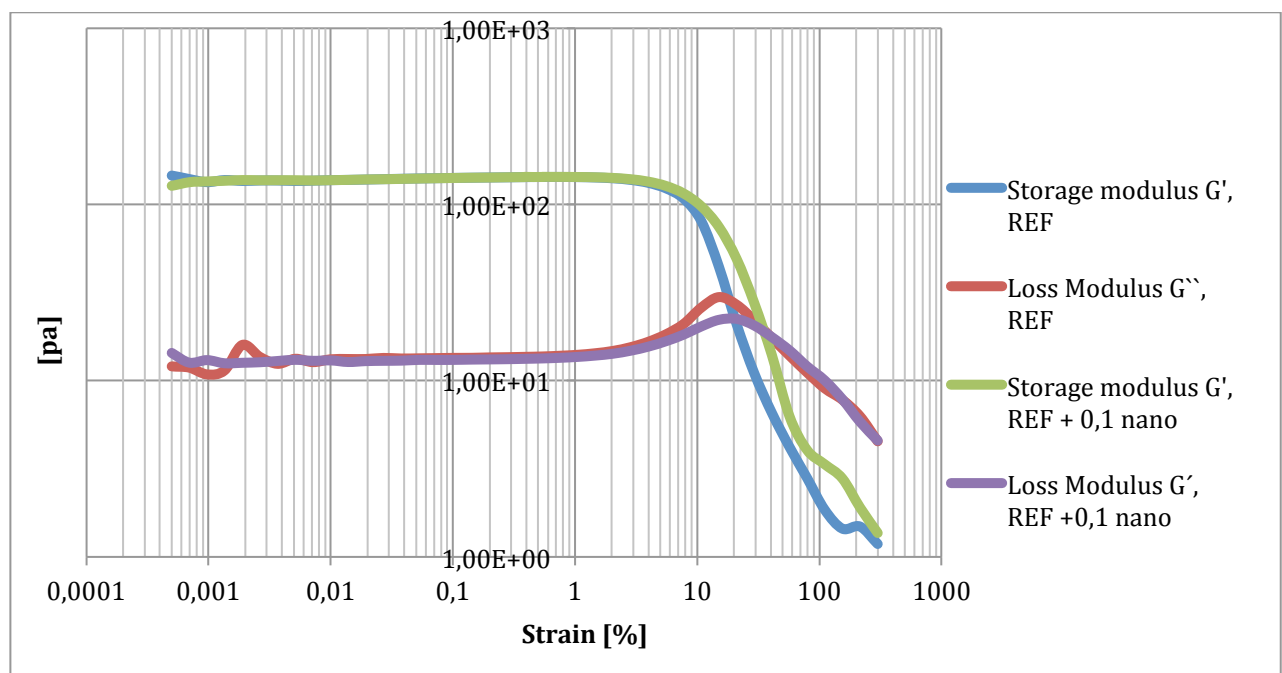


**Figure 46: Plots showing amplitude sweep for the two fluid systems.**

The point where the Loss Modulus and the Storage Modulus are equal is called the flow point, as reviewed in the literature section. At this point the fluid starts to flow. The data can be found in Table 14. We register that the

flow point for the system with nano exhibits higher flow point than the reference fluid with 26.73% increase.

Fluid	Flow point [Pa]
REF	7,6120
REF+ 0,1g nano	9,6465

**Table 14: Comparison of flow points for the two fluids by Anton Paar instrument**

The yield point calculated from the Anton Parr software measurements is found at the limit of the LVE range, where LVE plateau begins to deviate. Comparison between the yield point from Anton Paar software and the yield point from the Bingham model can be found in Table 15.

	Anton Paar	Bingham model
Fluid	Yield point ( $\tau_y$ ) [Pa]	Yield point( $\tau_y$ ) [Pa]
REF	0,7777	7,7
REF+ 0,1g nano	0,7778	19,4

**Table 15: Comparison of the yield point calculated by the Anton Paar instrument and the Bingham model for both fluids**

As expected the yield points that are calculated by the Bingham model, are significantly larger than the yield points calculated by the Anton Paar software. The value that is calculated from the rheological model, assumes that the liquid behaves as a theoretical Bingham plastic drilling fluid. This is not the real yield strength that is required to maintain the liquid in motion. The calculated yield strength from the Bingham model will be larger. [6]

The Anton Paar measurements show nearly identical yield strength for the two fluid systems. The difference is larger for the calculated values in the Bingham model. For the reference system and the system with nano, there is an increase of 890.1% and 2394.2% respectively, comparing the Anton Paar measurement to the rheology model. This result supports how the yield strength from the Bingham model differs from the true yield strength.

### 4.2.3 Oscillatory frequency sweep test results

The linear viscoelastic range was determined in the amplitude sweep test, with a value of approximately 1%. In the frequency sweep test, the viscoelastic property of a drilling fluid in its linear viscoelastic range is shown. The tests were performed on both fluid samples. Angular frequency was ramped from 0.01rad/s to 100rad/s.

Figure 47 shows the results from the fluid samples that were tested. The blue lines display the Complex Viscosity, Storage Modulus and Loss Modulus for the reference sample as the frequency of oscillation is ramped. The red lines display the same data for the reference sample with 0.1gram nanoparticles. Both fluids exhibit the same trend, showing that the Storage Modulus ( $G'$ ) is independent of frequency. The Storage Modulus ( $G'$ ) is also larger than the Loss Modulus ( $G''$ ) for both fluids. As reviewed in the theory section, when  $G' > G''$ , the samples response to deformation is dominated by elastic behavior. The fluids show a solid like property and have a stable gel structure, which is a characterization of a viscoelastic fluid. The stable structure is important for drilling fluids, as it keeps small particles in suspension. [25]

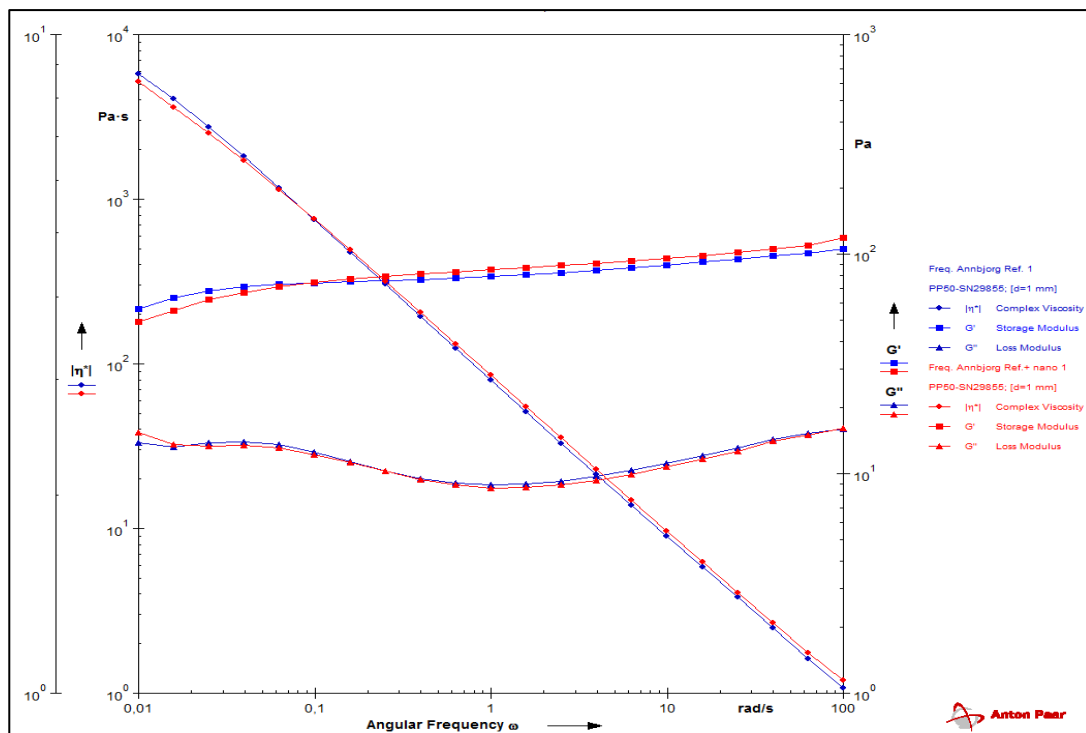


Figure 47: Comparison of fluids with and without nanoparticles, oscillatory frequency sweep test

### **4.3 Rheology Modeling and Analysis of nanoparticles fluid system**

The measured Fann data was compared against the different rheology models, to investigate how well they correlated. None of the fluids that were used in the calculations conformed exactly to either of the models. However, by comparing % deviation for all the models, one can find the one(s) that deviates the least.

Figure 48 shows to what extent the readings from reference system and reference system with 0.1 and 0.2g nano silica deviate from the rheology models. Herschel Buckley, Unified, Power law and Robertson and Stiff model all exhibited low % deviation compared to the two other models. According to the figure, there seem to be no clear differences in rheology models for the different fluids, but for the two fluids with nanoparticles, Robertson and Stiff exhibit the lowest % deviation, with 1.44% and 1.32% respectively. The reference system deviates the least from the Unified model, with 2.60%.

As expected, all three fluids differ a lot from the Newtonian model. As reviewed in the theory section, most drilling fluids are non-Newtonian, i.e. they don't obey the laws and equations that apply for Newtonian fluids. The same trend can be found observing Figure 49, displaying the viscosity curves for the reference system with 0.1g nano. All systems with nanoparticles exhibited similar behaviour.



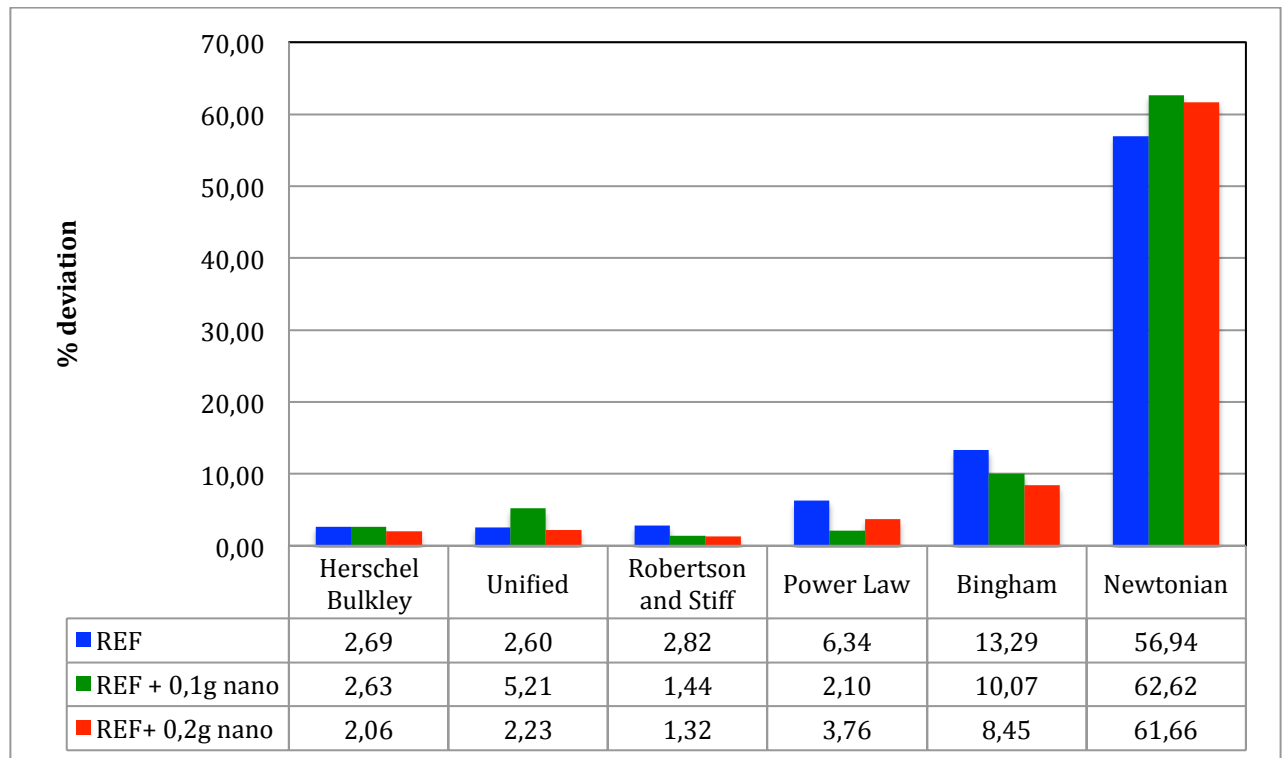


Figure 48: Comparison of the different rheology models %deviation to the reference system

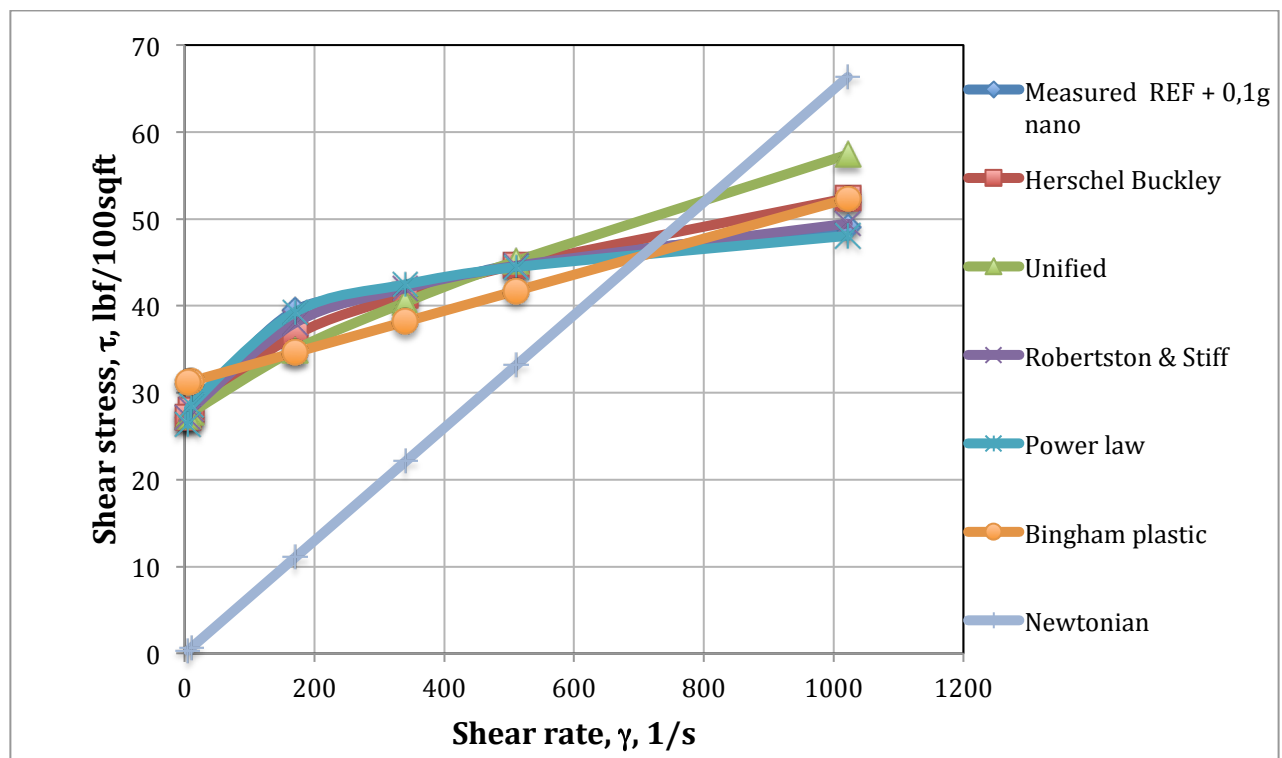


Figure 49: Comparison of the different rheology models with REF + 0,1g nano silica at 72 °F

Table 16, 17 and 18 are rheology models and model parameters derived from reference, Ref+0.1g nano and Ref +0.2g nano fluid systems, respectively.

Model	Equation for "REF" fluid system	Parameters					
		$\tau_o, \tau_y, \tau_{yL}$ A	k, C	n, B	$\mu_p, \mu$	%Error	$\mu_p, \mu$ cP
Herschel Bulkley	$6.641+0.4058*\gamma^{0.56170}$	6,64	0,41	0,56		2,69	
Unified	$6.402+0.5287*\gamma^{0.5215}$	6,40	0,53	0,52		2,60	
Power Law	$5.0236*\gamma^{0.2213}$		5,02	0,22		6,34	
Bingham	$9.534+0.0176*\gamma$	9,53			0,02	13,29	8,43
Newtonian	$0.09311*\gamma$				0,03	56,94	14,89
Robertson & Stiff	$2.0597*(33.9199+\gamma)^{0.3619}$	2,06	33,92	0,36		2,82	

Table 16: Rheology models and parameters for Ref fluid system

Model	Equation for Ref+0.1g Nano Fluid system	Parameters					
		$\tau_o, \tau_y, \tau_{yL}$ A	k, C	n, B	$\mu_p, \mu$	%Error	$\mu_p, \mu$ cP
Herschel Bulkley	$25.003+0.996*\gamma^{0.4785}$	25,00	1,00	0,48		2,63	
Unified	$26.675+0.1913*\gamma^{0.7329}$	26,68	0,19	0,73		5,21	
Power Law	$21.963*\gamma^{0.1131}$		21,96	0,11		2,10	
Bingham	$31.099+0.0208*\gamma$	31,10			0,02	10,07	9,96
Newtonian	$0.0649*\gamma$				0,06	62,62	31,07
Robertson & Stiff	$17.144*(15.3305+\gamma)^{0.1526}$	17,14	15,33	0,15		1,44	

Table 17: Rheology models and parameters for Ref + 0,1g nano

Model	Equation for Ref+0.2g Nano Fluid system	Parameters					
		$\tau_o, \tau_y, \tau_{yL}$ A	k, C	n, B	$\mu_p, \mu$	%Error	$\mu_p, \mu$ cP
Herschel Bulkley	$22.304+0.5436*\gamma^{0.5535}$	22,30	0,54	0,55		2,06	
Unified	$22.403+0.4928*\gamma^{0.5685}$	22,41	0,49	0,57		2,23	
Power Law	$18.712*\gamma^{0.119}$		18,71	0,12		3,76	
Bingham	$26.467+0.0208*\gamma$	26,47			0,02	8,45	9,96
Newtonian	$0.0584*\gamma$				0,06	61,66	27,96
Robertson & Stiff	$10.829*(40.3503+\gamma)^{0.205}$	10,83	40,35	0,21		1,32	

Table 18: Rheology models and parameters for Ref + 0,2g nano

## **5 Drilling fluid performance simulation studies**

The performance of the best system formulated in section §4.1.6, will be further evaluated with respect to hole cleaning and hydraulics.

### **5.1 Hydraulics performance simulation**

As reviewed in the introduction section the Equivalent circulation density (ECD) combines the annular pressure drop and the density of the fluid. Hence, an accurate prediction of annular pressure drop can give a good estimation of the ECD. To predict the annular pressure loss and the pump pressure loss one can use hydraulic models. In this section, the Unified model was chosen to compare the hydraulic behaviour of five mud formulations containing various amounts of nanoparticles. Details of the Unified model can be found in Appendix E. As the friction losses are dependent on several factors, the following factors will be taken into account for the estimation: rheology of the fluid, properties of the fluid (density and viscosity), wellbore and drill string geometry and flow rate.

#### **5.1.1 Simulation arrangement**

To study the hydraulic effects of the various muds, an uncomplicated, vertical well with a depth of 12.000 ft was configured. The well has an open hole section, and only one casing (for the convenience), both with the size of 8.5". The drill string has an inner and outer diameter of 4.8" and 5" respectively. The bit has three nozzles, and each of them has size of 28/32". The surface pressure is set to be zero. During the simulation the flow rate was increased from 1 to 600 gpm, with an interval of 50 gpm. Figure 50 shows the well configuration.

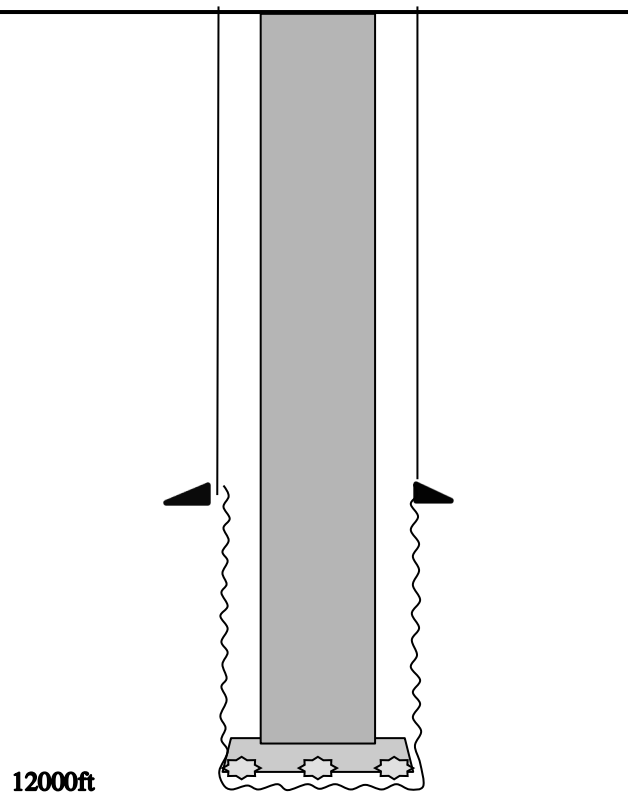


Figure 50: Illustration of well for hydraulic simulations

### 5.1.2 Description of drilling fluids

Five drilling mud formulations with various amounts of nanoparticles were mixed prior to the experiment. The Fann 35 data is shown in Table 19. The reference system, “REF”, contains 25gram of bentonite, 500gram of water, 2.5gram of KCl and 0.5gram of Xanthan. The remaining mud formulations, contains an increasing amount of nano particles. The mud density is 1.025 s.g for all the fluid systems.

RPM	REF	REF + 0.1g Nano	REF + 0.2g Nano	REF + 0.3g Nano	REF + 0.4 g Nano
600	24	46	42	38	41
300	19,5	42	38	31	35
200	16	38,5	34	29	31
100	13	37	30	27	30,5
6	8	26	23	21	22,5
3	7	25,5	22	20	22

Table 19: Fann 35 data for the simulation

### 5.1.3 Simulation results

The result from the hydraulic performance simulation is shown in Figure 51, where all the fluid systems are plotted as a function of annular pressure and flow rate. As expected, the annular pressure losses increase with increasing flow rate. All the fluid systems with nanoparticles exhibited higher annular pressure losses than the fluid system without nanoparticles. The system that shows the lowest annular pressure loss is the system with 0.3g nano. As the ECD is directly affected by the annular pressure loss, it will exhibit similar behaviour. In conventional drilling, it should be mentioned that the increase in ECD caused by annular pressure losses is usually small compared to the pressure of hydrostatic head.

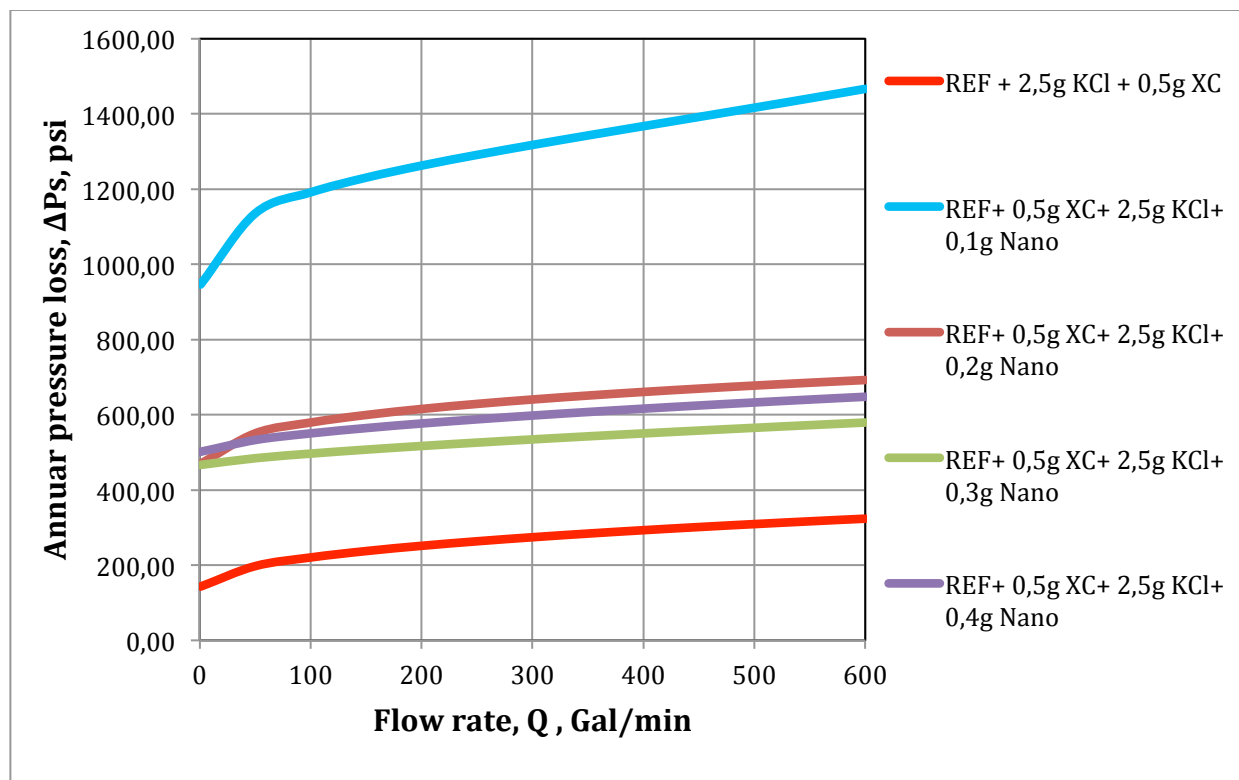


**Figure 51: Comparison of annular pressure loss at increasing flowrate for fluid samples containing various amounts of nanoparticles, based on the Unified model**

Figure 52 shows %ECD change of nano treated fluid systems with respect to the reference nano-free system. According to the Unified model, the system with 0.1g nanoparticles increases the ECD of the reference system compared to higher gram nano additives. From both systems with 0.1g and 0.2g nanoparticles we can see a rapid increase in %ECD change when the flow

rate is low. As the flow rate increases the changes is minor, and it stabilizes around 7.94% and 6.54%, respectively. The %ECD change system with 0.3g and 0.4g nanoparticles show a decreasing trend and stabilizes towards 4.52% and 5.74% respectively. In general, the addition of nanoparticles in XC system, increase the ECD since the additive creates a more viscous system. For this particular simulation set up and the considered fluid systems, as flow rate increase to 600gpm, the ECD obtained from the Unified model is found out to be gently increasing.

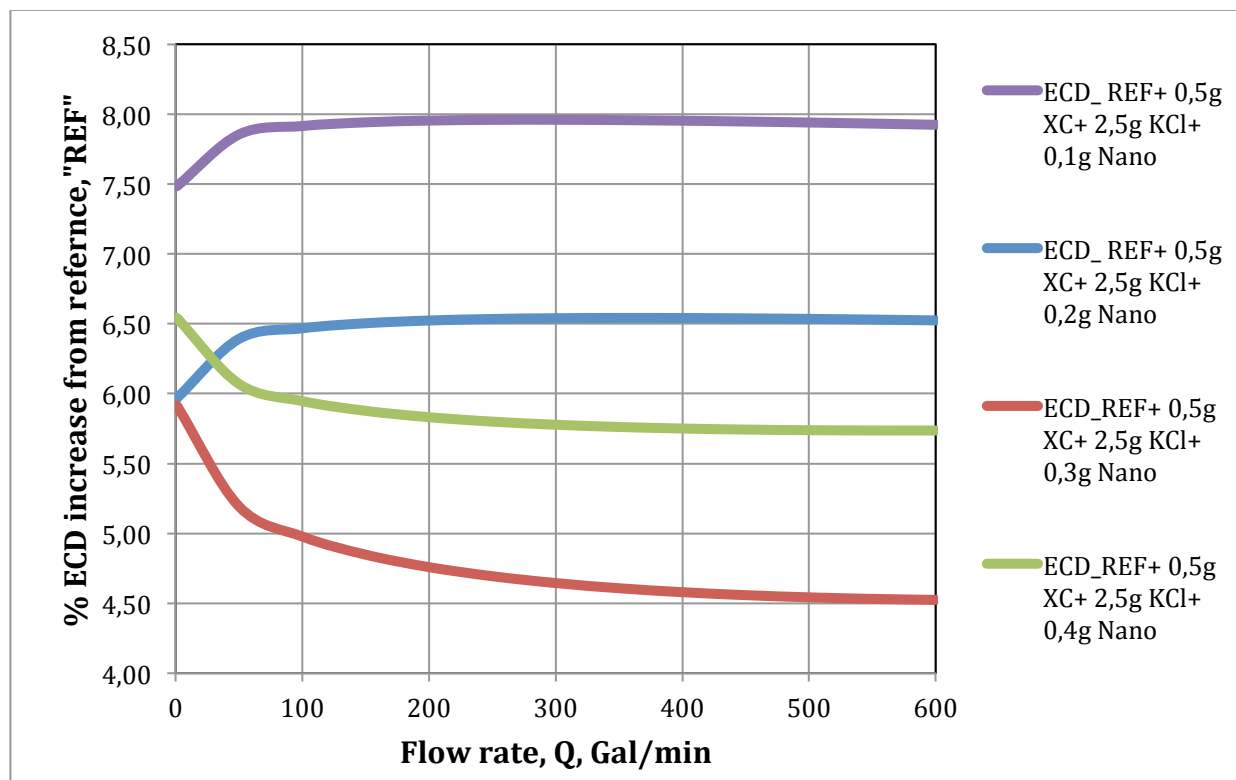


Figure 52: %ECD increase from reference system

## 5.2 Cutting transport

In this section, rheology data from six water based mud samples containing various amounts of nano particles were used in a simulation setup to study flow velocity and bed height composition. The simulation was performed on a deviated well, with fixed operational data.

### 5.2.1 Simulation arrangement

The cutting transport simulation is performed using the software Well Plan™ [20] and the Power law rheology model. The simulation was conducted on a deviated well that can be seen in Figure 53. It is 11003 feet long and has an open hole section. Detailed drill string data and hole data can be found in Appendix F.

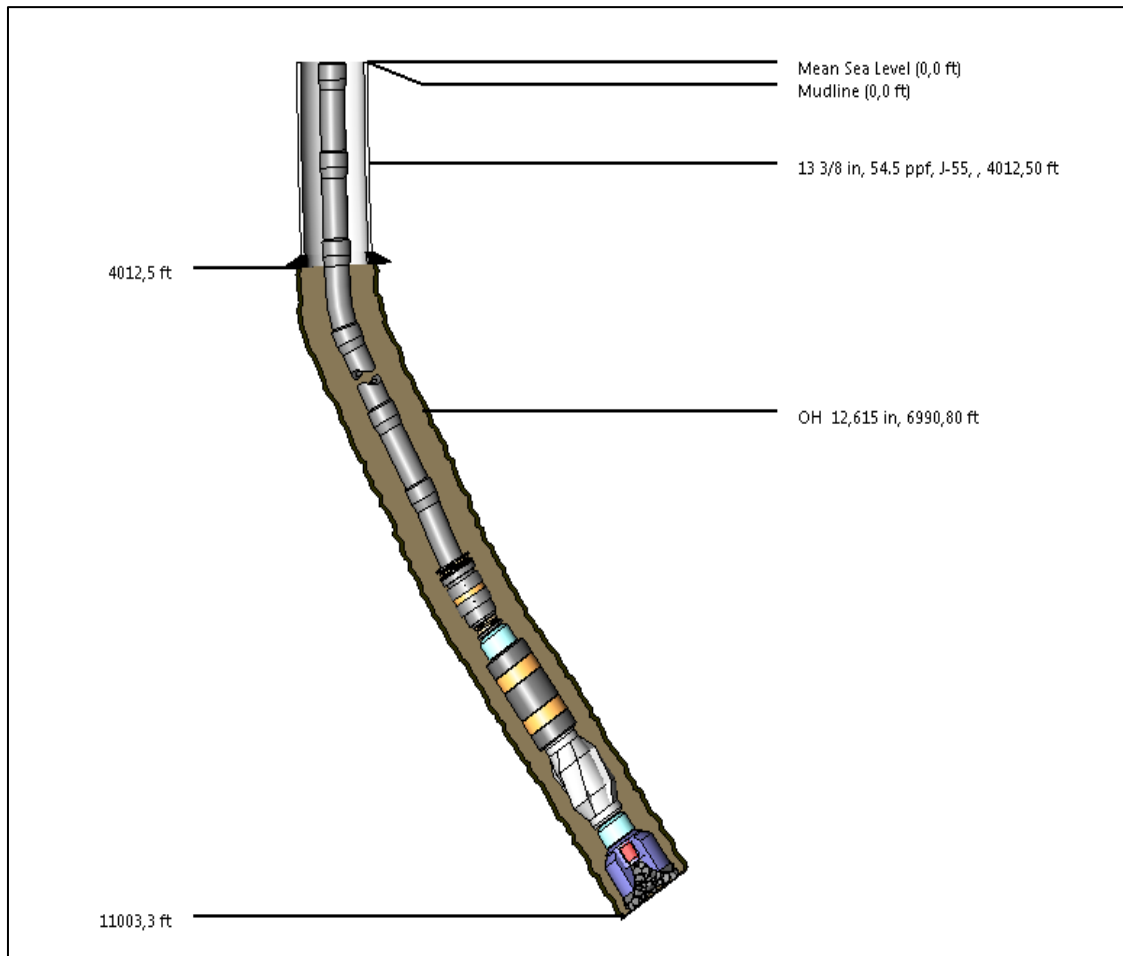


Figure 53: Experimental well for simulation

### 5.2.2 Description of drilling fluids

The Fann 35 data for the drilling fluids used to evaluate the cutting transport can be seen in Table 20. The reference system, “REF”, contains the following: 25gram of bentonite, 500gram of water, 2.5gram of KCl and 0.5gram of Xanthan. The remaining samples consist of the reference system

and increasing concentrations of nanoparticles, from 0.1gram to 0.5gram, respectively.

RPM	REF	REF + 0.1g Nano	REF + 0.2g Nano	REF + 0.3g Nano	REF + 0.4g Nano	REF + 0.5g Nano
600	24	46	42	38	41	31
300	19,5	42	38	31	35	27
200	16	38,5	34	29	31	23,5
100	13	37	30	27	30,5	21
6	8	26	23	21	22,5	15
3	7	25,5	22	20	22	14,5

**Table 20: Fann 35 data for the simulation**

### 5.2.3 Simulation result

#### 5.2.3.1 Minimum flow rate

The ability to predict the effective cleaning efficiency of a given mud and flow rate is very important. The prediction is performed by calculating the minimum flow rate for cutting transport. Minimum flow rate also known as Critical transport fluid velocity (CTFV) is defined as minimum fluid velocity required to prevent cutting bed formation. It also allows cutting transport upwards. [12] Table 21 displays the transport analysis data used in this simulation.

Figure 54 shows minimum flow rate for removing cuttings. As can be seen from the figure, the minimum flow rate increases with inclination. Well angles between 40-60° are critical as the cuttings have a tendency to slide down the wall and accumulate. The result is higher friction and the risk of various well issues. [23]

From the figure we see that when the hole angle exceeds a critical angle a significant increase in minimum flow rate is required. By comparing the results it is shown that “REF” with 0.1g nano silica has the lowest minimum



flow rate required and “REF” system has the highest minimum flow rate required to remove cuttings.

Parameters	Value
Cuttings diameter	0,125 in
Cuttings density	2,500 s.g
Bed Porosity	36,00 %
Rate of penetration	60,0 ft/hr
Rotary Speed	90 rpm
Bit Diameter	8,500 in
Annulus Diameter	8,500 in
Pipe Diameter	5,000 in
Joint Diameter	5,500 in
Minimum Pump Rate	100,0 gpm
Increment Pump Rate	200,0 gpm
Maximum Pump Rate	600,0 gpm

Table 21: Transport Analysis data: minimum flow rate

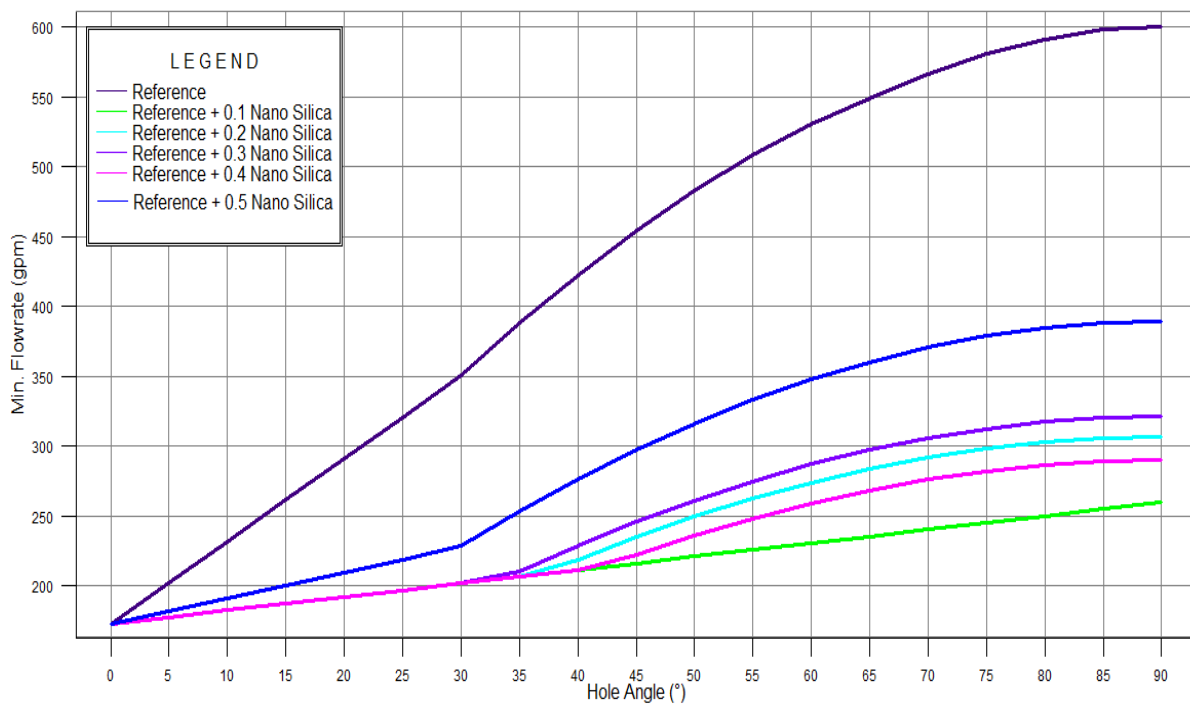


Figure 54: Comparison of the minimum flow rate for the different fluid systems with nano particles

### 5.2.3.2 Bed height deposition

The cutting capacity of “REF” system and “REF” system with increasing amounts of nano particles were investigated through bed height deposition. The results from the minimum flow rate simulation showed that minimum flow rate for “REF” was 873 gpm. The fluid systems REF + 0.1, 0.2, 0.3 and 0.4g nanoparticles all had the same minimum flow rate of 499 gpm. This was reflected in the input data, where the data for these four fluids was quite similar. Minimum flow rate for REF + 0.5g nanoparticles was calculated to be 563 gpm. In order to compare the simulated data from the different fluids, a circulation rate (pump rate) of 400 gpm was selected. This rate is below the minimum flow rate of each fluid. In that way it was possible to get cutting deposition and bed height from all the fluids. Transport analysis data can be found in Table 22.

Observing the results in Figure 55, we see that the fluid system with 0.1g nano has lower bed height and provides better performances compared to the others. As mention in previous section, greater inclination will require higher minimum flow rate in order to avoid deposition of cuttings. The simulation of well inclination against depth can be found in Appendix F.

Parameters	Value
Rate of Penetration	60 ft/hr
Rotary Speed	90 rpm
Pump Rate	400,0 gpm
Cuttings diameter	0,125 in
Cuttings density	2,500 sg
Bed Porosity	36,00 %
MD Calculation Interval	100,0 ft

**Table 22: Transport analysis data: Bed height**

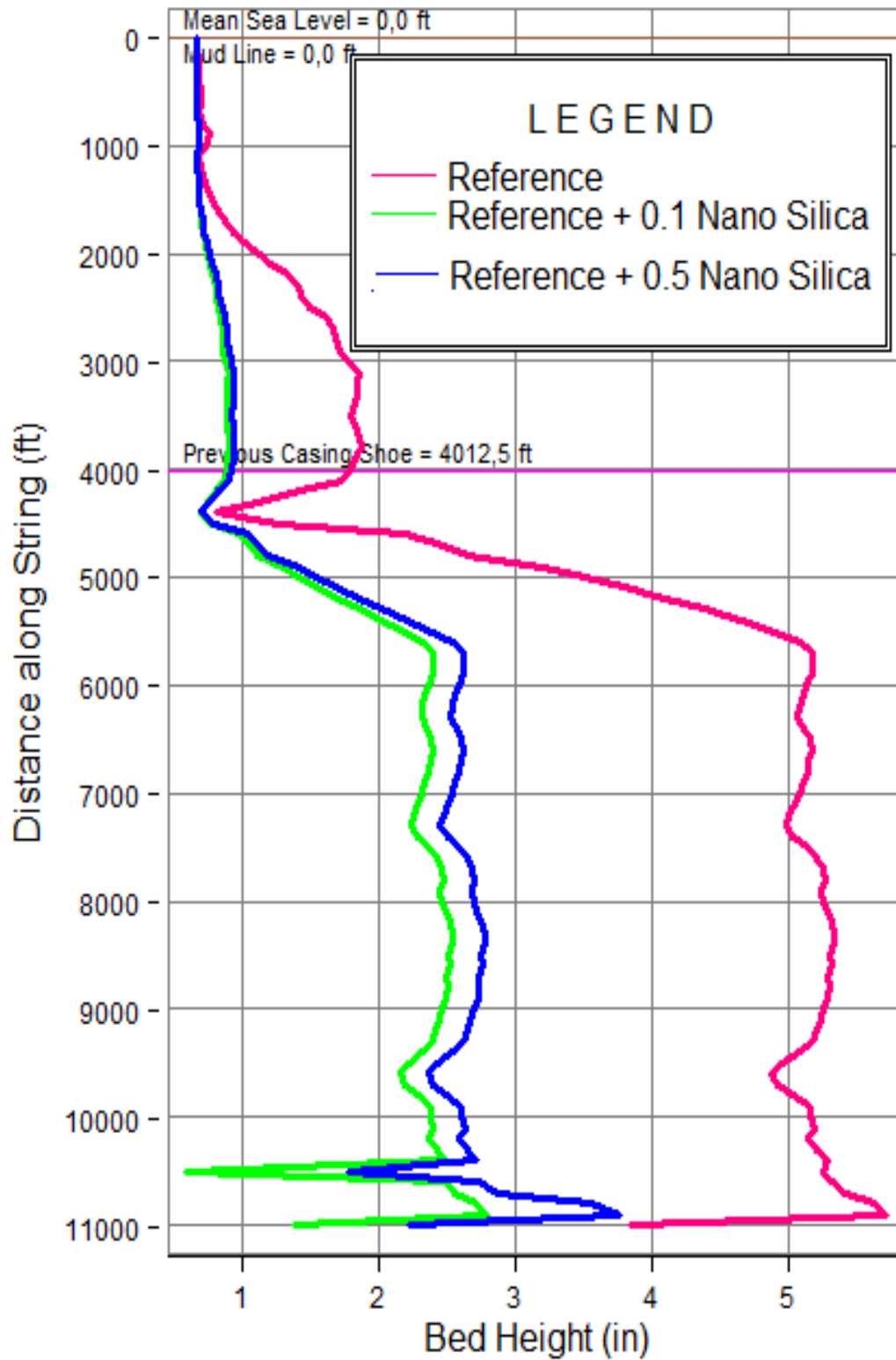


**Figure 55: Comparison of bed height for the various fluid systems containing nanoparticles**

## **6 Summary and discussion**

This section presents the summary and discussion for the thesis, comprising experimental part (Part I) and performance simulation part (Part II). The idea of the experimental part was to formulate a mud system containing nano particles that exhibited favorable rheology and filtrate properties. The viscoelastic properties of the obtained mud system were further investigated. In Part II, hydraulic performance and cutting transport for the selected fluid systems were conducted.

### **Part I: Rheology and Viscoelasticity**

#### **6.1 Effect of Xanthan concentration**

A screening test based on various amounts of polymer Xanthan in 500g H<sub>2</sub>O and 25g bentonite was conducted to select a system for further additives. The results showed that the fluid samples had increasing PV, AV, YS and k as the amount of Xanthan increased. According to Figure 5, an increase in plastic viscosity, yield and gel strength, as well as decrease in filter loss, indicated that the fluid system became more dispersed and flocculated. Based on the results from this test, the fluid system with 0.5g XC was selected for further additives. It was justified by observing the physical behavior of the fluids as well as economical aspects.

#### **6.2 Temperature effects on 0.5g XC fluid system**

For practical operations, to investigate how temperature affected the selected screening system, the system were heated up to 72, 120 and 150°F before Fann measurements. The results were in accordance with the expectations; the fluid systems became more viscous with increasing PV and AV as temperature raised.

### **6.3 Effect of KCl and NaCl on polymer system**

This study was undertaken to investigate how NaCl and KCl affected the polymer system. Comparing the potassium systems to the salt free system, increase in filter losses and decrease in YS was found, indicating that addition of KCl made the system more aggregated. The system with 2.5 g KCl was chosen over the NaCl systems, because of the inhibitive properties of the potassium ion.

### **6.4 Effect of nanoparticles on polymer system**

By introducing nanoparticles to the fluid systems significant changes were observed regarding rheological and filtrate properties. There were observed an increase in AV and YS for all nano fluid systems compared to the system without nano. The fluid system with the least amount of nanoparticles (0.1 g) exhibited the greatest change in AV and YS with 91.67% and 153.33% increase, respectively. Higher YS as well as increasing consistency index (k) and decreasing flow behavior index (n) for all the nano systems indicated that the addition of nano particles can provide better cutting transport than the fluid system without nano. Again, the system with 0.1g nano stood out with the greatest change in consistency and flow behavior index. Also, this system showed superior filtrate properties with a reduction of 16.67% filtrate compared to the system without nano. Based on the results from this experiment, the fluid system with 0.1g nano was selected for a viscoelasticity test for further investigation of its rheological properties.

### **6.5 Effect of salt types on Nano based system (NaCl and KCl)**

To investigate whether a mixture of salt types had positive effects on rheological properties on the nano fluid system, fluid samples with both KCl and NaCl were mixed. The amount of KCl was held constant as varying amounts of NaCl. The YS was found to be decreasing as the amount of NaCl was increasing. The fluid sample with 0.2g NaCl exhibited lower filter loss

than the reference fluid without NaCl. Unlike the YS, the “n” and “k” values were not consistent with regards to increasing NaCl.

## **6.6 Rheology Modeling and Analysis of nanoparticles fluid system**

Two nanoparticle fluid system (0.1g and 0.2g nano) and nano-free fluid were considered to study which rheology model described the shear stress-strain behaviour the best. The measured Fann data were compared with Newtonian and non-Newtonian models. The absolute average sum deviation between the models data and the measured data were calculated. The result obtained from 0.1g and 0.2g nano fluids showed that Robertson and Stiff exhibited the lowest % deviation, with 1.44% and 1.32%, respectively.

## **6.7 Viscoelasticity**

The oscillatory -amplitude and frequency sweep test were carried out on the selected 0.1g nano-treated mud system. Also, a similar mud system, without the presence of nano particles was tested for comparison. From the amplitude tests, yield point, flow point and LVE range was determined. One could observe a nearly identical behavior of the two fluid samples within the LVE range that was close to 1%. For both fluid samples, the Storage Modulus ( $G'$ ) was greater than the Loss Modulus ( $G''$ ) within the LVE range, indicating that the elastic portion was dominating. When exceeding LVE range the viscous portion became the dominant one. The flow point of the nano fluid was measured to be 26.73% higher than the reference fluid, whereas the YP of the fluids were nearly identical. As expected, comparing the measured YP's to the calculated YP's from Bingham model, major differences were seen, as the fluids are not behaving as a theoretical Bingham plastic fluid.

As for the oscillatory frequency test, the two fluid samples exhibited similar trends. The samples response to deformation was dominated by elastic

behavior, as the Storage Modulus was greater than the Loss Modulus for both fluids.

## **Part II: Performance simulation**

### **6.8 Hydraulics**

In order to evaluate how the rheology of the selected drilling fluids affected the ECD, the Unified model was chosen. For comparison of hydraulic behavior in this simulation, the formulated fluids (in section §4.4) containing various amounts of nano particles were considered. The results showed that all the fluids with nanoparticles exhibited higher annular pressure loss than the fluid system without nano. Clearly, the system with 0.1g showed the highest impact on the ECD but we observe that it flattens out as the flow rate is increased. The system with 0.3g nano affected the ECD the least with an increase of approximately 4.54%.

### **6.9 Cutting transport**

Poor hole cleaning can cause drilling related problems. In this thesis, a total of six rheology data of nano particles based fluids formulated in section §4.4 were used in a simulation setup on a deviated well to study minimum flow velocity and bed height (cutting deposition). The results showed that all the fluids containing nano particles exhibited lower minimum flow rate than the fluid with nano. A pump rate of 400 gpm was selected for bed height deposition. The best performance was done by fluid system with 0.1g nano, which had the lowest minimum flow rate and bed height composition. We observe that this system has a higher viscosity, allowing the particles to be transported instead of settled.

## 7 Conclusion

The main objective of this thesis was to come up with an improved fluid system by the use of nanotechnology. Several conventional (without nano) and nano based water based mud systems were formulated and tested. The systems were evaluated in various concentration of polymer, KCL and NaCl.

After several attempts, the composition of the best nano-system obtained is:  
*500g H<sub>2</sub>O+ 25g Bentonite+ 0.5g XC+ 2.5g KCl+ 0.1g Nano silica*

Based on the experimental part, viscoelasticity test and simulations the following conclusions can be drawn.

- As the amount of KCl additives increases in XC polymer system (nano-free), the shear stress of Fann measured data shift downward. As a result a decrease in YS and PV is observed, as well as an increase in filter losses.
- Unlike KCl, the addition of 2.5g and 5g NaCl shift Fann measured data upward and downward from the reference systems, respectively.
- The addition of nanoparticles to the polymer system (with KCl) showed higher shear stress for all amounts of nanoparticles that were added in the experiment.
- Significant increases in AV and YS were seen for especially two of the nano fluid systems, the system with 0.1g and 0.2g nano. Also, Power Law parameters indicated a substantial increase in consistency index (k) and decreasing flow behaviour index (n).
- The highest filtrate reduction was obtained from the system treated with 0.1g nano particles. The reduction was by 16.67% as compared with the nano-free system.
- Results from the oscillatory tests indicated that the nano-treated fluid exhibited similar viscoelastic behavior as the nano free fluid system.



- In the hydraulic performance simulation, all the fluids containing nanoparticles exhibited higher annular pressure losses than the system without nano particles. The fluid with 0.1g nano particles was highly viscous. It showed a higher annular pressure loss.
- During cutting transport simulation all the fluids containing various amounts of nano particles proved better performances than the nano untreated fluid, exhibiting lower minimum flow rates and bed height composition.
- Out of the considered nano treated systems, the 0.1g nano treated system shows the best transport efficiency.

## References

- [1] Aadnøy, B.S. and Looyeh, R. (2010) Petroleum Rock Mechanics. USA: Elsevier's Science.
- [2] Aadnøy, B.S. (1998) "Geomechanical Analysis for Deep-water Drilling", SPE 39339, presented at the IADC/SPE Drilling Conference, Dallas, TX, 3 - 6 March.
- [3] Fjær, E. et al. (2008) Petroleum Related Rock Mechanics. UK: Elsevier's science.
- [4] Versan, M. and Tolga, A. (2005) "Effect of Polymers on the Rheological properties of KCl/Polymer Type Drilling Fluid" Energy Sources, 27(5), pp. 405-415.
- [5] Kaarstad, E. and Aadnoy, B.S. (2006) "Fracture Model for General Offshore Applications", SPE 101178, presented at 2006 SPE Asia Pacific Oil and Gas Conference and Exhibition, Adelaide, Australia, 11-13 September.
- [6] Skjeggstad, O. (1989) Boreslamteknologi: teori og praksis, Bergen: Alma Mater forlag.
- [7] Xiuhua, Z. and Xiaochun, M. (2010) Drilling Fluids. China: Prospection and Technology Institute.
- [8] Caenn, R. et al. (2011) Compostion and properties of drilling and completion fluids. USA: Elsevier Inc.
- [9] MI SWACO (1998) Drilling fluids and Engineering handbook.

- [10] Olad, A. (2011) “Polymer/ Clay Nanocomposites”, Reddy, B. (ed.) Advances in Diverse Industrial Applications of Nanocomposites, Croatia: InTech, pp. 113-138.
- [11] Zakaria, M. Husein, M.M. Harland, G. (2012) “Novel Nanoparticle-Based Drilling Fluid with Improved Characteristics”, SPE-156992-MS, SPE International Oilfield Nanotechnology Conference and Exhibition, 12-14 June, Noordwijk, The Netherlands.
- [12] Belayneh, M. (2013) PET 525 Advanced drilling lecture note, [Lecture].
- [13] Nwosu, O.U. and Ewulonu, C. M. (2014) “Rheological Behaviour of Eco-friendly Drilling Fluids from Biopolymers”, Journal of Polymer and Biopolymer Physics Chemistry, 2(3), pp. 50-54.
- [14] Bourgoyne jr., A.T. et al. (1986) SPE Textbook Series, Volume 2: Applied Drilling Engineering. Texas: Society of Petroleum Engineers.
- [15] Ochoa, M.V. (2006) Analysis of Drilling Fluid Rheology and Tool Joint Effect to Reduce Errors in Hydraulics Calculations. PhD Thesis. Texas: A&M University.
- [16] Skaugen, E. (1997) Kompendium i boring, Høyskolen i Stavanger, Stavanger.
- [17] Strand, S. (1998) Øvinger i bore- og brønnvæsker, Høyskolen i Stavanger, Stavanger.
- [18] Mitchell, R. F. Miska, S. Z. & Aadnoy, B.S. (2011) SPE Textbook Series, Volume 12: Fundamentals of Drilling Engineering. Texas: Society of Petroleum Engineers.

- [19] EPRUI Nanoparticles and Microspheres Co. Ltd. (2015) Available at:  
<http://www.nanoparticles-microspheres.com> (Accessed: 15.03.15).
- [20] WellPlan (Landmark)<sup>TM</sup> Software, Halliburton.
- [21] Nazari, T. Hareland, G. and Azar J.J. (2010) “A Review of Cuttings Transport in Directional Well Drilling: Systematic Approach”, SPE 132372, SPE Western Regional Meeting, Anaheim, California, U.S.A, 27-29 May.
- [22] Piroozian, A. et al. (2012) “Impact of drilling fluid viscosity, velocity and hole inclination on cuttings transport in horizontal and highly deviated wells”, Journal of Petroleum Exploration and Production Technology, 2(3), pp. 149-156.
- [23] Torbjørnsen, K. (1994) Borevæsketeknologi. Norway: Vett & Viten A/S.
- [24] Saasen, A. and Løklingholm, G. (2002) “The Effect of Drilling Fluid Rheological Properties on Hole Cleaning”, SPE-74558-MS, IADC/SPE Drilling Conference, 26-28 February, Dallas, Texas.
- [25] Binh, B. Saasen, A. Maxey, J. et al. (2012) “Viscoelastic Properties of Oil-Based Drilling Fluids” Annual Transactions of the Nordic Rheology Society. Vol 20.
- [26] Mezger, T.G. (2011) The Rheology Handbook. Hanover: European Coating Tech Files.
- [27] Fann viscometer (2015) Available at:  
[http://www.glossary.oilfield.slb.com/en/Terms/f/fann\\_viscometer.aspx](http://www.glossary.oilfield.slb.com/en/Terms/f/fann_viscometer.aspx)  
(Accessed: 23.04.15).

- [28] Amandullah, Md. Al-Arfaj, M.K. Al-Abdullatif, Z.A. (2011) “Preliminary Test Results of Nano-based Drilling Fluids for Oil and Gas Field Application”, SPE-139534-MS, SPE/IADC Drilling Conference and Exhibition, 1-3 March, Amsterdam, The Netherlands.
- [29] Kelco Oil Field Group (2005) “Drilling Fluid Rheology, “n” and “K” Applications” Technical bulletin.
- [30] Khodja, M. Khodja-Saber, M. Canselier, J.P. Cohaut, N. Bergaye, F. (2010) “Drilling Fluid Technology: Performances and Environmental Considerations” Fuerstner I. (ed.) Products and Services; from R&D to Final Solutions, Publisher: Sciyo.
- [31] Aadnøy, B.S. (2010) Modern Well Design. CRC Press.
- [32] Fundamentals of Onshore Drilling (2015) Available at: [http://geologie.vsb.cz/DRILLING/drilling/presentations/presentation\\_No\\_5.pdf](http://geologie.vsb.cz/DRILLING/drilling/presentations/presentation_No_5.pdf) (Accessed: 16.04.15).
- [33] Aston, M.S. Alberty, M.W et al. (2004) “Drilling Fluids for Wellbore Strengthening”, SPE-87130-MS, IADC/SPE Drilling Conference, 2-4 March, Dallas, Texas.
- [34] Aadnøy, B.S. et al. (2008) “Design of Well Barriers To Combat Circulation Losses”, SPE-105449-PA.
- [35] Nwaoji, C.O. Hareland, G. Husein, M. Nygaard, R. Zakaria, M.F. (2013) “Wellbore Strengthening- Nano-Particle Drilling Fluid Experimental Design Using Hydraulic Fracture Apparatus”, SPE 163434 presented at SPE / IADC Drilling Conference and Exhibition, Mar 05 - 07, 2013 2013, Amsterdam, The Netherlands.

- [36] Sharma, M.M. Zhang, R. Chenevert, M.E. Ji, L. Guo, Q. Friedheim, J. (2012) “A New Family of Nanoparticle Based Drilling Fluids” SPE 160045 presented at the SPE Annual Technical Conference and Exhibition held in San Antonio, Texas, USA, 8-10 October.
- [37] Ramadan, A. M. (2001) Solids Bed Removal in Deviated Boreholes. PhD thesis.
- [38] Amanullah, Md. and Al-Tahini, A.M. (2009) “Nano-technology-Its Significant in Smart Fluid Development for Oil and Gas field Application”, SPE-126102-MS, SPE Saudi Arabia Section Technical Symposium, 9-11 May, Al-Khobar, Saudi Arabia.

## Abbreviations

API – American Petroleum Institute  
AV – Apparent viscosity  
XC – Xantam gum  
CaCO<sub>3</sub> – Calcium carbonate  
CEC – Cation Exchange capacity  
CMC – Carboxyl methyl cellulose  
CTFV – Critical transport fluid velocity  
DF – Drilling Fluid  
ECD – Equivalent circulation density  
EDS – Elemental Dispersive Spectroscopy  
Fe – Iron  
G' – Storage modulus  
G'' – Loss modulus  
gel – Gel strength  
gpm – Gallons per minute  
k – Consistency index  
K – Potassium  
KCl – Potassium chloride  
LCM – Loss circulation materials  
Li – Lithium  
LPLT – Low Pressure Low Temperature  
LVE – Linear viscoelastic  
M – C – Mohr-Coulomb  
Mg – Magnesium  
n – Flow behaviour index  
NaCl – Sodium Chloride  
NP – Nano particle  
O – Oxygen  
OBM – Oil Based Mud  
OH – Hydroxide

PAC – Polyanionic celluloses

Pd – Palladium

PV – Plastic viscosity

ROP – Rate of penetration

RPM – Revolutions per minute

S.G – Specific gravity

SEM – Scanning Electron Microscopy

Si – Silicon

TVD – True vertical depth

WBM – Water Based Mud

YP – Yield Point

YS – Yield Strength



## Nomenclature

- A - Model parameter  
B - Model parameter  
C - Model parameter  
 $C_D$  - Particle drag coefficient  
D - Hydraulic diameter of the pipe  
 $d_p$  - Particle diameter  
g - Gram  
g - Gravity  
k - Consistency index  
n - Flow behaviour index  
 $P_w$  - Well pressure  
 $P_0$  - Pore pressure  
 $P_0$  - Pore pressure  
 $P_{wf}$  - Fracturing pressure  
 $P_y$  - Plasticity term  
Q - Pump rate  
Re - Reynolds number  
 $V_s$  - Settling velocity  
V - Mean fluid velocity  
 $\delta$  - Phase shift angel  
 $\tan(\delta)$  - Damping factor  
 $\rho_{st}$  - Static mud density  
 $\rho_p$  - Density of particle  
 $\rho_f$  - Fluid density  
 $\rho$  - Fluid density  
 $\gamma$  - Shear rate  
 $\mu$  - Dynamic viscosity of fluid  
 $\mu_p$  - Plastic viscosity  
 $\sigma$  - In situ stress, external load  
 $\sigma_h$  - Minimum horizontal stress

$\sigma_H$  - Maximum horizontal stress

$\sigma_t$  - Tensile rock strength

$\tau$  - Shear stress

$\tau_y$  - Yield point, Bingham

$\tau_o$  - Yield point, Herschel Buckley

$\tau_{min}$  - Minimum shear strain

$\tau_{max}$  - Maximum shear strain

$\gamma_{min}$  - Minimum shear rate

$\gamma_{max}$  - Maximum shear rate

$\tau_{yL}$  - Lower shear yield point

$\nu$  - Poisson's ratio

$\Delta P_s$  - Pressure loss in surface equipment

$\Delta P_{ds}$  - Pressure loss inside the drill string

$\Delta P_b$  - Pressure loss across the bit

$\Delta P_p$  - Pump pressure

$\Delta P_{annulus}$  - Pressure loss in the annulus

Wt.% - Weight percent

# List of Figures

Figure 1: Drilling fluid circulation system [30]	8
Figure 2: Median line principle weight selection [31]	9
Figure 3: Mud invasion [17]	10
Figure 4: Investigation methodology	13
Figure 5: Different behaviors of clay pellets with respect to rheology and filtrate of fluid systems [32]	13
Figure 6: Compressive and tensile failure in shale formation [3]	15
Figure 7: The penetrating model [2]	16
Figure 8: The non-penetrating model [2]	17
Figure 9: Lost circulation formations [18]	19
Figure 10: Stress cage concept to enhance wellbore strength [33]	20
Figure 11: Description of the filtrate cake formation, fracture process and bridging mechanisms. [34]	21
Figure 12: Schematic representation of flocculation and deflocculating, dispersed and aggregation mechanisms [8]	25
Figure 13: Simple Octahedron structure. Oxygen and aluminum atoms [6]	27
Figure 14: Simple tetrahedral structure. Oxygen and Silicon atoms. [6]	27
Figure 15: Tetrahedral sheet with octahedron sheet in the middle [6]	28
Figure 16: Distribution of charges in a montmorillonite crystal [6]	29
Figure 17: Effect of cation concentration and species on linear swelling. Clay mineral analysis of shale: 9.2% montmorillonite, 11.2% mixed layer, 35% illinite, 5.5% chlorite, 4.4% kaolonite.	30
Figure 18: Structure of polymers: a) linear b) branched c) cross linked [6]	32
Figure 19: Structure of Xanthan gum [8]	33
Figure 20: Surface area to volume ratio versus particle diameters [38]	34
Figure 21: Mud cakes of commercial and in house nano particles [11]	35
Figure 22: Rheological models [12]	41
Figure 23: Periodic oscillations illustrated by two plate model [26]	46
Figure 24: Oscillatory test showing viscoelastic behaviour [26]	47
Figure 25: Left figure: Illustrates a strain amplitude showing a gel-like character in the LVE range. Right figure: Illustrates a strain amplitude sweep of a sample showing the character of a viscoelastic liquid in the LVE range. [26]	48
Figure 26: Pressure drop [12]	49
Figure 27: Drilling Fluid Circulation System [15]	50
Figure 28: Forces acting on a single particle at an active erosion site of a cutting bed [37]	52
Figure 29: Parts of Fann VG 35 viscometer [27]	55
Figure 30: Photograph picture of API filter test	56
Figure 31: Photograph picture of density measuring equipment	56
Figure 32: Element analysis of Nano- Silica	57
Figure 33: SEM picture of Nano- Silica	58
Figure 34: Rheology measurements for screening test at 72°F	60
Figure 35: Consistency index (k) for screening system at 72, 120 and 150 °F	62
Figure 36: Flow behaviors flow index (n) for screening system at 72, 120 and 150 °F	62
Figure 37: Plastic viscosity for screening system at 72, 120 and 150 °F	63
Figure 38: Apparent viscosity for screening system at 72,120 and 150 °F	63
Figure 39: Yield strength for screening system at 72, 120 and 150 °F	64
Figure 40: Rheology measurements for REF+ 0,5gXC at 72, 120 and 150 °F	66
Figure 41: Rheology measurements for REF+0,5gXC system with various amounts of salt. (72 °F)	68
Figure 42: Rheology measurements for REF+ 0,5gXC +2,5gKCl and various amounts of nano	71
Figure 43: Mud cake from fluid system with 0.1g nanoparticles	73
Figure 44: Rheology measurements for 0.2g nano system with various amounts of NaCl	75
Figure 45: Anton Paar rheometer	76
Figure 46: Plots showing amplitude sweep for the two fluid systems.	77

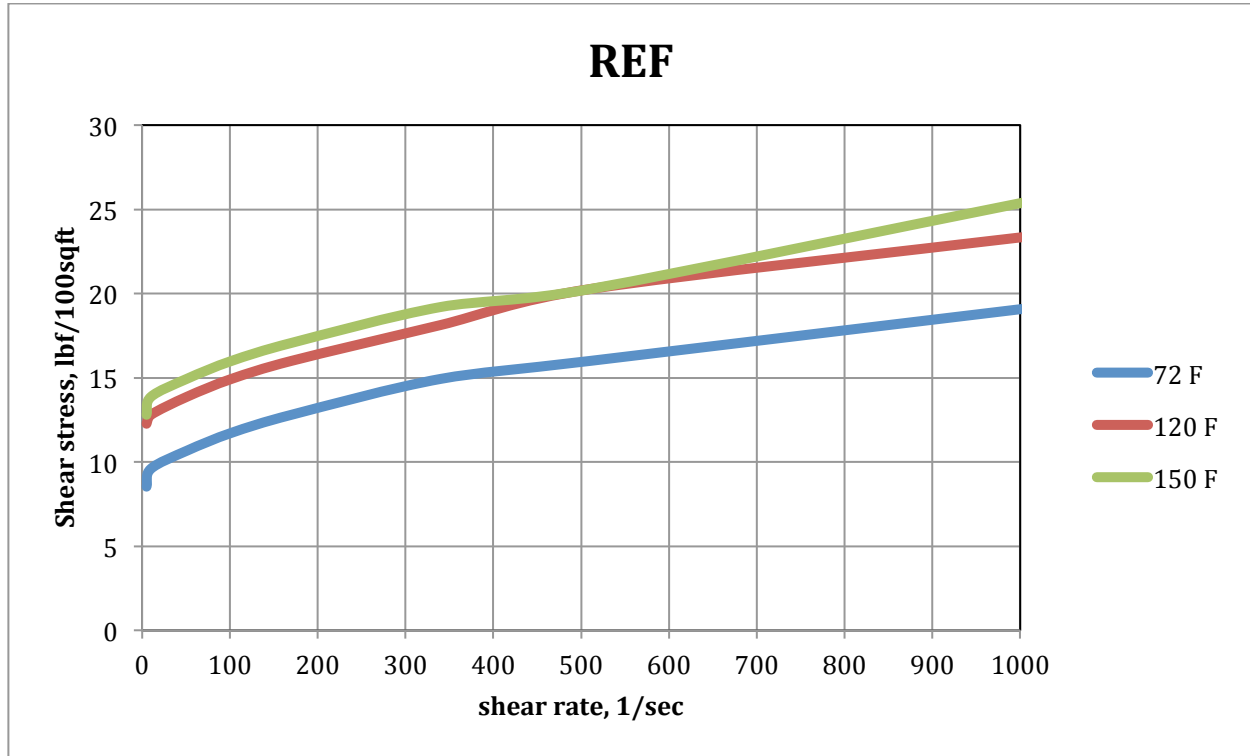
<b>Figure 47: Comparison of fluids with and without nanoparticles, oscillatory frequency sweep test</b>	<b>79</b>
<b>Figure 48: Comparison of the different rheology models %deviation to the reference system</b>	<b>81</b>
<b>Figure 49: Comparison of the different rheology models with REF + 0,1g nano silica at 72 °F</b>	<b>81</b>
<b>Figure 50: Illustration of well for hydraulic simulations</b>	<b>84</b>
<b>Figure 51: Comparison of annular pressure loss at increasing flowrate for fluid samples containing various amounts of nanoparticles, based on the Unified model</b>	<b>85</b>
<b>Figure 52: %ECD increase from reference system</b>	<b>86</b>
<b>Figure 53: Experimental well for simulation</b>	<b>87</b>
<b>Figure 54: Comparison of the minimum flow rate for the different fluid systems with nano particles</b>	<b>89</b>
<b>Figure 55: Comparison of bed height for the various fluid systems containing nanoparticles</b>	<b>91</b>
<b>A1-Figure 56: Fann data for reference system at 72, 120 and 150°F</b>	<b>110</b>
<b>A2-Figure 57: Rheology parameters for REF system at 72, 120 and 150°F</b>	<b>110</b>
<b>A3-Figure 58: Fann data for REF + 0,75gXC at 72, 120 and 150°F</b>	<b>111</b>
<b>A4-Figure 59: Rheology parameters for REF + 0,75gXC at 72, 120 and 150°F</b>	<b>111</b>
<b>A5-Figure 60: Fann data for REF+ 1,0gXC at 72, 120 and 150 °F</b>	<b>112</b>
<b>A6-Figure 61: Rheology parameters for REF + 1,0gXC at 72, 120 and 150 °F</b>	<b>112</b>
<b>A7-Figure 62: Fann data for REF + 1,5gXC at 72, 120 and 150 °F</b>	<b>113</b>
<b>A8-Figure 63: Rheology parameters for REF +1,5gXC at 72, 120 and 150°F</b>	<b>113</b>
<b>B1-Figure 64: Fann data for REF+ 4gNaCl and REF + 4gNaCl+ 0,5gNano at 72, 100 and 130 °F</b>	<b>114</b>
<b>B2-Figure 65: Rheology parameters for REF + 4gNaCl and REF + 4gNaCl+ 0,5gNano at 72°F</b>	<b>114</b>
<b>B3-Figure 66: Rheology parameters for REF + 4gNaCl and REF + 4gNaCl+ 0,5gNano at 100 °F</b>	<b>115</b>
<b>B4-Figure 67: Rheology parameters for REF + 4gNaCl and REF + 4gNaCl+ 0,5gNano at 130°F</b>	<b>115</b>
<b>B5-Figure 68: Comparison filtrate loss of REF + 4gNaCl and REF + 4gNaCl + 0,5gNano</b>	<b>116</b>
<b>C1-Figure 69: Fann data for REF + 0,5gXC and REF + 0,5gXC + 0,5gNano at 72°F</b>	<b>117</b>
<b>C2-Figure 70: Rheology parameters for REF + 0,5gXC and REF + 0,5gXC + 0,5gNano at 72°F</b>	<b>117</b>
<b>C3-Figure 71: Comparison filter loss for REF + 0,5gXC and REF +0,5gXC + 0,5gNano</b>	<b>118</b>
<b>D1-Figure 72: Fann data for REF+ 4gNaCl + 0,5gXC and REF + 4gNaCl +0,5gXC +0,5gNano at 72, 100 and 130°F</b>	<b>119</b>
<b>D2-Figure 73: Rheology parameters for REF+ 4gNaCl + 0,5gXC and REF + 4gNaCl +0,5gXC +0,5gNano at 72°F</b>	<b>119</b>
<b>D3-Figure 74: Rheology parameters for REF+ 4gNaCl + 0,5gXC and REF + 4gNaCl +0,5gXC+ 0,5gNano at 100 °F</b>	<b>120</b>
<b>D4-Figure 75: Rheology parameters for REF+ 4gNaCl + 0,5gXC and REF + 4gNaCl +0,5gXC + 0,5gNano at 130 °F</b>	<b>120</b>
<b>D5-Figure 76: Comparison filtrate loss for REF+ 4gNaCl+ 0,5gXC and REF+ 4gNaCl +0,5gXC +0,5gNano</b>	<b>121</b>
<b>F3-Figure 77: Well inclination for the simulation</b>	<b>126</b>

# List of Tables

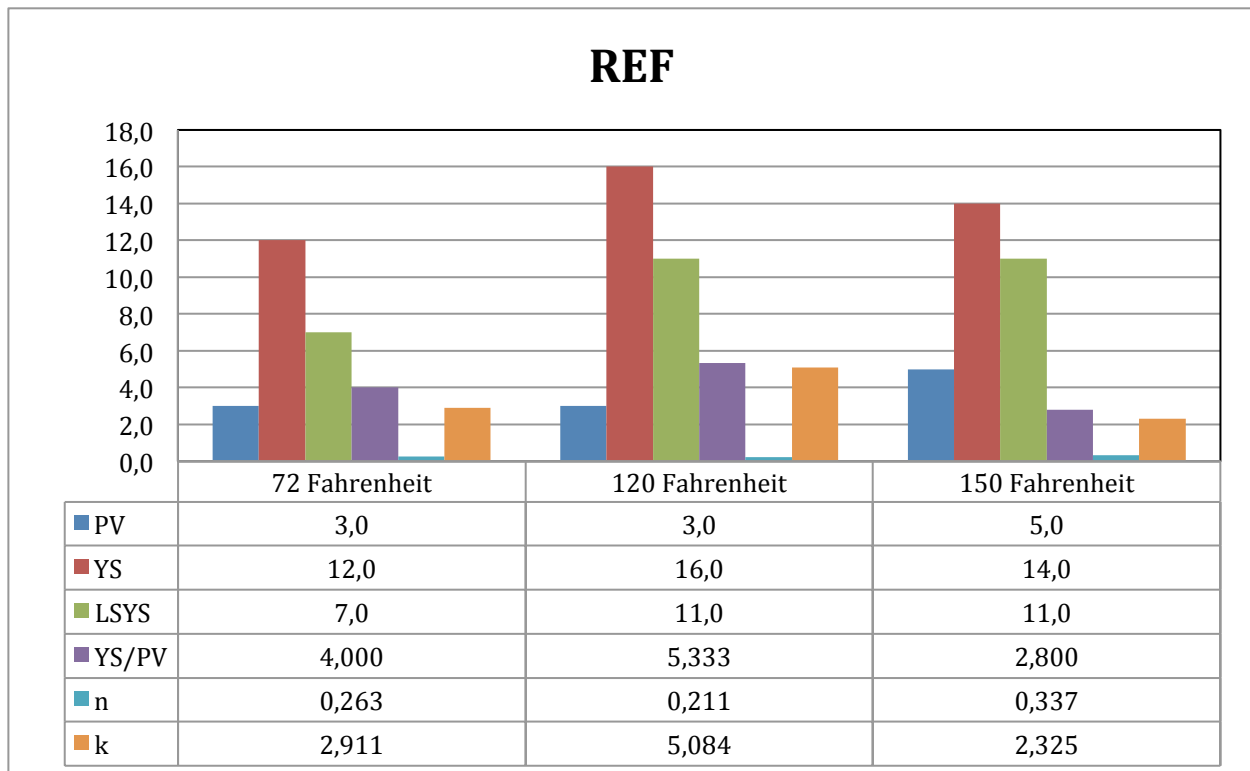
<b>Table 1: API LPLT Fluid loss of drilling samples using commercial nanoparticles [11]</b>	<b>36</b>
<b>Table 2: Comparative study of API LPLT fluid loss property of in-house prepared nanoparticle and drilling fluids [11]</b>	<b>36</b>
<b>Table 3: Fluid sample composition of screening test</b>	<b>59</b>
<b>Table 4: Extracted parameters from screening test performed at 72 °F</b>	<b>61</b>
<b>Table 5: Fluid sample composition of screening test</b>	<b>65</b>
<b>Table 6: Extrated parameters for REF + 0,5gXC system at 72,120 and 150 °F</b>	<b>67</b>
<b>Table 7: Fluid composition for reference system + 0,5gXC with various amounts of NaCl and KCl</b>	<b>67</b>
<b>Table 8: Extracted paramters for REF + 0,5gXC with various amounts of salt</b>	<b>69</b>
<b>Table 9: Fluid composition for polymer system (with KCL) with various amounts of nano particles</b>	<b>70</b>
<b>Table 10: Extracted parameters for REF + 0,5g XC + 2,5g KCl with various amounts of nanoparticles</b>	<b>73</b>
<b>Table 11: Fluid composition for 0.2g nano fluid system with various amounts of NaCl</b>	<b>74</b>
<b>Table 12: Extracted parameters for 0,2g nano particles with various amounts NaCl</b>	<b>75</b>
<b>Table 13: Fluid composition for viscoelasticity test</b>	<b>76</b>
<b>Table 14: Comparison of flow points for the two fluids by Anton Paar instrument</b>	<b>78</b>
<b>Table 15: Comparison of the yield point calculated by the Anton Paar instrument and the Bingham model for both fluids</b>	<b>78</b>
<b>Table 16: Rheology models and parameters for Ref fluid system</b>	<b>82</b>
<b>Table 17: Rheology models and parameters for Ref + 0,1g nano</b>	<b>82</b>
<b>Table 18: Rheology models and parameters for Ref + 0,2g nano</b>	<b>82</b>
<b>Table 19: Fann 35 data for the simulation</b>	<b>84</b>
<b>Table 20: Fann 35 data for the simulation</b>	<b>88</b>
<b>Table 21: Transport Analysis data: minimum flow rate</b>	<b>89</b>
<b>Table 22: Transport analysis data: Bed height</b>	<b>90</b>
<b>E1-Table 23: Summary of Unified hydraulics model [15]</b>	<b>124</b>
<b>F1-Table 24: Hole data (Casing + open hole)</b>	<b>125</b>
<b>F2-Table 25: Drill String data (Drill pipe + BHA)</b>	<b>125</b>

# Appendix

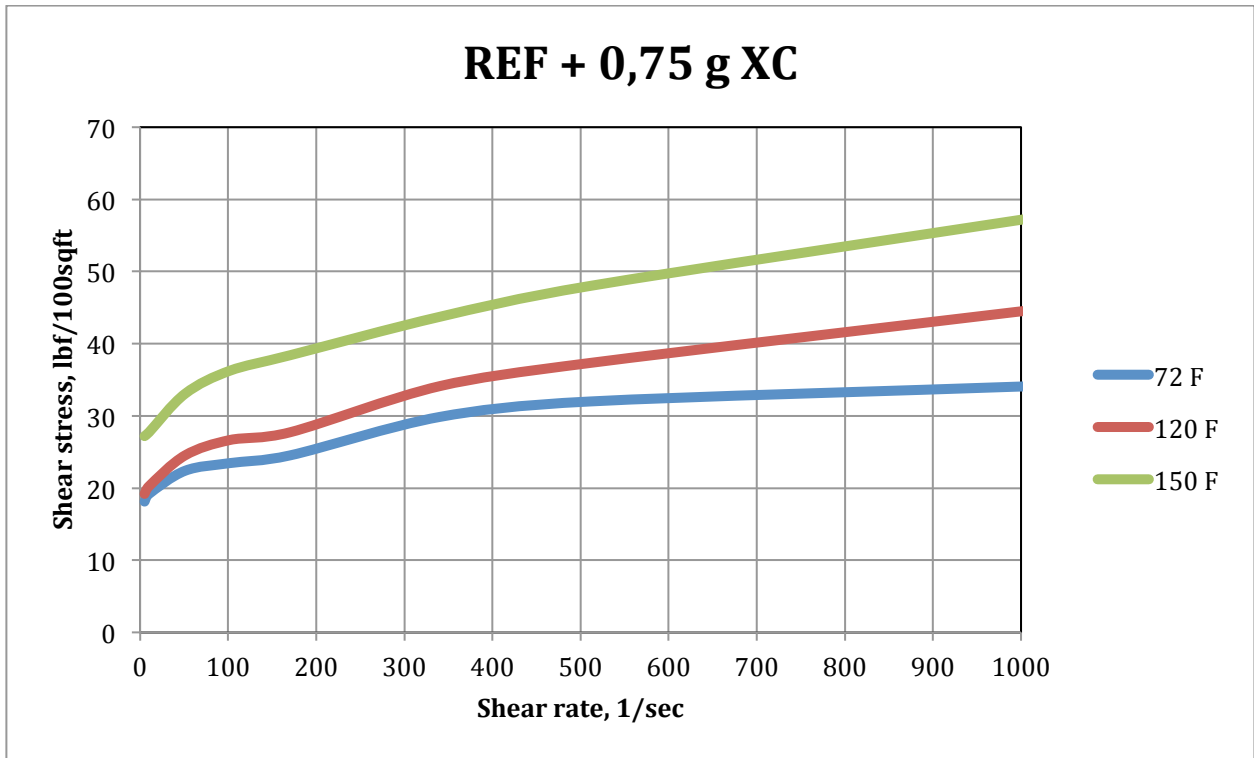
## Appendix A: Effect of temperature on polymer system



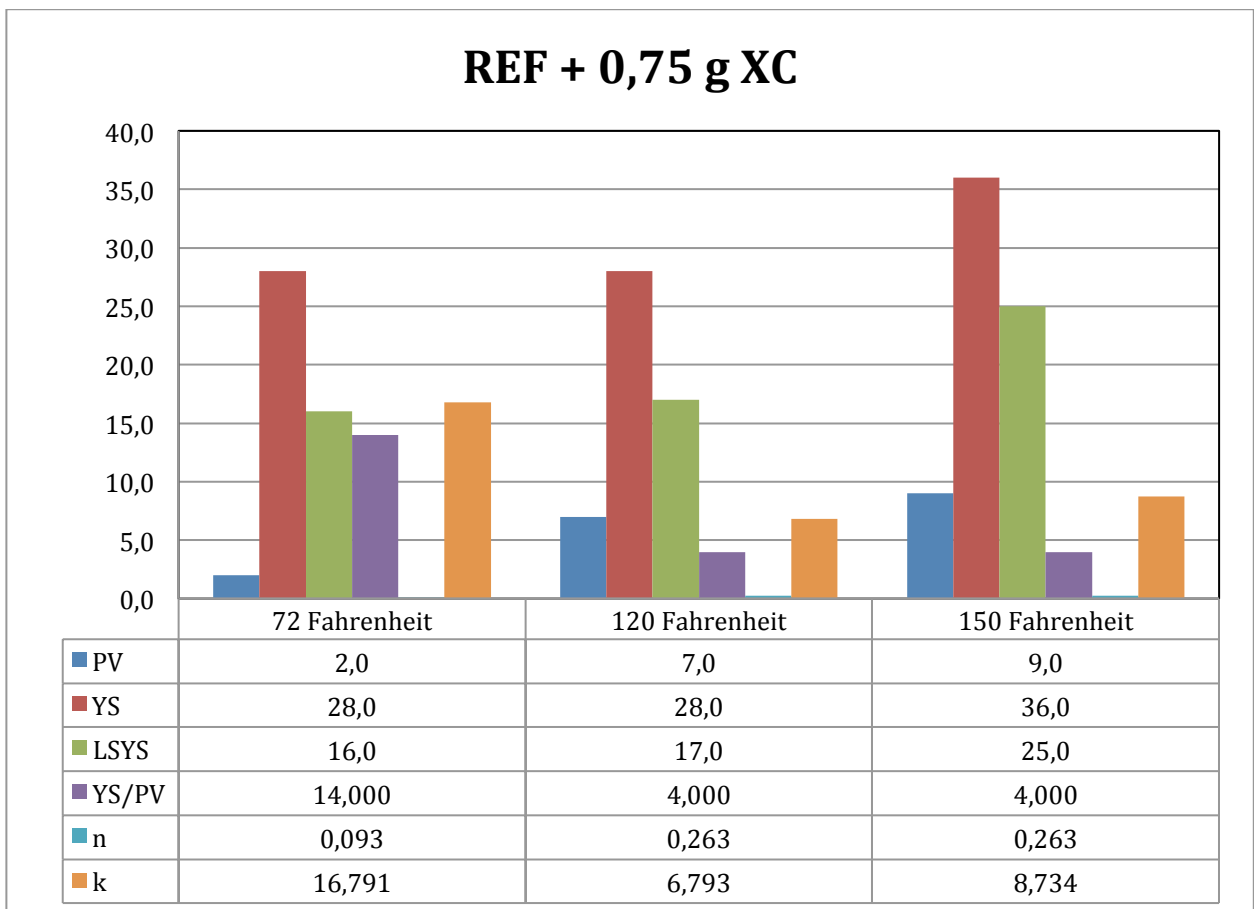
A1-Figure 56: Fann data for reference system at 72, 120 and 150°F



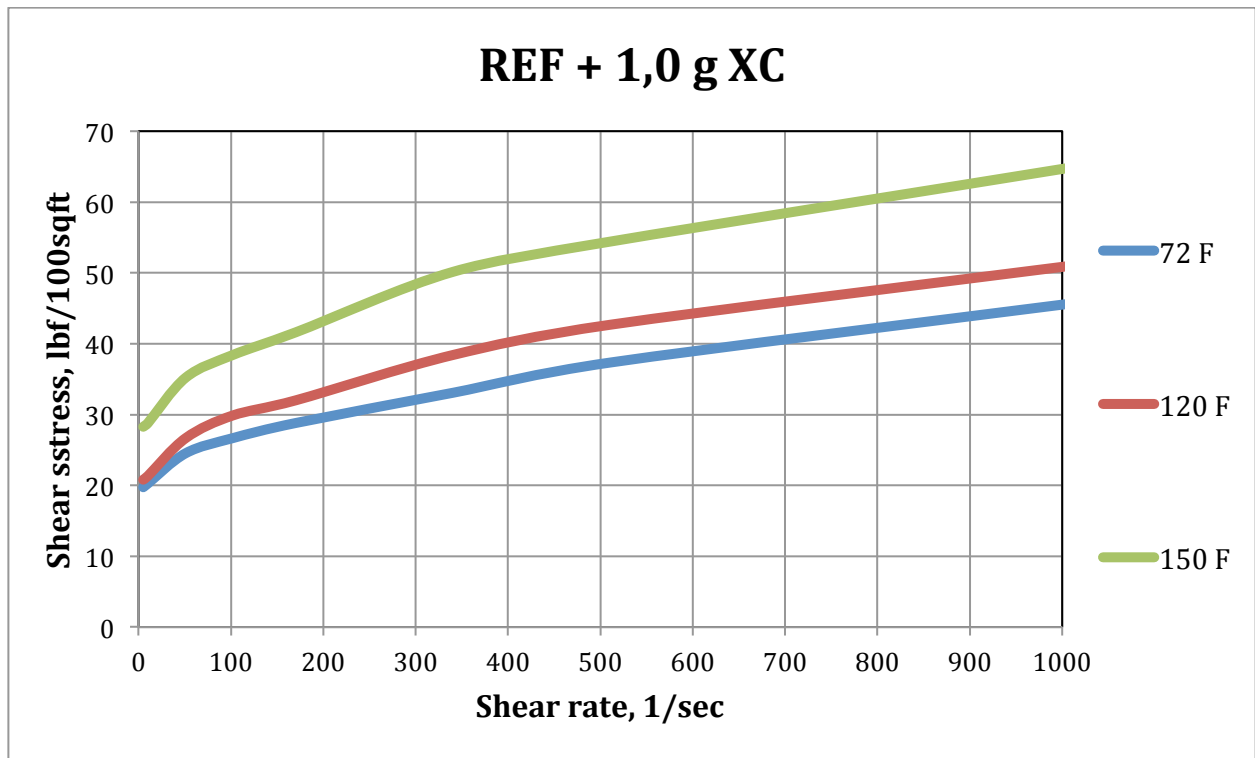
A2-Figure 57: Rheology parameters for REF system at 72, 120 and 150°F



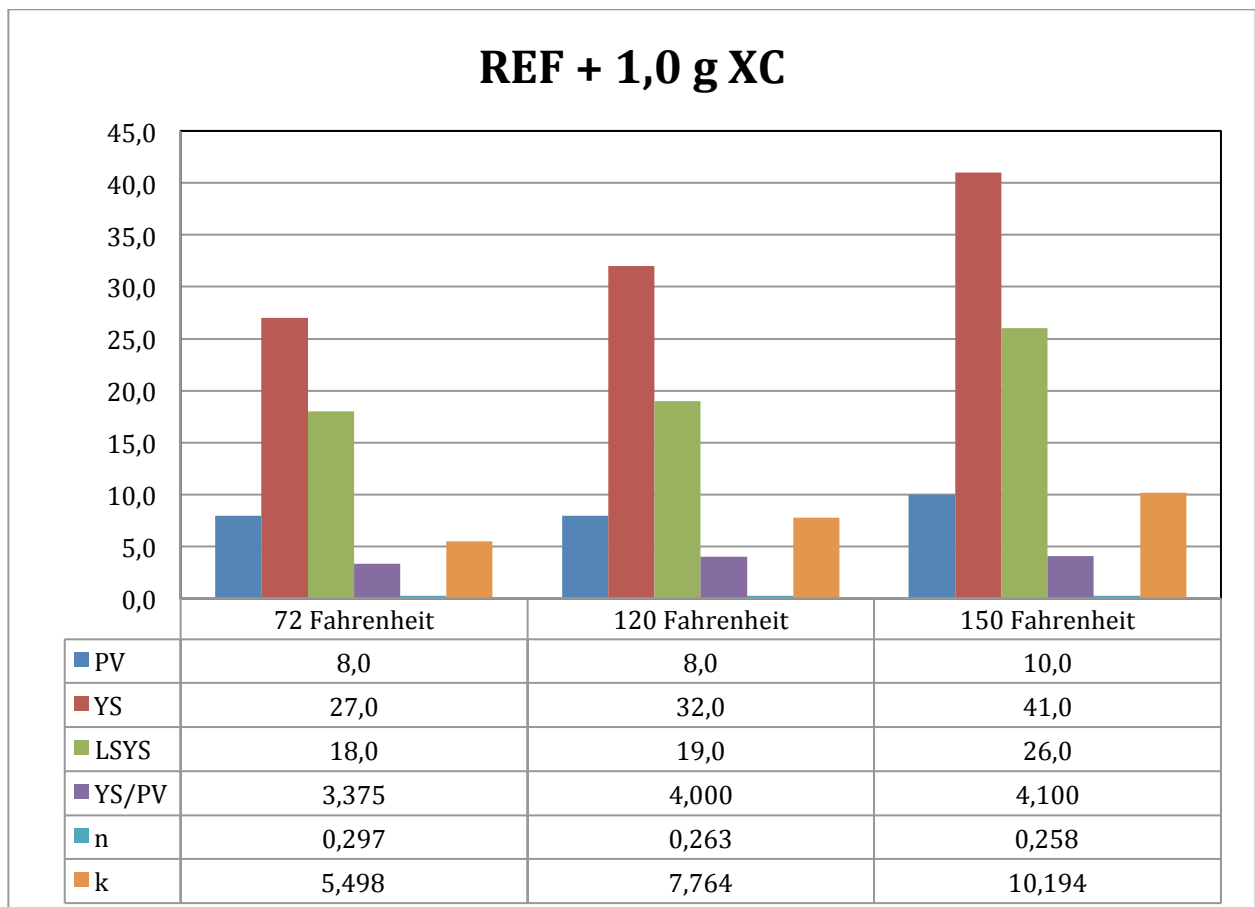
**A3-Figure 58: Fann data for REF + 0,75gXC at 72, 120 and 150°F**



**A4-Figure 59: Rheology parameters for REF + 0,75gXC at 72, 120 and 150°F**

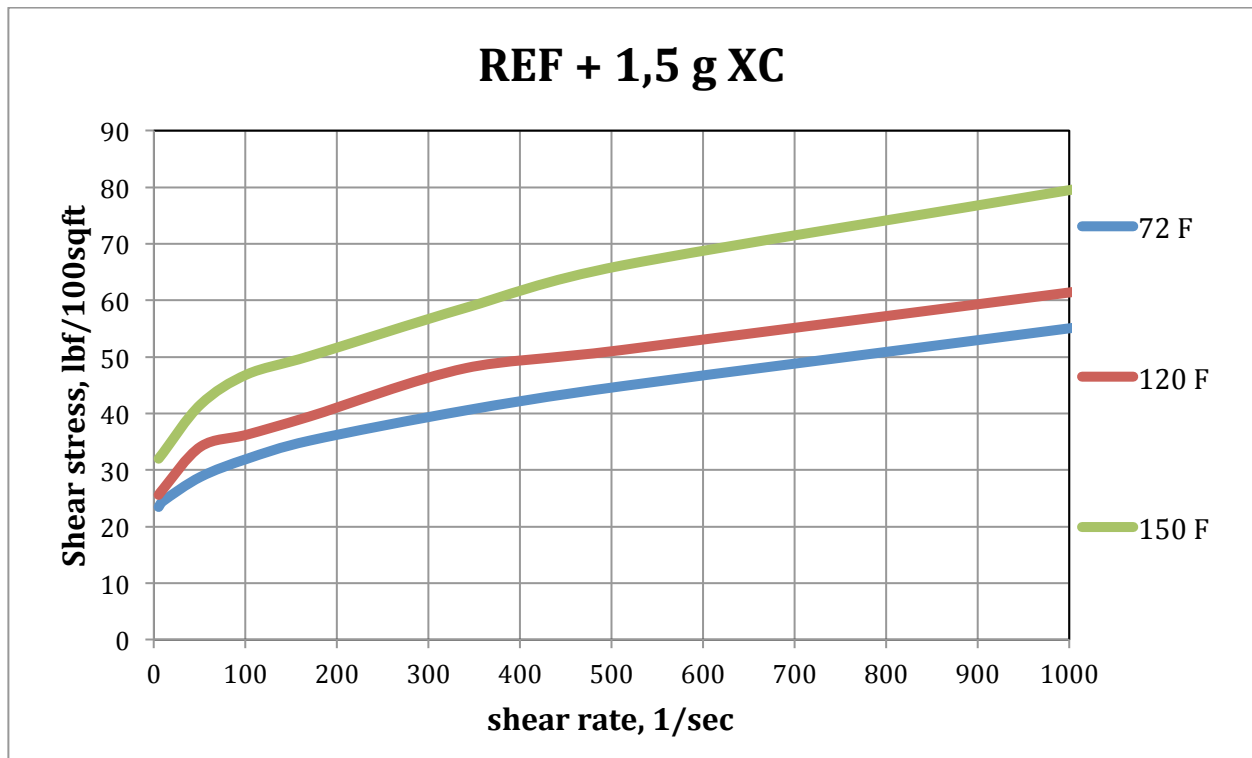


A5-Figure 60: Fann data for REF+ 1,0gXC at 72, 120 and 150 °F

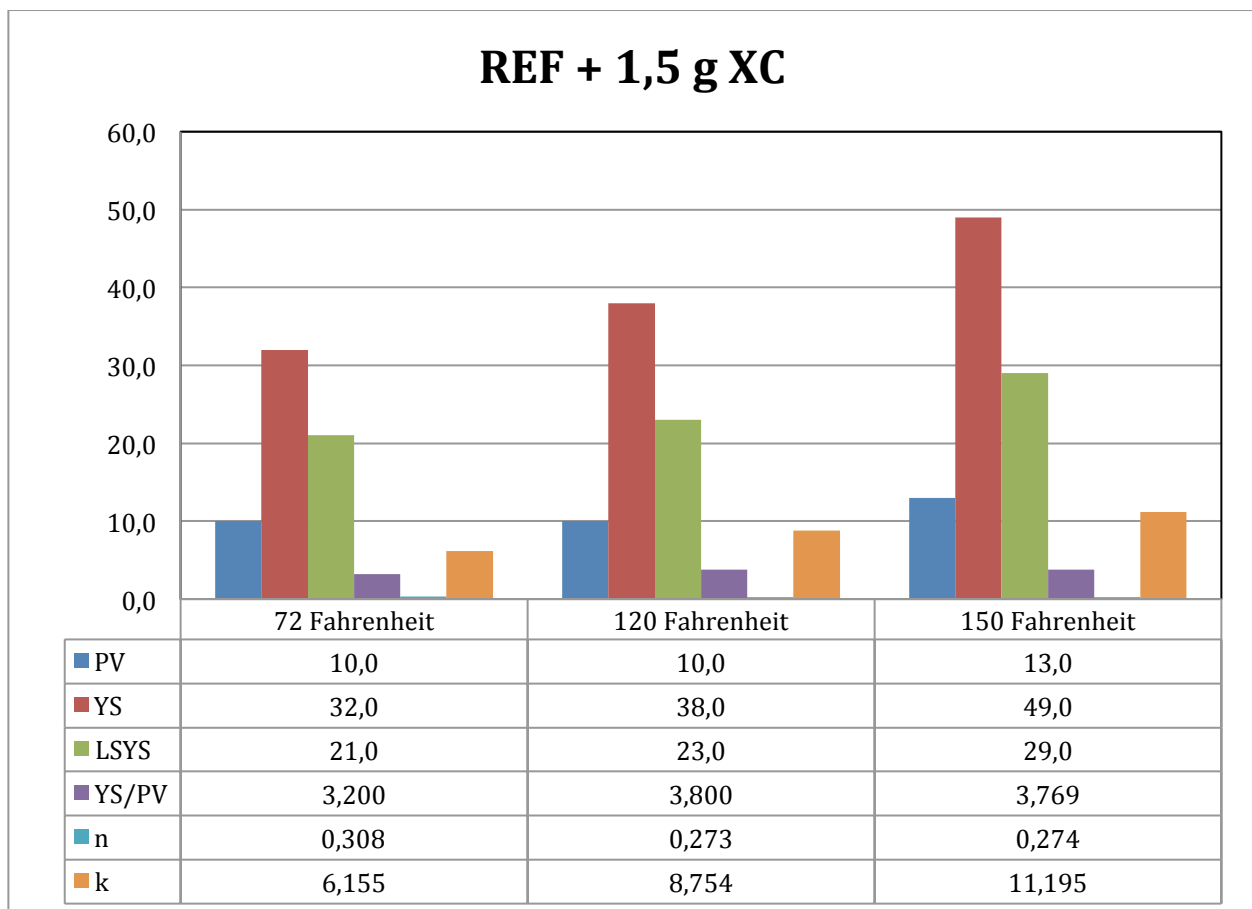


A6-Figure 61: Rheology parameters for REF + 1,0gXC at 72, 120 and 150 °F



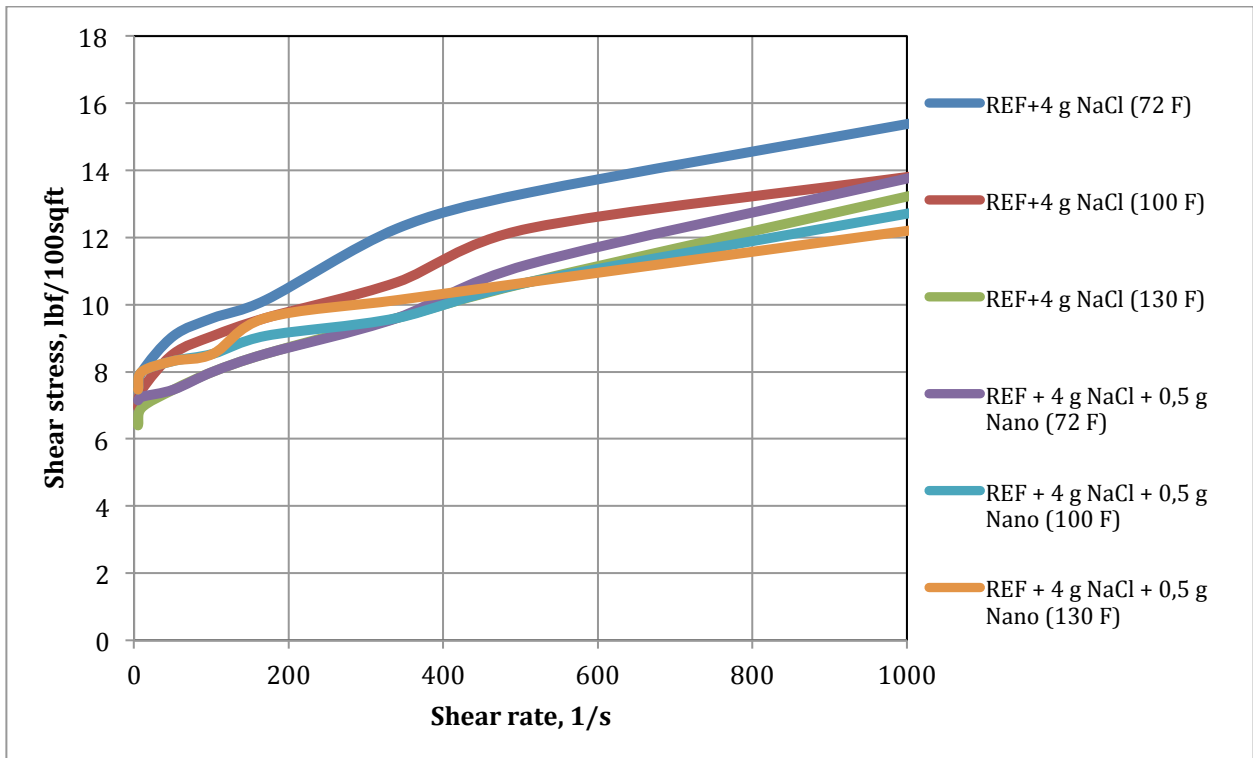


A7-Figure 62: Fann data for REF + 1,5gXC at 72, 120 and 150 °F

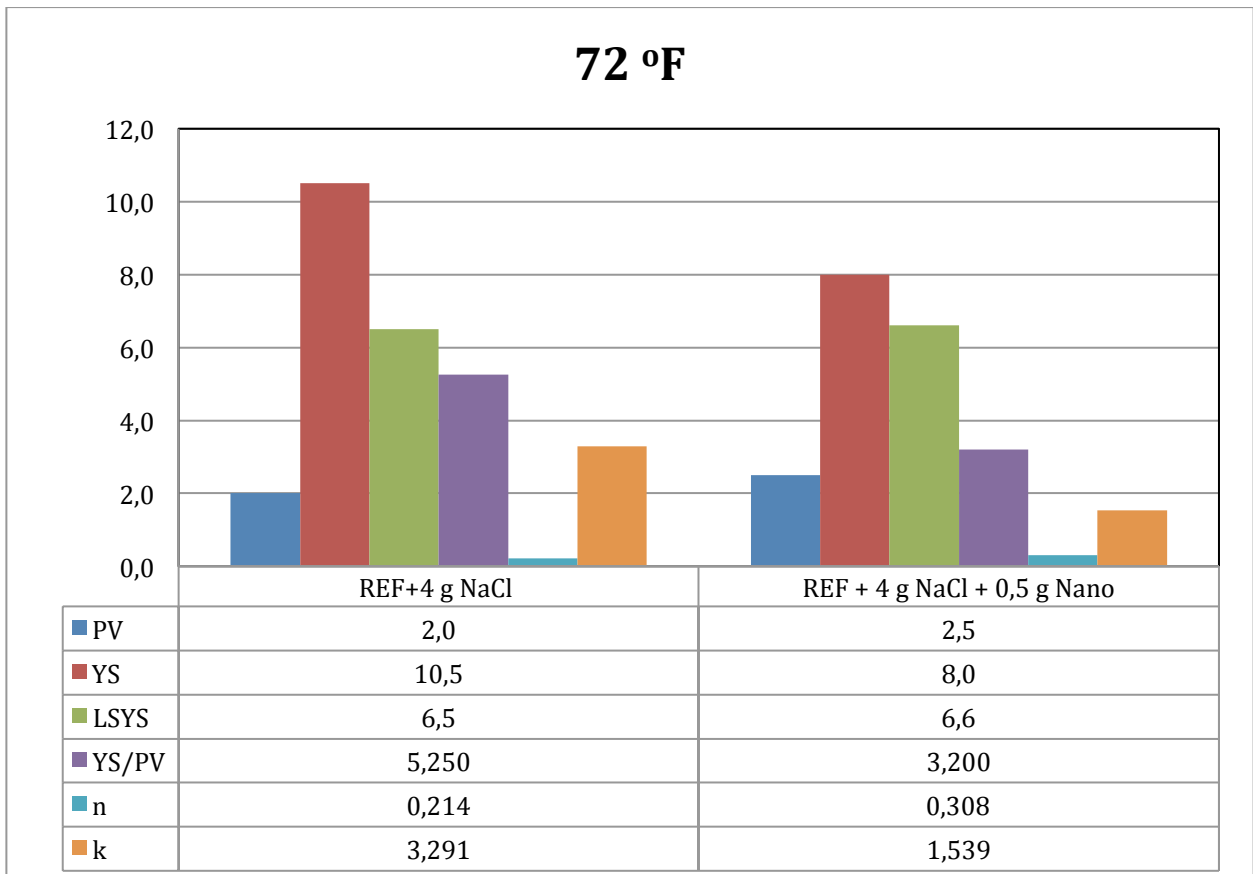


A8-Figure 63: Rheology parameters for REF +1,5gXC at 72, 120 and 150°F

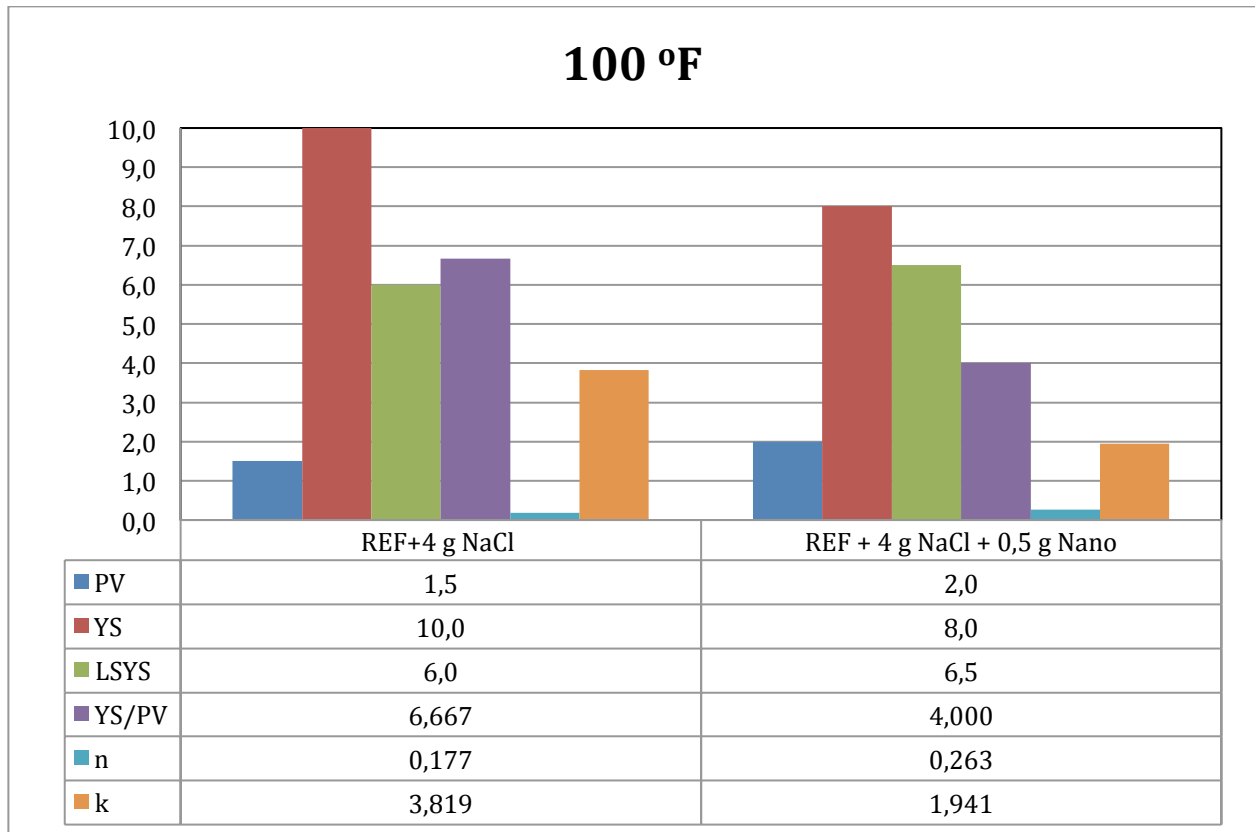
### Appendix B: Effect of nano on salt system (NaCl)



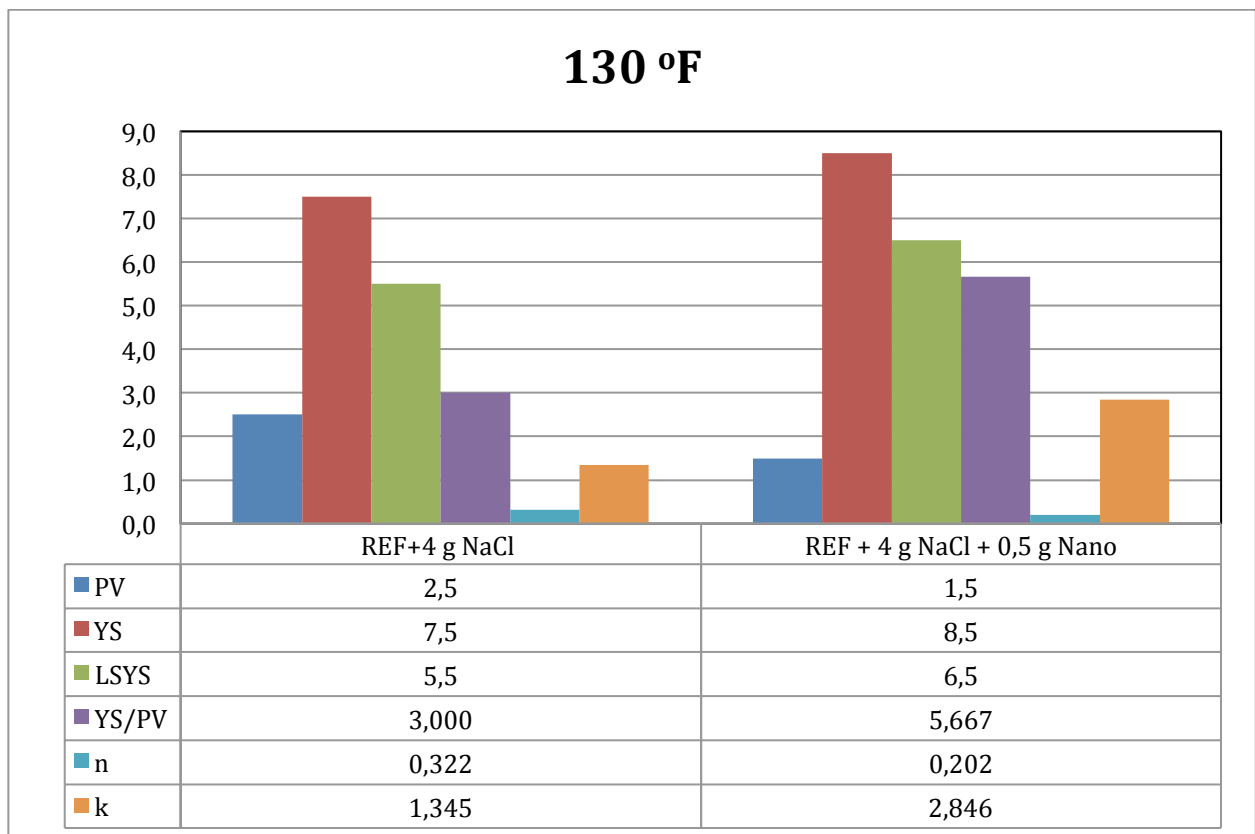
B1-Figure 64: Fann data for REF+ 4gNaCl and REF + 4gNaCl+ 0,5gNano at 72, 100 and 130 °F



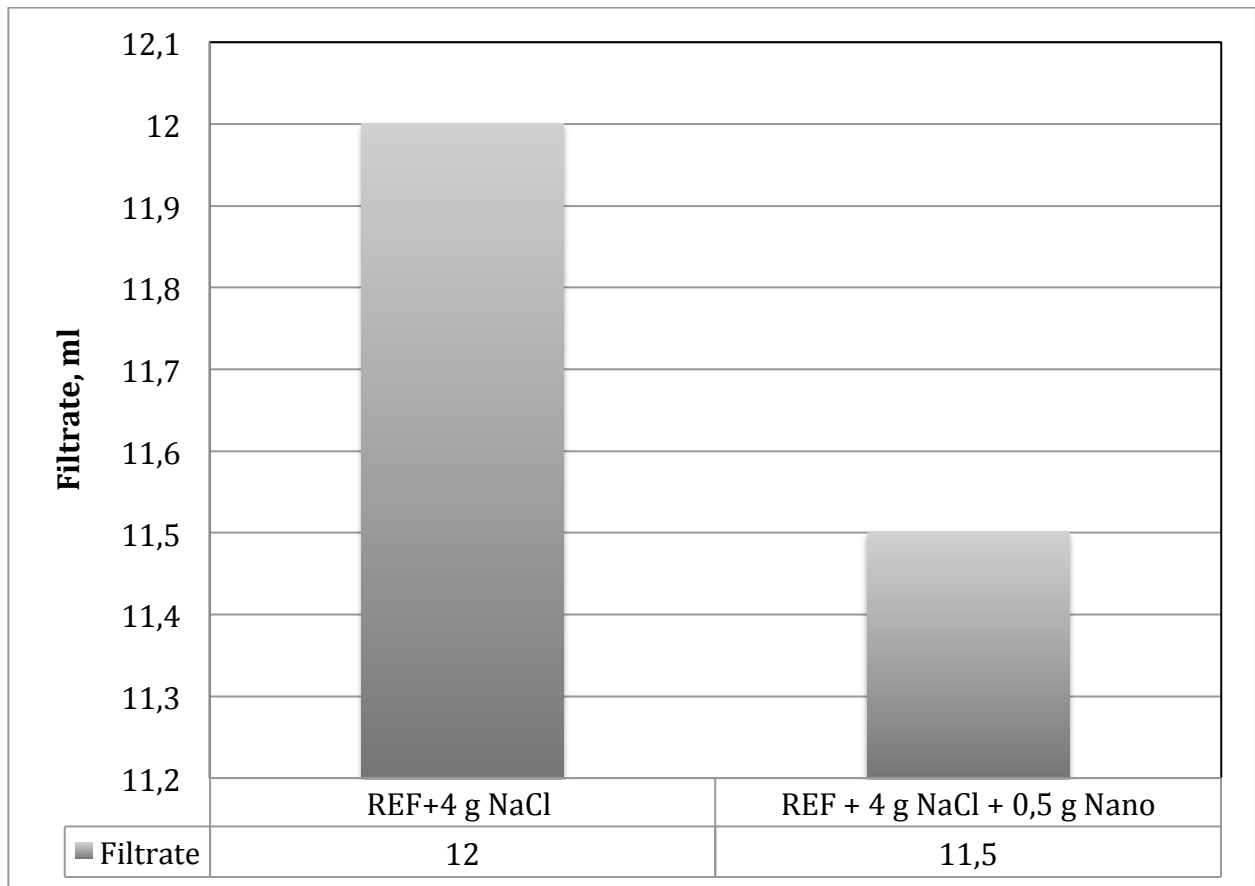
B2-Figure 65: Rheology parameters for REF + 4gNaCl and REF + 4gNaCl+ 0,5gNano at 72°F



**B3-Figure 66: Rheology parameters for REF + 4gNaCl and REF + 4gNaCl+ 0,5gNano at 100 °F**

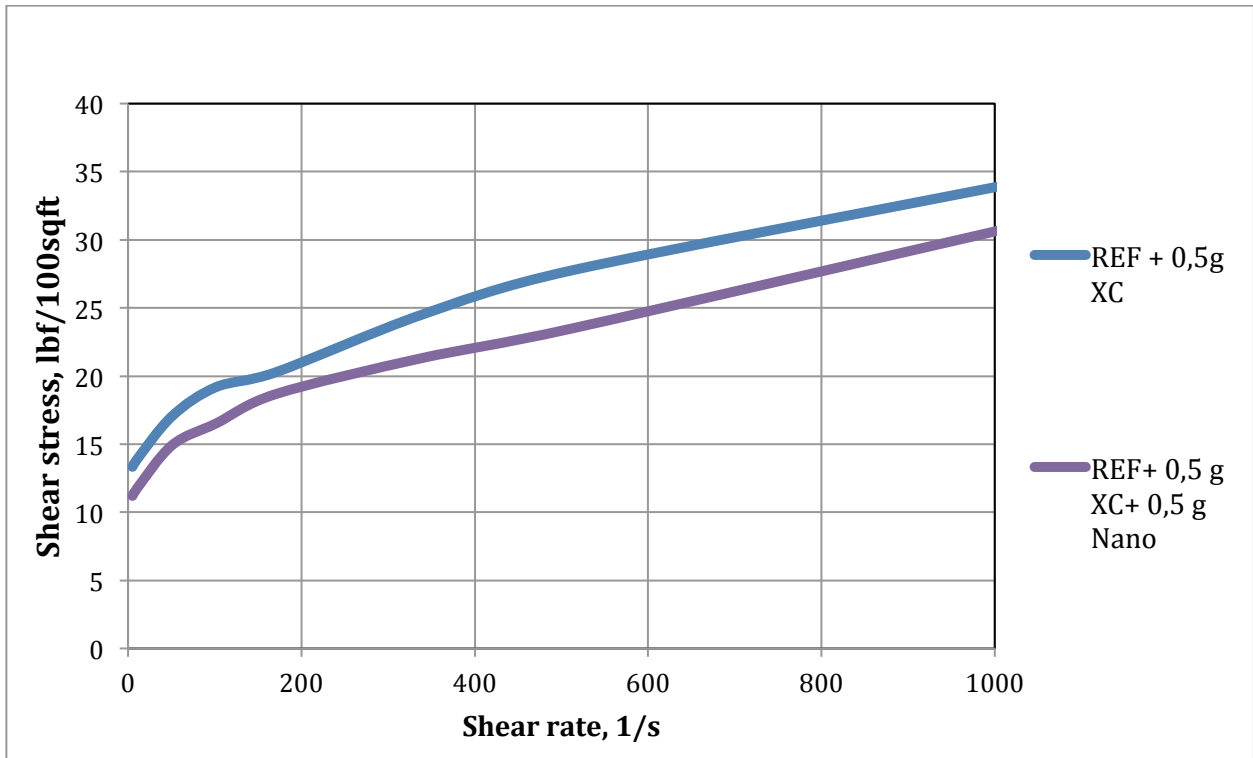


**B4-Figure 67: Rheology parameters for REF + 4gNaCl and REF + 4gNaCl+ 0,5gNano at 130°F**

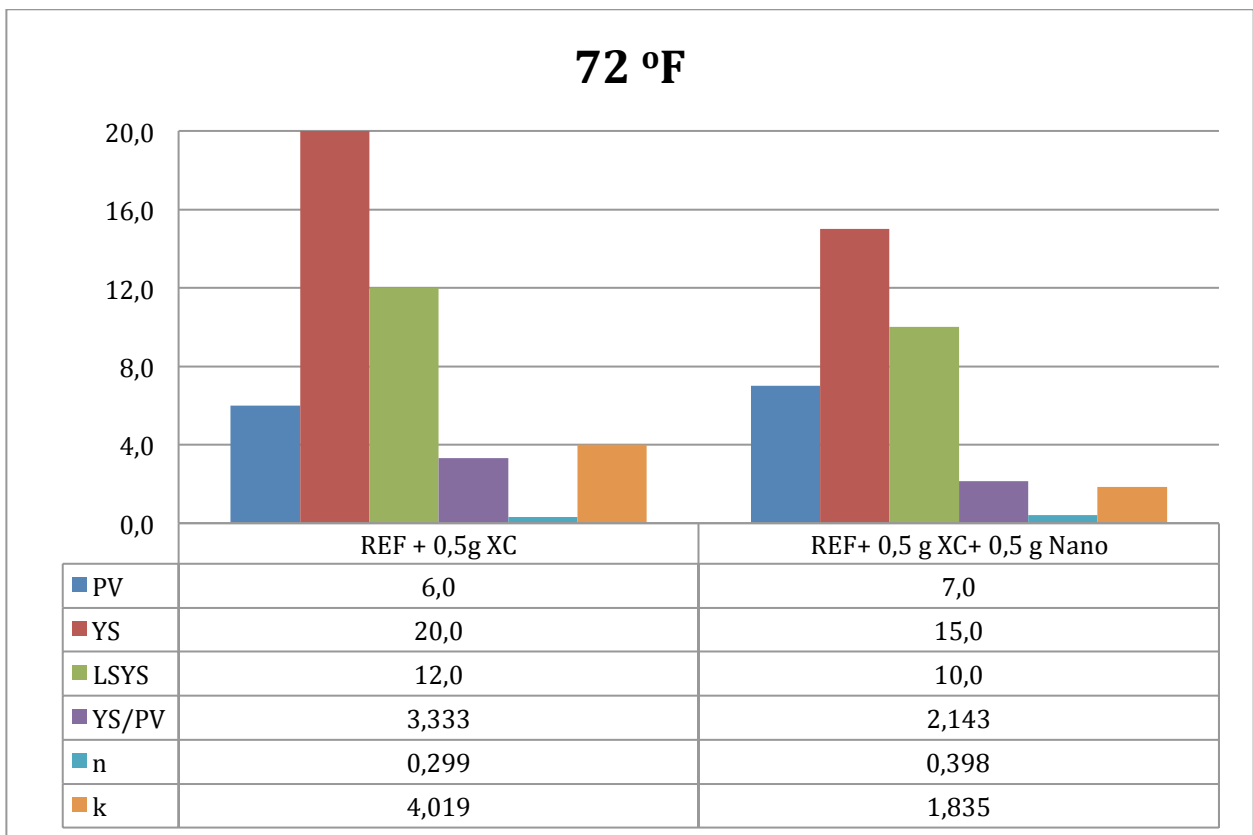


**B5-Figure 68: Comparison filtrate loss of REF + 4gNaCl and REF + 4gNaCl + 0,5gNano**

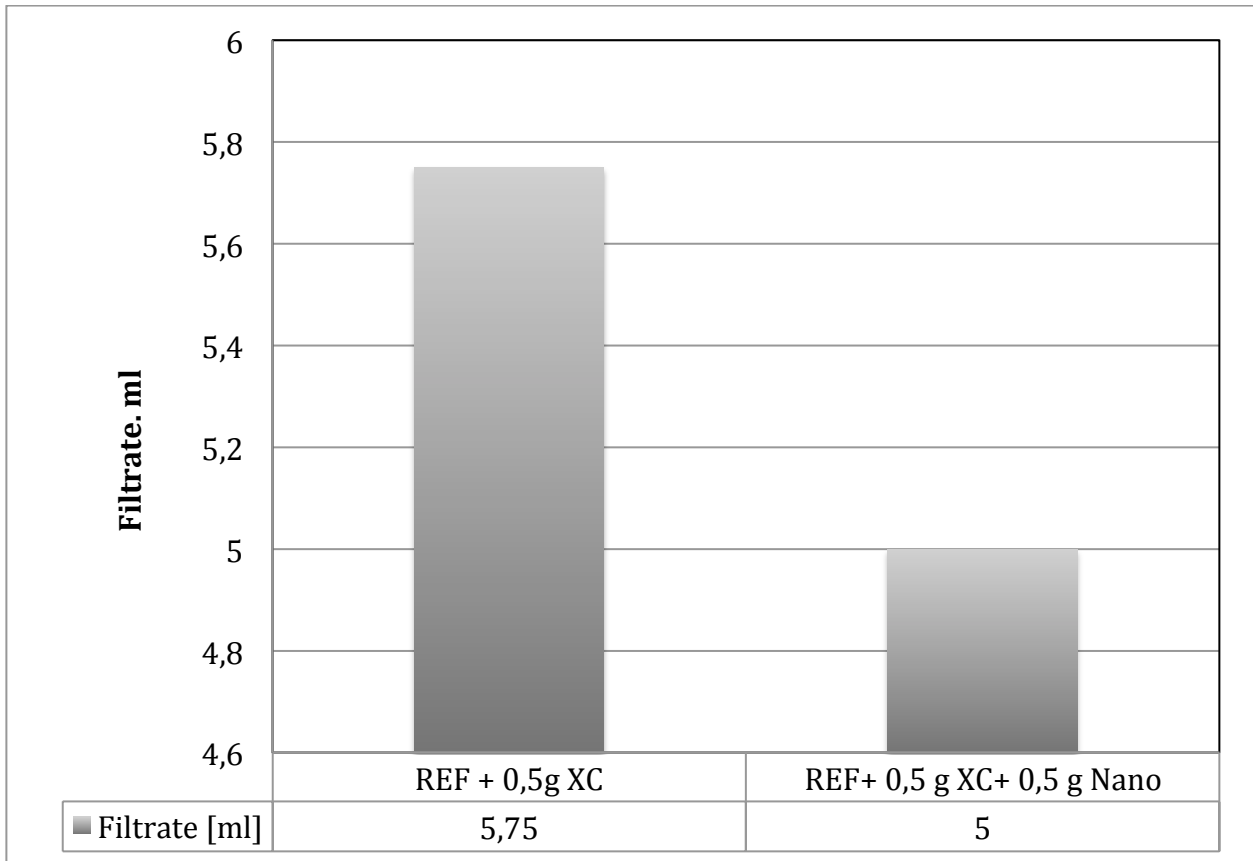
### Appendix C: Effect of nano on polymer system



C1-Figure 69: Fann data for REF + 0,5gXC and REF + 0,5gXC + 0,5gNano at 72°F

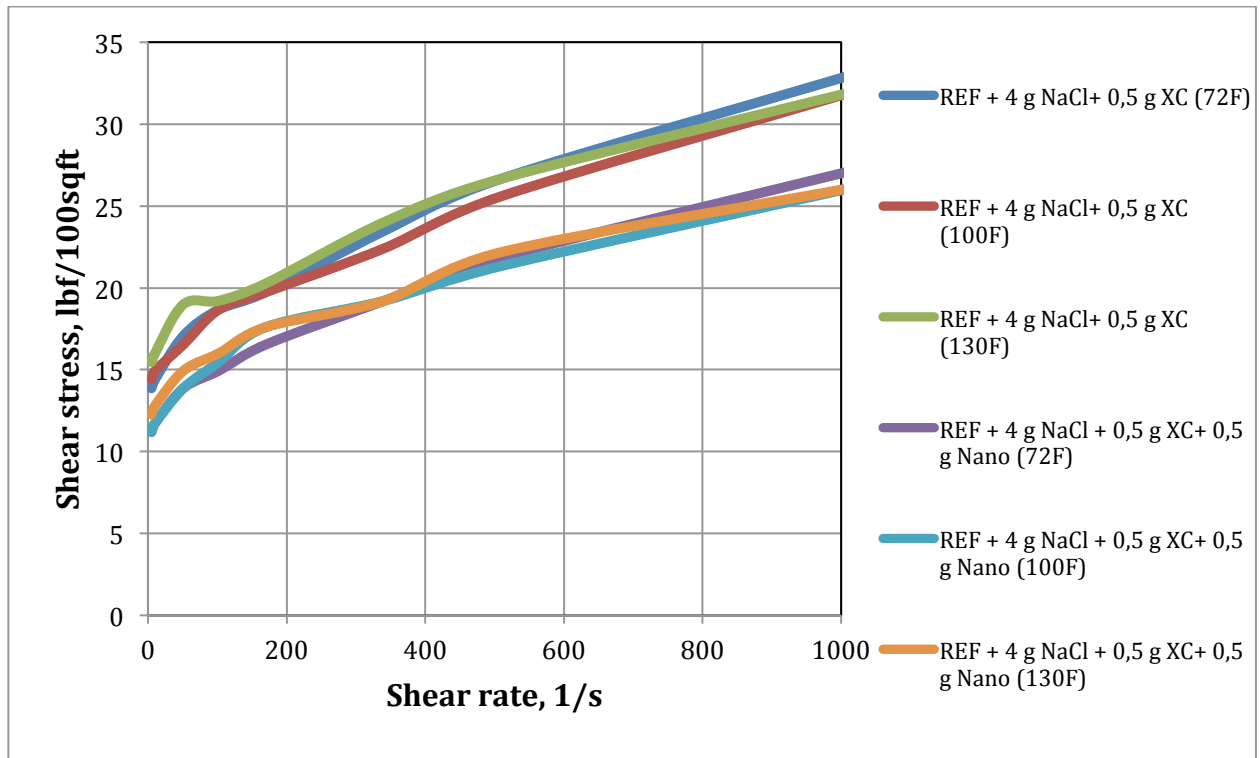


C2-Figure 70: Rheology parameters for REF + 0,5gXC and REF + 0,5gXC + 0,5gNano at 72°F

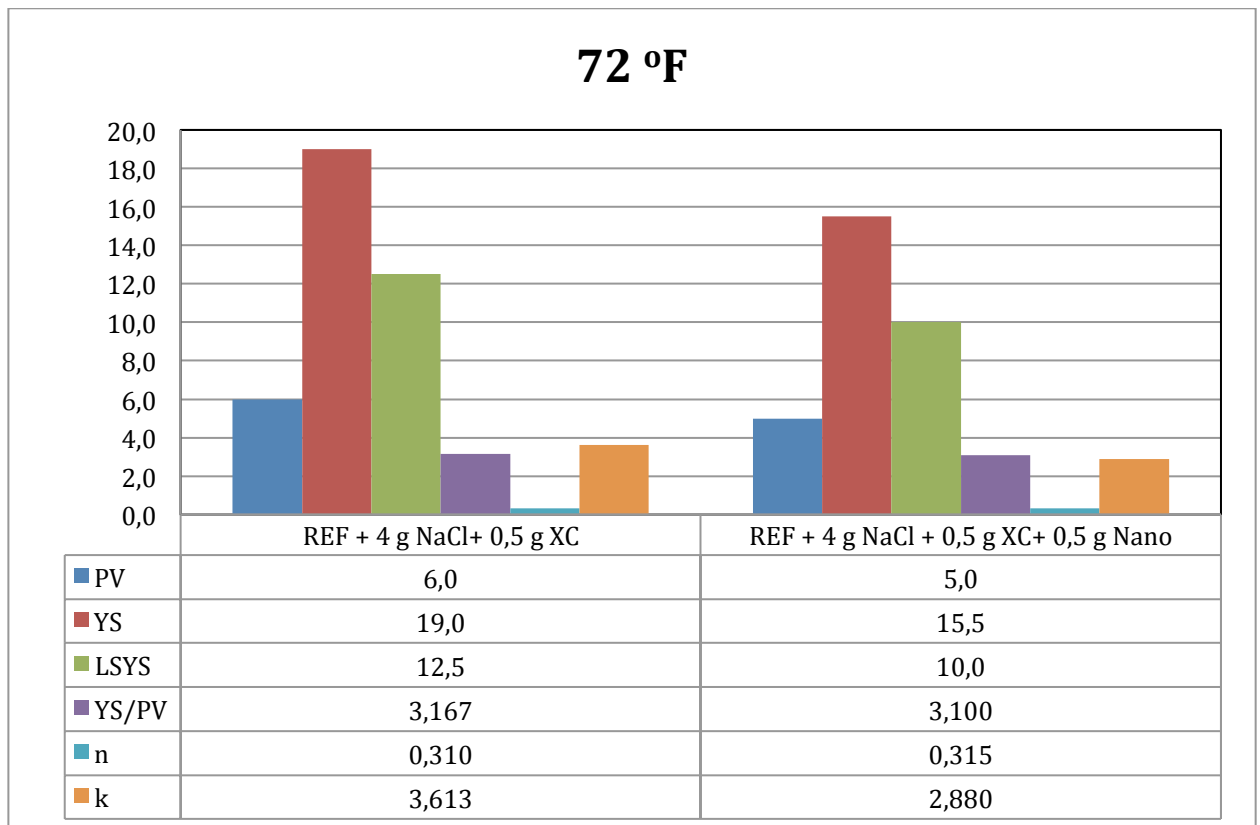


**C3-Figure 71: Comparison filter loss for REF + 0,5gXC and REF +0,5gXC + 0,5gNano**

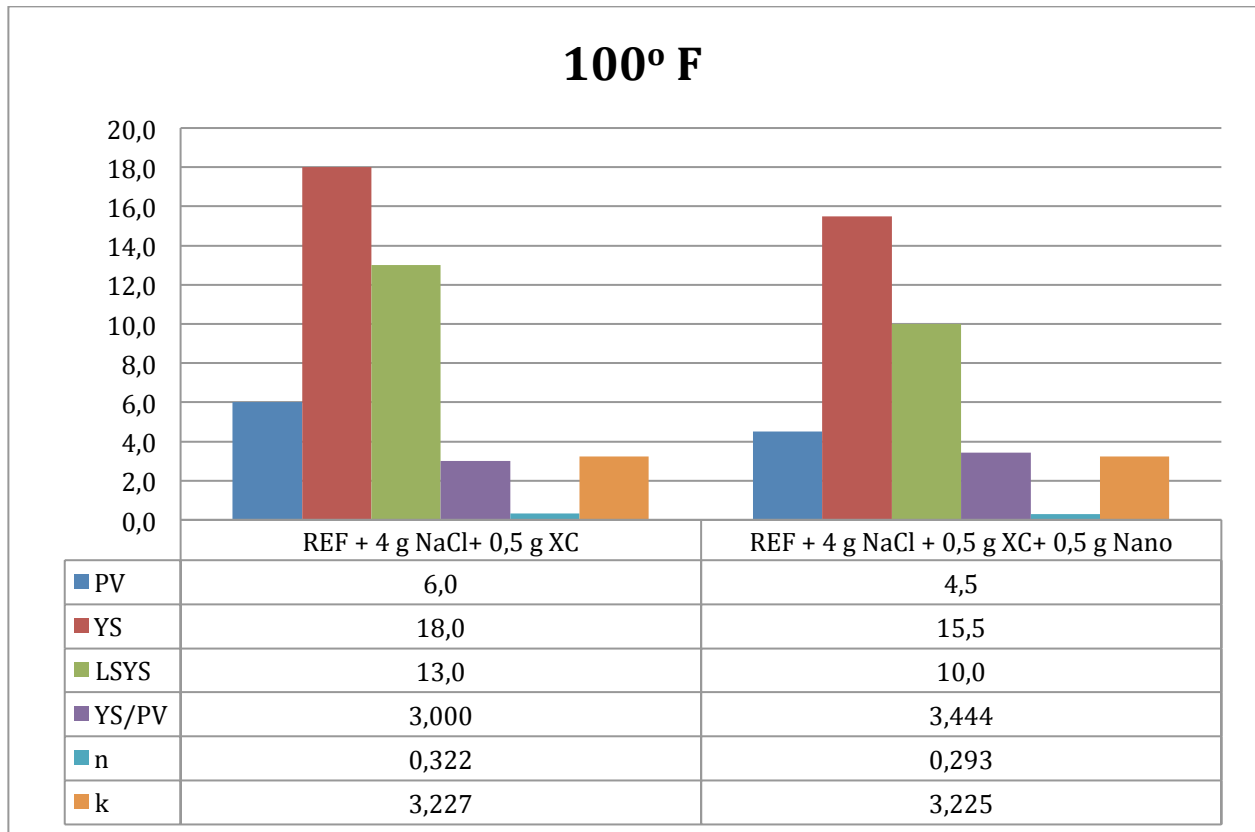
### Appendix D: Effect of nano on polymer system (with NaCl)



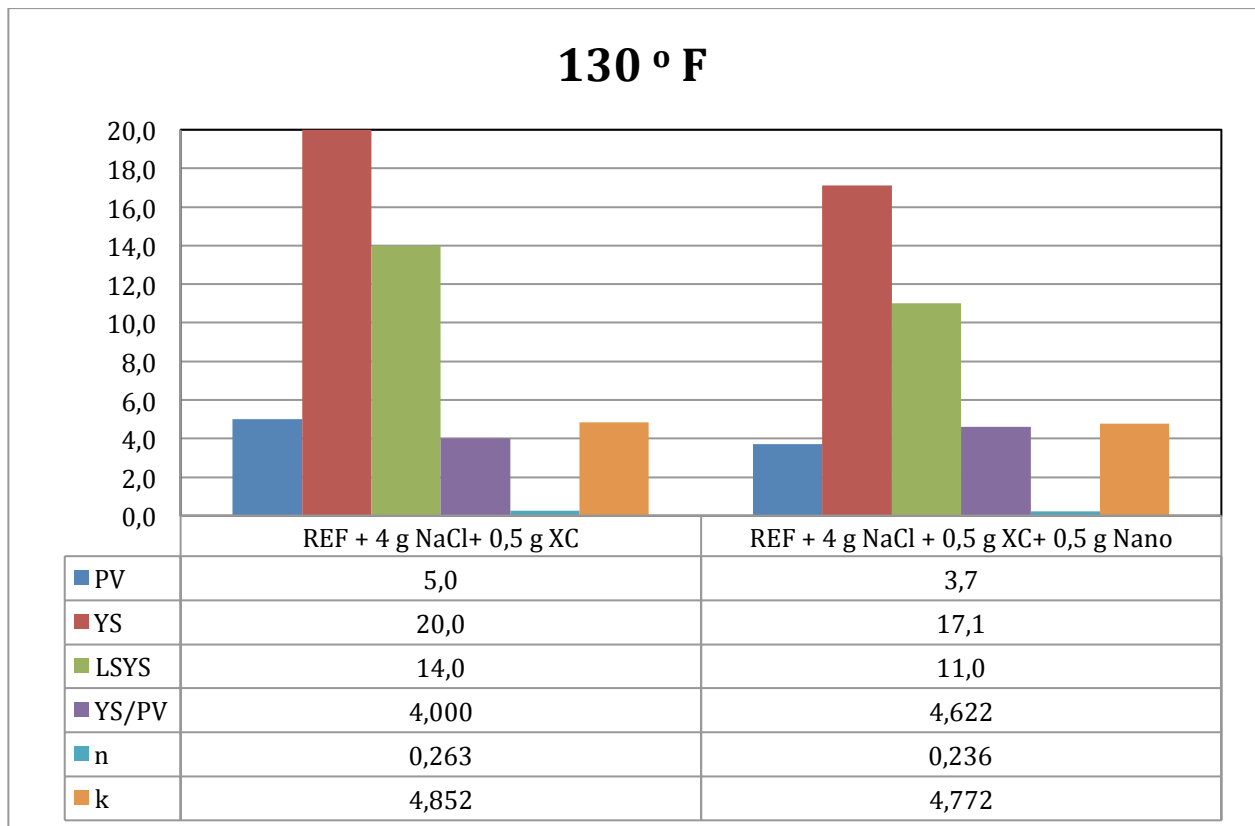
D1-Figure 72: Fann data for REF+ 4gNaCl + 0,5gXC and REF + 4gNaCl +0,5gXC +0,5gNano at 72, 100 and 130°F



D2-Figure 73: Rheology parameters for REF+ 4gNaCl + 0,5gXC and REF + 4gNaCl +0,5gXC +0,5gNano at 72°F

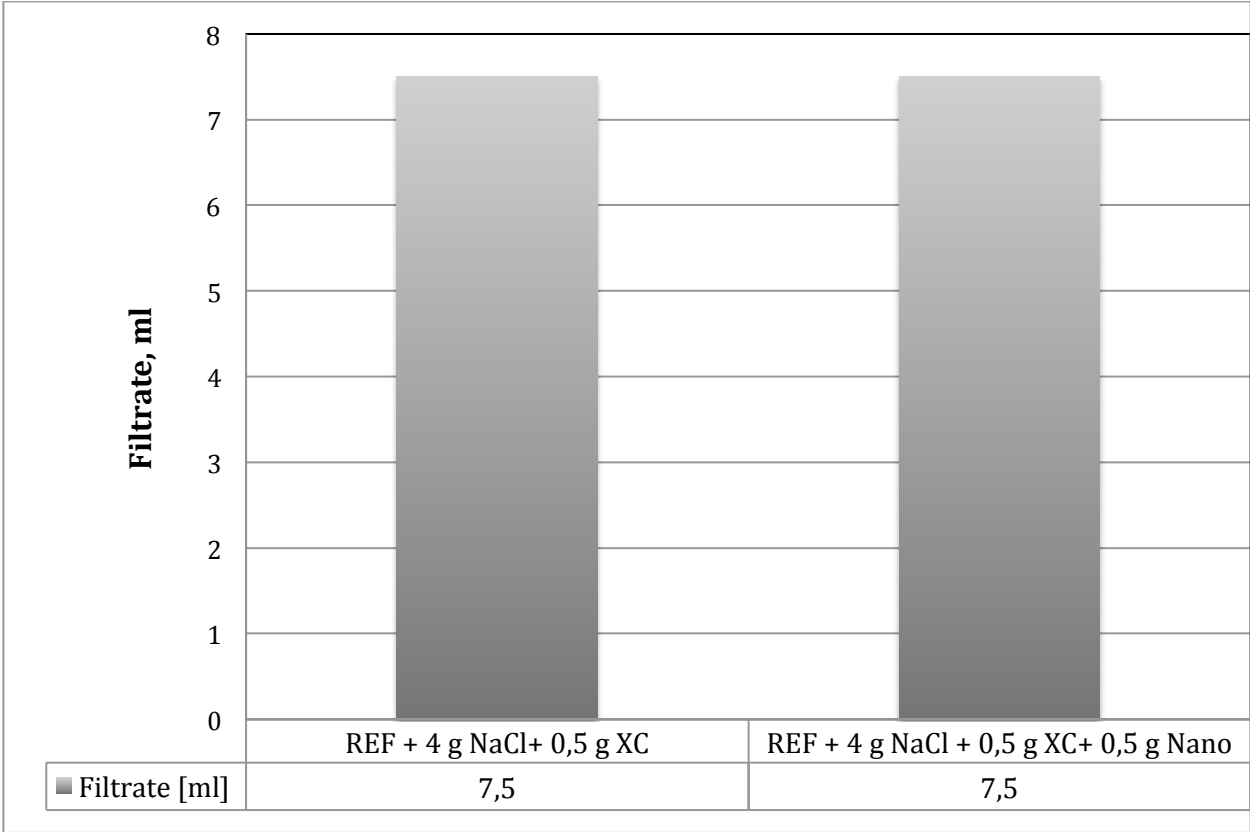


**D3-Figure 74: Rheology parameters for REF+ 4gNaCl + 0,5gXC and REF + 4gNaCl +0,5gXC+ 0,5gNano at 100 °F**



**D4-Figure 75: Rheology parameters for REF+ 4gNaCl + 0,5gXC and REF + 4gNaCl +0,5gXC + 0,5gNano at 130 °F**





**D5-Figure 76: Comparison filtrate loss for REF+ 4gNaCl+ 0,5gXC and REF+ 4gNaCl +0,5gXC +0,5gNano**

## Appendix E: Unified model

### Unified: Pipe Flow

$$\mu_p = R_{600} - R_{300}$$

$$\tau_y = R_{300} - \mu_p$$

$$\tau_0 = 1.066(2R_3 - R_6)$$

$$\mu_p = cp$$

$$n_p = 3.32 \log \left( \frac{2\mu_p + \tau_y}{\mu_p + \tau_y} \right)$$

$$k_p = 1.066 \left( \frac{\mu_p + \tau_y}{511} \right)$$

$$G = \left( \frac{(3-\alpha)n+1}{(4-\alpha)n} \right) \left( 1 + \frac{\alpha}{2} \right)$$

$$\alpha = 1 \text{ for anulli}$$

$$\alpha = 1 \text{ for pipe}$$

$$v_p = \frac{24.51 q}{D_p^2}$$

$$\gamma_w = \frac{1.6 * G * v}{D_R}$$

$$\gamma_w = \text{sec}^{-1}$$

$$\tau_w = \left[ \left( \frac{4-\alpha}{3-\alpha} \right) \right] \tau_0 + k \gamma_w^n$$

$$N_{Re} = \frac{\rho v_p}{19.36 \tau_w}$$

Laminar:

$$f_{laminar} = \frac{16}{N_{Re}}$$

Transient:

$$f_{transient} = \frac{16 N_{Re}}{(3470 - 1370 n_p)}$$

Turbulent: $f_{turbulent} = \frac{a}{N}$	$a = \frac{\log n + 3.93}{50}$ $b = \frac{1.75 - \log n}{7}$
---	---

$$f_{\text{partial}} = (f_{\text{transient}}^{-8} + f_{\text{turbulent}}^{-8})^{-1/8} \text{ and } f_p = (f_{\text{partial}}^{12} + f_{\text{laminar}}^{12})^{1/12}$$

$$\left(\frac{dp}{dL}\right) = 1.076 \frac{f_p v_p^2 \rho}{10^5 D_p}$$

psl/ft

$$\Delta p = \left(\frac{dp}{dL}\right) \Delta L$$

### Unified Annular Flow

$$\mu_p = R_{600} - R_{300}$$

$$\tau_y = R_{300} - \mu_p$$

$$\tau_0 = 1.066(2R_3 - R_6)$$

$$\mu_p = cp$$

$$n_p = 3.32 \log \left( \frac{2\mu_p + \tau_y - \tau_y}{\mu_p + \tau_y - \tau_y} \right)$$

$$k_p = 1.066 \left( \frac{\mu_p + \tau_y - \tau_0}{511} \right)$$

$$G = \left( \frac{(3-\alpha)n+1}{(4-\alpha)n} \right) \left( 1 + \frac{\alpha}{2} \right)$$

$\alpha = 1$  for annuli  
 $\alpha = 1$  for pipe

$$v_a = \frac{24.51 q}{D_2^2 - D_1^2}$$

$v = \text{ft}/\text{min}$

$$\gamma_w = \frac{1.6 * G * v}{D_R}$$

$$\gamma_w = \text{sec}^{-1}$$

$\tau_w = \left[ \left( \frac{4-\alpha}{3-\alpha} \right) \right] \tau_0 + k \gamma_w^n$
$N_{Re} = \frac{\rho v_e}{19.36 \tau_w}$
<p>Laminar:</p> $f_{laminar} = \frac{24}{N_{Re}}$ <p>Transient:</p> $f_{transient} = \frac{16 N_{Re}}{(3470 - 1370 n_p)}$ <p>Turbulent:</p> $a = \frac{\log n + 3.93}{50} \quad b = \frac{1.75 - \log n}{7} \quad \left. \vphantom{\begin{matrix} a \\ b \end{matrix}} \right\} f_{turbulent} = \frac{a}{N}$
$f_{partial} = (f_{transient}^{-8} + f_{turbulent}^{-8})^{-1/8}$ $f_a = (f_{partial}^{12} + f_{laminar}^{12})^{1/12}$
$\left( \frac{dp}{dL} \right) = 1.076 \frac{f_a v_a^2 \rho}{10^5 (D_2 - D_1)}$ <p style="text-align: center; margin-left: 100px;">psl/ft</p> $\Delta p = \left( \frac{dp}{dL} \right) \Delta L$ <p style="text-align: center; margin-left: 100px;">psl</p>

## Pressure loss at bit

$\Delta p_{Nozzles,psi} = \frac{156 \rho q^2}{(D_{N1}^2 + D_{N2}^2 + D_{N3}^2)^2}$
--

**E1-Table 23: Summary of Unified hydraulics model [15]**

## Appendix F: Hole and drill string, and well inclination data hole cleaning simulation

### Hole data (Casing + Open hole)

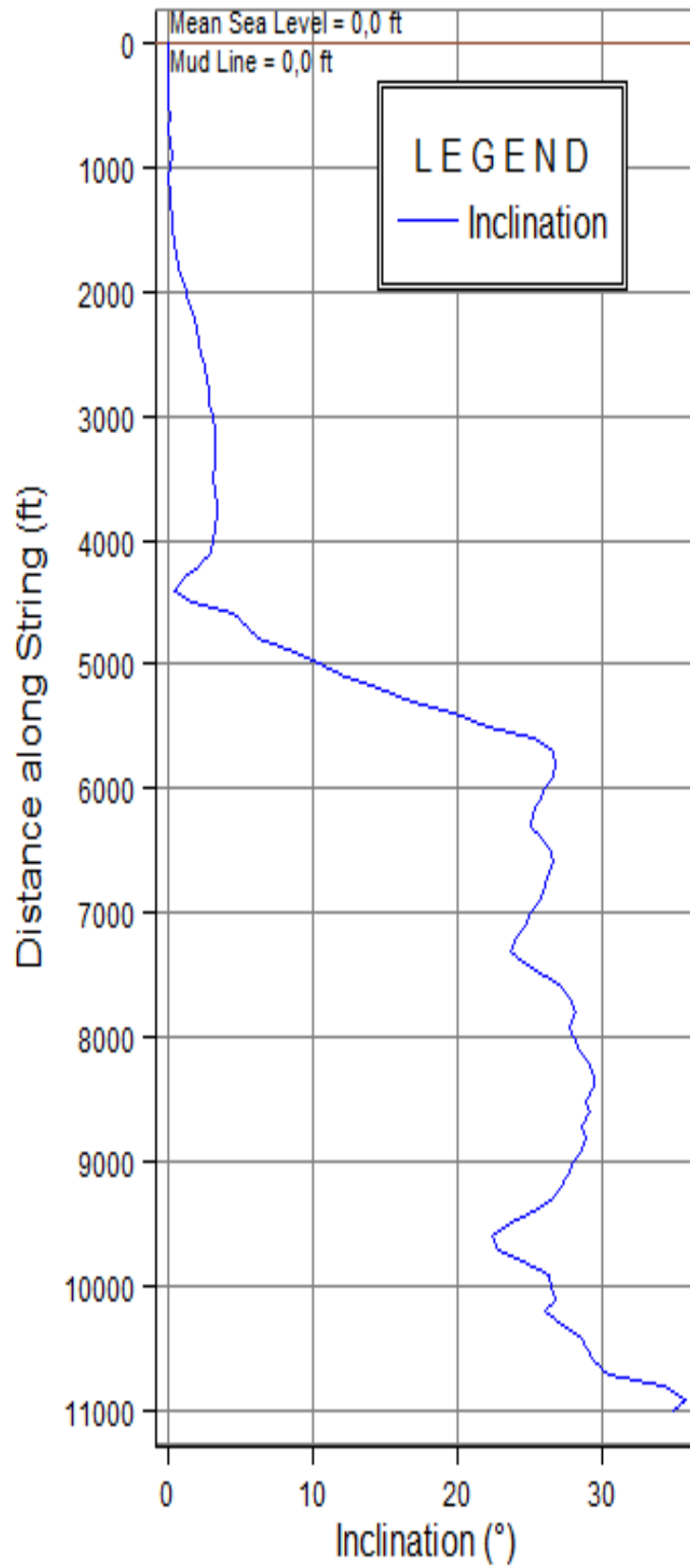
	Section type	Measured Depth (ft.)	Length (ft.)	Shoe Measured Depth (ft.)	Id (In)	Drift (In)	Effective Hole Diameter (In)	Friction factor	Linear Capacity (bbl/ft)	Excess (%)	Item Description
1	Casing	4012.5	4012.5	4012.5	12.250	12.459	12.615	0.25	0.1458		13 3/8in, 54.5ppf, J-55
2	Open Hole	11003.0	6990.50		12.250		12.250	0.30	0.1458	0.00	

**F1-Table 24: Hole data (Casing + open hole)**

### Drill String data (Drill pipe + BHA)

Type	Length (ft)	Depth (ft)	Body	Stabilizer/tool joint					Weight (ppf)	Material	Grade	Class
			OD (in)	ID (in)	Avg.joint Length (ft)	Length (ft)	OD (in)	ID (in)				
Drill pipe	10445	10445.00	5.0	4.276	30.00	1.42	6.406	3.75	22.26	CS_API 5D/7	E	P
Heavy weight Drill pipe	120.0	10565.0	6.625	4.5	30.00	4.00	8.25	4.5	70.50	CS_1340 MOD	1340 MOD	
Hydraulic Jar	32.00	10597	6.5	2.75					91.79	CS_API 5D/7	4145H MOD	
Heavy weight Drill pipe	305.0	10902	5.0	3.0	30.00	4.00	6.50	3.063	49.7	CS_1340 MOD	1340 MOD	
Bit sub	5.00	10907	6.0	2.4					79.51	CS_API 5D/7	4145H MOD	
MWD tool	85.00	10992	8.0	2.5					154.36	SS_15-15LC	15-15LC MOD	
Integral blade stabilizer	5.00	10997	6.25	2.0		1.00	8.453		93.72	CS_API 5D/7	4145H MOD	
Bit sub	5.00	11002	6.0	2.4					79.51	CS_API 5D/7	4145H MOD	
Tri-cone bit	1.00	11003	10.625						166.0			

**F2-Table 25: Drill String data (Drill pipe + BHA)**



F3-Figure 77: Well inclination for the simulation

## Appendix G: Well plan cutting transport models

### Hole Cleaning Calculations

Calculate  $n, K, \tau_y$ , and Reynold's Number

$$n = \frac{(3.32)(\log 10)(YP + 2PV)}{(YP + PV)}$$

$$K = \frac{(PV + YP)}{511}$$

$$\tau_y = (5.11K)^n$$

$$R_A = \frac{\rho V_a^{(2-n)}(D_H - D_p)^n}{(2/3)G_{ra}K}$$

Concentration Based on ROP in Flow Channel

$$C_o = \frac{(V_r D_B^2 / 1471)}{(V_r D_B^2 / 1471) + Q_m}$$

Fluid Velocity Based on Open Flow Channel

$$V_a = \frac{24.5Q_m}{D_H^2 - D_p^2}$$

Coefficient of Drag around Sphere

If  $R_e < 225$  then,

$$C_D = \frac{22}{\sqrt{R_e}}$$

else,

$$C_D = 1.5$$

Mud carrying capacity

$$C_M = \frac{4g\left(\frac{D_c}{12}\right)(\rho_c - \rho)}{3\rho C_D}$$

Slip Velocity

If  $V_A < 53.0$ , then  $V_{sv} = (0.00516)V_A + 3.0006$

If  $V_A \geq 53.0$ , then  $V_{sv} = (0.02554)(V_A - 53.0) + 3.28$

**Settling Velocity in the Plug in a Mud with a Yield Stress**

$$U_{\#} = \left[ \frac{4}{3} \frac{g D_c^{1+b} (\rho_c - \rho)}{a K_b \rho_c^{1-b}} \right]^{\frac{1}{2-b(2-n)}}$$

Where:

$$a = 42.9 - 23.9n$$

$$b = 1 - 0.33n$$

**Angle of Inclination Correction Factor**

$$C_a = (\sin(1.33\alpha))^{1.33} \left( \frac{5}{D_H} \right)^{0.66}$$

**Cuttings Size Correction Factor**

$$C_s = 1.286 - 1.04 D_c$$

**Mud Weight Correction Factor**

If  $(\rho < 7.7)$ , then

$$C_m = 1.0$$

else

$$C_m = 1.0 - 0.0333(\rho - 7.7)$$

**Critical Wall Shear Stress**

$$\tau_{wc} = [ag \sin(\alpha)(\rho_c - \rho) D_c^{1+b} \rho_c^{b/2}] \frac{2n}{2n - 2b + bn}$$

Where:

$$a = 1.732$$

$$b = -0.744$$

**Critical Pressure Gradient**

$$F_{gc} = \frac{2\tau_{wc}}{\gamma_h [1 - (\frac{r}{r_h})^2]}$$

**Total Cross Sectional Area of the Annulus without Cuttings Bed**

$$A_A = \frac{\pi (D_H^2 - D_P^2)}{4 \cdot 144}$$



**Dimensionless Flow Rate**

$$\Pi_{g_b} = \Pi \left[ 8 \times \frac{\frac{n}{2(1+2n)}}{\left(a\right) \frac{1}{b}} \right]^{\frac{1}{2-(2-n)\delta}} \times \left(1 - \left(\frac{r_p}{r_h}\right)^2\right) \left(1 - \left(\frac{r_p}{r_h}\right)^{\frac{\delta}{2-(2-n)\delta}}\right)$$

Where:

$$a = 16$$

$$b = 1$$

**Critical Flow Rate (CFR)**

$$Q_{crit} = r_h^2 \left[ \frac{\rho_g b^{\frac{1}{\delta}} r_k^{\left(\frac{1}{\delta+n}\right)}}{K \rho^{\left(\frac{1}{\delta-1}\right)}} \right]^{\frac{\delta}{2-\delta(2-n)}} \Pi_{g_b}$$

**Correction Factor for Cuttings Concentration**

$$C_{BED} = 0.97 - (0.00231 \mu_a)$$

**Cuttings Concentration for a Stationary Bed by Volume**

$$C_{mov} = C_{BED} \left(1.0 - \frac{Q_m}{Q_{crit}}\right) (1.0 - \phi_B)(100)$$

Where:

$D_B$  = Bit diameter

$D_H$  = Annulus diameter

$D_P$  = Pipe diameter

$D_{TJ}$  = Tool joint diameter

$D_C$  = Cuttings diameter

$\tau_y$  = Mud yield stress

$G_{\#}$  = Power law geometry factor

$R_A$  = Reynolds number

$R_e$  = Particle Reynolds number

$\rho$  = Fluid density

$\rho_c$  = Cuttings density

$V_a$  = Average fluid velocity for annulus

$V_R$  = Rate of penetration, ROP

$V_{av}$  = Cuttings travel velocity

$V_{\infty}$  = Original slip velocity

$V_{sv}$  = Slip velocity

$V_{cav}$  = Critical transport fluid velocity

$V_{TC}$  = Total cuttings velocity

$K$  = Consistency factor

$n$  = Flow behavior index

$a, b, c$  = Coefficients

$YP$  = Yield point

$PV$  = Plastic viscosity

$Q_C$  = Volumetric cuttings flow rate

$Q_m$  = Volumetric mud flow rate

$Q_{crit}$  = Critical flow rate for bed to develop

$C_o$  = Cuttings feed concentration

$C_D$  = Drag coefficient

$C_m$  = Mud carrying capacity

$C_A$  = Angle of inclination correction factor

$C_S$  = Cuttings size correction factor

$C_{mud}$  = Mud weight correction factor

$C_{BED}$  = Correction factor for cuttings concentration

$C_{dms}$  = Cuttings concentration for a stationary bed by volume

$U_{\text{set}}$  = Settling velocity

$U_s$  = Average settling velocity in axial direction

$U_{mix}$  = Average mixture velocity in the area open to flow

$\alpha$  = Wellbore angle

$\phi_B$  = Bed porosity

$\mu_a$  = Apparent viscosity

$\lambda_p$  = Plug diameter ratio

$\xi$  = Gravitational coefficient

$r_0$  = Radius of which shear stress is zero

$r_p$  = Radius of drill pipe

$r_k$  = Radius of wellbore or casing

$P_{\text{crit}}$  = Critical frictional pressure gradient

$\tau_{wc}$  = Critical wall shear stress